Aus dem Institut für Virologie
des Fachbereichs Veterinärmedizin
der Freien Universität Berlin

Structural and functional research on glycoprotein 3 of porcine reproductive and respiratory syndrome virus

Inaugural-Dissertation
zur Erlangung des Grades eines
Doctor medicinae veterinariae
an der Freien Universität Berlin

vorgelegt von
Bang Qian
aus Yunnan, Volksrepublik China

Berlin 2024
Journal-Nr.: 4485

Gedruckt mit Genehmigung
des Fachbereichs Veterinärmedizin
der Freien Universität Berlin

Dekan: Univ.-Prof. Dr. Uwe Rösler
Erster Gutachter: PD Dr. Michael Veit
Zweiter Gutachter: Univ-Prof. Dr. Benedikt Kaufer
Dritter Gutachter: Prof. Dr. Robert Klopfleisch

Deskriptoren (nach CAB-Thesaurus):
Porcine reproductive and respiratory syndrome virus, PRRSV, Glycoprotein 3, structure and function, Virus Replication, Inhibitor

Tag der Promotion: 15.10.2024

Table of contents

List of Figures

List of tables

Abbreviations

PRRS	Porcine reproductive and respiratory syndrome
PRRSV	Porcine reproductive and respiratory syndrome virus
LDV	lactate dehydrogenase-elevating virus
SHFV	simian hemorrhagic fever virus
EAV	equine arteritis virus
WPDV	wobbly possum disease virus
PNGase F	Peptide-n-glycosidase
GP2	Glycoprotein 2
GP3	Glycoprotein 3
GP4	Glycoprotein 4
GP5	Glycoprotein 5
N	Nucleocapsid protein
ORF	Open reading frame
ORF5a	Open reading frame 5a protein
UTR	Untranslated region
ER	Endoplasmic reticulum
Endo H	Endoglycosidase H
GFP	Green fluorescent protein
kb	Kilo base pair
kDa	Kilo Dalton
BHK-21	Baby hamster kidney cells
C	Carboxyl terminus
cDNA	Complementary DNA
CHO-K1	Chinese hamster ovary cells
HR	Hydrophobic region
M	Membrane protein
MAb	monoclonal antibody
MOI	Multiplicity of infection
mRNA	Messenger RNA
N	Amino terminus
nsp	Non-structural protein
PAM	Porcine alveolar macrophage
PBS	Phosphate-buffered saline
SDS	Sodium dodecyl sulfate

SDS-PAGE	SDS polyacrylamide gel electrophoresis
sgRNA	subgenomic RNA
SP	Signal peptide
TM	Transmembrane
TMD	Transmembrane domain
TMR	Transmembrane region
VLPs	Virus-like particles
WT	Wild type
WB	Western blot
RdRp	RNA dependent RNA polymerase
M^{pro}	Proteinase

1 Introduction

1.1 Porcine respiratory and reproductive syndrome virus

Porcine reproductive and respiratory syndrome (PRRS) is a highly contagious and virulent infectious disease caused by the etiologic agent known as porcine reproductive and respiratory syndrome virus (PRRSV). This virus, classified as an enveloped and positive-stranded RNA virus, belongs to the Nidovirales order and the Arterviridae family, which also includes murine lactate dehydrogenase-elevating virus (LDV), simian hemorrhagic fever virus (SHFV), and equine arteritis virus (EAV) (E. J. Snijder, Kikkert, & Fang, 2013). PRRSV first emerged in the late 1980s as a mysterious disease. Subsequently, Lelystad virus and VR2332 were isolated in Europe (PRRSV type 1) and North America (PRRSV type 2), respectively(Benfield et al., 1992; Bryans, Crowe, Doll, & McCollum, 1957; Notkins & Scheele, 1963; Wensvoort et al., 1991).

However, several new strains have been reported recently, including eleven highly divergent simian Arteriviruses in diverse African non-human primates and a novel Arterivirus, the wobbly possum disease virus (WPDV) in common brushtails in New Zealand (Dunowska, Biggs, Zheng, & Perrott, 2012; Lauck et al., 2011). Each Arterivirus infects only one animal species, unlike some coronaviruses, which have been shown to transmit between species(Hilgenfeld & Peiris, 2013). There has been no discovery that Arterivirus infects humans, at least to date (Balasuriya, Go, & MacLachlan, 2013; Meulenberg, 2000; E. J. Snijder et al., 2013).

Over the past few decades, PRRS has become the most significant infectious disease affecting pigs, resulting in substantial financial losses for the global pork industry. In the United States, the annual estimated economic impact of PRRS-related pig morbidity stands at around 600 million USD, carrying significant implications for food security (Holtkamp et al., 2013). Currently, PRRSV-2 strains are prevalent in China, exhibiting high fatality rates and rapid variation and recombination in piglets (C. Li et al., 2016; Song, Shen, Cui, & Zhao, 2010; Tian et al., 2007). Due to the virus's continuous mutation and recombination, providing adequate protection against varying virus strains remains challenging for current vaccines. Nevertheless, vaccination

remains the primary measure for PRRS prevention, with domestic inactivated and attenuated vaccines widely used to combat classical strains like VR2332, CH-1R, and R98, as well as highly pathogenic strains JXA1, TJ, HuN4, and XH-GD(H. Zhang et al., 2023).

PRRSV is notoriously difficult to eliminate from pig farms, with several factors contributing to this persistence, including genetic variation and the presence of decoy epitopes. For instance, ORF3, encoding GP3, contains hypervariable regions (N. Chen et al., 2011). Some studies have shown that epitope A of GP5 may act as a decoy, potentially delaying the neutralizing antibody response, a hallmark of PRRSV infections (Thaa, Sinhadri, Tielesch, Krause, & Veit, 2013). Many epitopes in GP3 are also non-neutralizing and may function as decoys (J. Z. Chen et al., 2014), while the secreted fraction of GP3 might divert antibodies away from virus particles. Therefore, it is crucial for us to unravel the structure and biological function of GP3 in the process of PRRSV persistent infection, aiding our comprehension of PRRSV pathogenesis.

1.1.1 Clinical symptoms and pathogenesis of PRRSV

1.1.1.1 Clinical symptoms of PRRSV

In its early stages, PRRS was known by various names such as mystery swine disease, mystery reproductive syndrome, and blue-ear pig disease (Keffaber, 1989; Wensvoort et al., 1991). However, it later emerged as a globally devastating clinical condition marked by severe reproductive disorders affecting pregnant sows, perinatal losses, and respiratory distress in piglets. Highly infectious PRRS outbreaks manifest as episodes of reproductive failure, including third-trimester abortions, premature parturition, and elevated fetal losses such as mummies, stillbirths, and neonatal deaths (Meulenberg, 2000). Additionally, reduced growth performance and heightened mortality occur, often secondary to respiratory disease (Keffaber, 1989; Loula, 1991).

However, the disease's intensity appears to vary among isolates, and experiments with PRRSV have revealed variations in virulence. Studies involving pigs experimentally infected with nine different PRRSV isolates from the USA demonstrated significant differences in clinical disease, rectal temperatures, and gross and histological lung lesions (Halbur et al., 1996; Halbur et al., 1995). Animals infected with mildly virulent

isolates of the LV strain exhibited transient pyrexia, dyspnea, and tachypnea, while those infected with highly virulent isolates displayed labored breathing, pyrexia, lethargy, and anorexia. Moreover, the impact on reproductive performance was found to be isolate-dependent (Mengeling, Vorwald, Lager, & Brockmeier, 1996).

The severity of clinical PRRS is linked to elevated viral concentrations in blood and tissues, attributed to the efficient replication of highly virulent isolates in the host (W. Johnson et al., 2004). It was concluded that infection of susceptible pigs with highly virulent PRRSV isolates resulted in longer periods of viremia, increased severity of clinical signs and mortality, and significantly higher viral loads in blood and tissues compared to mildly virulent or cell culture-adapted strains (W. Johnson et al., 2004). Other factors, such as animal age and bacterial co-infection, can influence virus replication and clinical signs. Studies comparing age groups determined that younger animals (4–8 weeks of age) infected with PRRSV exhibited longer viremia, higher excretion rates, and increased replication rates in macrophages compared to older pigs (16–24 weeks) (Thanawongnuwech, Thacker, & Halbur, 1998; van der Linden, Voermans, van der Linde-Bril, Bianchi, & Steverink, 2003).

Additionally, certain bacterial agents, such as *Bordetella bronchiseptica* and *Mycoplasma hyopneumoniae*, appeared to enhance the duration and severity of PRRSV-induced pneumonia and lung lesions (Brockmeier, Palmer, & Bolin, 2000; Thacker, Halbur, Ross, Thanawongnuwech, & Thacker, 1999). Furthermore, PRRSV infection increased the susceptibility of pigs *to Streptococcus suis* type 2 infection and enhanced the severity of *Salmonella choleraesuis* infection (Feng et al., 2001; Wills et al., 2000).

1.1.1.2 Pathogenesis of PRRSV

The pathogenesis of PRRSV entails a complex sequence of events. Initially, PRRSV gains entry into host cells through clathrin-mediated endocytosis (Lunney et al., 2016). Subsequently, the viral genome is liberated into the cytosol through a process involving endosome acidification and membrane fusion. The receptor-mediated viral entry of PRRSV has been the subject of extensive research (Welch & Calvert, 2010). To date, CD163 has been identified as the primary receptor responsible for mediating viral

internalization and disassembly (Van Breedam et al., 2010). Notably, the overexpression of CD163 renders various nonpermissive cell lines susceptible to PRRSV infection. Additionally, two minor structural proteins, GP2a and GP4, have been identified as viral attachment proteins facilitating virus entry into susceptible host cells by interacting with CD163 (Calvert et al., 2007).

PRRSV enters the host body through the respiratory tract, primarily through the inhalation of contaminated air. The virus predominantly reproduces in macrophages and dendritic cells located in the lungs and upper respiratory tract, leading to viremia within 6–12 hours post-infection (pi). Notably, serum viremia may persist for several weeks, even in the presence of circulating antibodies (Lunney et al., 2016). PRRSV possesses the capability to modulate the host's immune response, enabling it to elude detection and clearance. As virus replication diminishes to the extent where it is no longer discernible in the blood and lungs, and pigs cease to manifest overt signs of clinical disease, PRRSV can disseminate systemically, infecting diverse tissues and organs throughout the pig's body. During this phase, viral replication is predominantly localized in lymphoid organs, including the tonsils and lymph nodes but excluding the spleen (Rowland, Lawson, Rossow, & Benfield, 2003; Wills et al., 1997). PRRSV demonstrates the capacity to establish persistent infections in certain pigs, contributing to the prolonged circulation of the virus within swine herds. The sustained replication of the virus in regional lymph nodes plays a crucial role in the efficient transmission of the virus to naive pigs through oral-nasal secretions and semen (Christopher-Hennings, Nelson, Althouse, & Lunney, 2008). In the end, virus replication gradually diminishes until the virus is eradicated within the host; nevertheless, viral replication can persist for as long as 250 days post-infection (Wills, Doster, Galeota, Sur, & Osorio, 2003).

It's important to highlight that in the typical swine production setting, where pigs are raised for 250 days, PRRSV establishes a 'life-long' infection (Lunney et al., 2016).Understanding the pathogenesis of PRRSV is crucial for the development of effective control and prevention strategies, encompassing vaccines and management practices within swine herds.

1.1.2 The PRRSV genome and virion structure

1.1.2.1 The virus genome organization

Viruses of the Arteriviridae family share similar genetic and biological features, such as genomic organization and content, morphology, and a cellular tropism for the macrophage lineage (Faaberg, Balasuriya, Brinton, Gorbalenya, & Yoo, 2012). The genome of the porcine reproductive and respiratory syndrome virus (PRRSV) is a single-stranded RNA molecule. Its genomic organization, approximately 15 kilobases in length, is depicted in figure 1 and contains several open reading frames (ORFs). The genome is organized into two main regions: the 5' and 3' untranslated region (UTR) and the coding region (K. Faaberg et al., 2012; Yun & Lee, 2013).

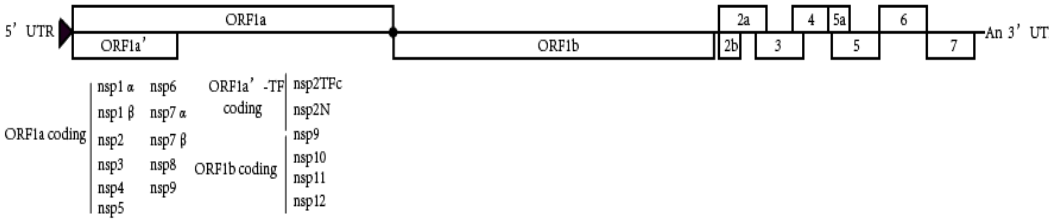

Figure 1 The viral genomic organization

The viral genome starts from the 5' terminal, including ORF1a, ORF1a', and ORF1b, which encode non-structural proteins, as shown below the genome. The remaining part of the viral genome includes ORF2a, ORF2b (E protein), ORF3, ORF4, ORF5, ORF5a, ORF6 (M protein), and ORF7 (N protein), which encode structural proteins. "•" denotes the Ribosomal Frame Shift (RFS) site. Modified from (Kappes & Faaberg, 2015).

The coding region of the PRRSV genome consists of at least 10 ORFs, encoding various viral proteins. These proteins play crucial roles in viral replication, immune evasion, and pathogenesis. Key proteins encoded by the PRRSV genome include the replicase polyproteins (pp1a and pp1ab), the structural proteins (such as the envelope glycoproteins GP2, GP3, GP4, and GP5), and non-structural proteins (such as nsp1 to nsp12).

Polyproteins pp1a and pp1ab are cleaved by four viral proteases, resulting in the release of at least 16 distinct non-structural proteins (nsps): nsp1α, nsp1β, nsp2-6, nsp2TF^{C}, nsp2N*, nsp7α, nsp7β, nsp8, the RNA-dependent RNA polymerase (nsp9), a helicase (nsp10), an endonuclease (nsp11), and nsp12. These nsps come together

to form membrane-associated complexes that play a critical role in regulating and executing the replication and transcription of the viral genome(E. J. Snijder et al., 2013). Subgenomic RNA2 (sgRNA2) encodes ORF2a/b, giving rise to glycoprotein 2 (GP2) and a small unglycosylated envelope protein (E). ORF3, expressed from sgRNA3, produces GP3. Meanwhile, sgRNA4 encodes ORF4, resulting in GP4. These three proteins, GP2, GP3, and GP4, form a trimeric complex, known as the minor glycoprotein complex. This complex plays a crucial role in viral entry and is heavily N-glycosylated (Das et al., 2010; E. H. Wissink et al., 2005).

Subgenomic RNA5 (sgRNA5) encodes both ORF5 and ORF5a. ORF5a codes for the ORF5a protein, a small unglycosylated protein essential for virus viability, while ORF5 codes for GP5, the major glycoprotein with a variable number of N-glycan residues surrounding the cell attachment domain (C. R. Johnson, Griggs, Gnanandarajah, & Murtaugh, 2011; Mardassi, Massie, & Dea, 1996; Meulenberg et al., 1995; Robinson, Abrahante, Johnson, & Murtaugh, 2013).

ORF6, expressed from sgRNA6, leads to the production of the membrane protein (M). GP5 and M form a disulfide-linked heterodimer, constituting the major glycoprotein complex on the virion, as initially demonstrated for LDV (Faaberg, Even, Palmer, & Plagemann, 1995; Mardassi et al., 1996).

Finally, the nucleocapsid protein (N) is encoded by ORF7 and is expressed from sgRNA7. N is the primary structural component within the PRRSV virion, forming disulfide-linked homodimers. It plays a key role in packaging the viral genomic RNA (gRNA). Notably, N is the only known structural protein without a transmembrane domain or ectodomain on the PRRSV virion (Bautista, Meulenberg, Choi, & Molitor, 1996; Dea, Gagnon, Mardassi, Pirzadeh, & Rogan, 2000; Doan & Dokland, 2003; Loemba, Mounir, Mardassi, Archambault, & Dea, 1996; Spilman, Welbon, Nelson, & Dokland, 2009; E. H. Wissink et al., 2005; Wootton & Yoo, 2003).

It's worth noting that PRRSV is a genetically diverse virus, and different strains have variations in their genome sequences. This genetic diversity contributes to the challenges in developing effective vaccines and control strategies against PRRSV.

1.1.2.2 The overlapping feature of virus genome

Most proteins of Arteriviruses are encoded by overlapping genes, especially those ORFs encoding the structural proteins (Figure 1). ORF2b encoding the E-protein is completely present inside ORF2. The 3´end of ORF2 is overlapping with the 5´end of the ORF3, while the 3´ end of ORF3 is overlapping to 5´end of the ORF4 which direct results in the C-terminus of GP3 overlapping to N-terminus of GP4. An exception is ORF4 of PRRSV-2, its stop codon is ultimately preceded by the start codon of ORF5a and separated by further nucleotides from the start codon of ORF5(Firth et al., 2011; Kappes & Faaberg, 2015). In the overlapping parts of the genes, mutations in one gene also cause a mutation in the overlapping gene. If this also leads to a change in the amino acid sequence, this complicates the interpretation of functional studies with recombinant viruses and appropriate control mutations must be conducted.

1.1.2.3 The virus particle

PRRSV exhibits a characteristic particle structure, consisting of an outer lipid envelope surrounding the viral RNA and a nucleocapsid (Figure 2). The virion typically presents as a roughly spherical or ellipsoidal particle. The approximate diameter of a PRRSV virion is typically 60 nanometers (nm), with a discernible 20–30 nm diameter core (Dokland, 2010).

The envelope houses various viral glycoproteins, such as GP2, GP3, GP4, GP5, and the major envelope protein E, alongside the non-glycosylated membrane protein M (Dea et al., 2000; E. J. J. S. I. o. V. Snijder, 2002; Wu et al., 2005). It has been found that the 2b protein, expressed from a second ORF entirely contained within ORF2, is also a minor structural component of PRRSV (Wu et al., 2001; Wu et al., 2005). These proteins play crucial roles in the virus's ability to infect host cells and evade the host's immune system.

The nucleocapsid consists of the N (nucleocapsid) protein (Dea et al., 2000), which binds to the viral RNA and plays a critical role in packaging the viral genome. Notably, GP5 and M combine to form a disulfide-linked heterodimer, constituting the major structural component of the virion. Contrastingly, GP2/3/4 form a disulfide-linked heterotrimeric complex within virus particles, categorized as minor structural proteins

along with E (E. H. Wissink et al., 2005). Additionally, studies have discovered that the membrane-anchored protein, ORF5a, encoded by an alternative open reading frame of the sub-genomic mRNA that also encodes GP5, is incorporated into virus particles, albeit as a minor component (C. R. Johnson et al., 2011). Likewise, the nsp2, as a non-structural protein, has been found to be integrated into virions of various PRRSV strains(Kappes, Miller, & Faaberg, 2013).

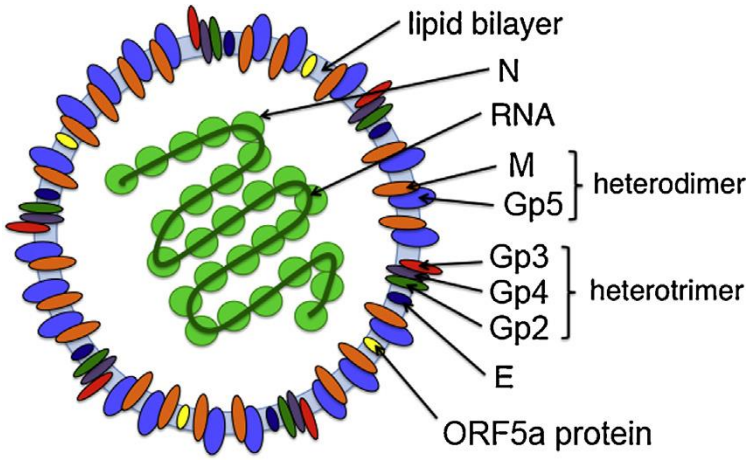

Figure 2 Scheme of an arterivirus particle

The membrane contains the major Gp5/M complex (blue and orange), the minor glycoprotein complex Gp2/3/4 (green, red, and purple, respectively), the small hydrophobic E protein (dark blue), and the ORF5a protein (yellow).(Veit, Matczuk, Sinhadri, Krause, & Thaa, 2014)

The assembly and formation of virions requires further exploration. To date, it is known that once the virus enters the host cell, the viral RNA genome is released and synthesis of the polyprotein, which generates the RNA dependent RNA polymerase (RdP), leading to the generation of complementary negative-sense RNA strands. Transcription follows, resulting in the synthesis of sgRNAs responsible for encoding various viral proteins. The host cell's machinery then translates these sgRNAs into viral proteins. Subsequently, new viral RNA and proteins assemble into virions within specific host cell compartments, such as the endoplasmic reticulum (ER) or Golgi apparatus (Veit et al., 2014). The structural proteins, including GP2, GP3, GP4, GP5, M, and E, play a vital role in forming the viral envelope (Molenkamp et al., 2000; Verheije, Welting, Jansen, Rottier, & Meulenberg, 2002; Welch et al., 2004). These assembled viral particles then bud into the ER or Golgi membranes, acquiring their envelope during this process. Finally, mature virions are released from the host cell,

primed to infect new cells.

1.1.3 The major envelope proteins GP5 and M of PRRSV.

Gp5 varies in length, encompassing approximately 200 amino acids in PRRSV and 255 in EAV. Sequence alignment indicates that the additional amino acids are likely situated in the ectodomain of Gp5. This protein consists of an N-terminal cleavable signal peptide that directs protein synthesis to the rough endoplasmic reticulum (ER), followed by an ectodomain of roughly 30 amino acids in PRRSV and 90 amino acids in EAV. Within this region, there is at least one N-glycosylation site in EAV and several in PRRSV. The segment between residues 60 and 125 in PRRSV or between 115 and 180 in EAV is hydrophobic and is thought to span the membrane three times (Balasuriya & MacLachlan, 2004; Dea et al., 2000; E. H. J. Wissink et al., 2004). However, the true membrane topology of GP5 has not yet been investigated experimentally (Dokland, 2010). The C-terminal part (128–200 in PRRSV, 181–255 in EAV) is hydrophilic and likely located in the cytosol, ultimately ending up in the virus's interior. Notably, in PRRSV, Gp5 is the most variable structural protein, with only approximately 50% amino acid homology between North American and European isolates (Kapur, Elam, Pawlovich, & Murtaugh, 1996; Murtaugh, Elam, & Kakach, 1995). The high degree of variation in GP5 is the probable cause of the absence of immunological cross-reaction between the viruses (Meng, 2000). The presence of large endodomains in major envelope proteins is a distinctive characteristic among Nidoviruses. In alphaviruses, the 33-residue endodomain of the envelope protein E2 was observed to establish specific interactions with the nucleocapsid (N) protein during virus budding (Owen & Kuhn, 1997). A comparable role could be envisaged for the endodomains of PRRSV's GP5.

The ORF5a protein, encoded by the ORF5a sgRNA, exhibits variable amino acid lengths, ranging from 43 to 51 in PRRSV and from 47 to 64 in other Arteriviruses. While the predicted molecular mass of the ORF5a protein is 5–6 kDa, it migrates in SDS-PAGE at approximately 10 kDa. This protein is anticipated to have a type III membrane topology, featuring a central hydrophobic transmembrane region that may function as a signal peptide, a short N-terminal ER-luminal ectodomain (5–12 aa) lacking

glycosylation sequons, and a longer C-terminal endodomain (14–31 aa) (Firth et al., 2011; C. R. Johnson et al., 2011). The function of ORF5a is still not fully known, to date, the ORF5a protein is essential for the replication of both type 1 and type 2 PRRSV strains. In contrast, recombinant EAV strains lacking the ORF5a protein could be generated, but their growth was significantly compromised(Firth et al., 2011; Sun et al., 2013).

The M protein is the most conserved membrane protein of Arteriviruses, and its molecular weight can vary slightly between different strains and genotypes of PRRSV. Generally, the molecular weight of the PRRSV M protein falls in the range of approximately 18 to 20 kDa. This size estimation is based on the amino acid sequence and protein structure of the M protein. It comprises a concise ectodomain spanning 15–17 amino acids, three putative transmembrane regions, each with 20 amino acids, interconnected by two short loops of approximately 6–9 amino acids, and an extensive hydrophilic cytoplasmic tail encompassing about 70–80 amino acids (de Vries, Chirnside, Horzinek, & Rottier, 1992). This protein is renowned for being the most highly conserved structural component of PRRSV. Additionally, it shares a 22% sequence identity with the corresponding protein in EAV.

The primary constituents of the PRRSV envelope are GP5 and M, accounting for at least half of the viral protein content. These two proteins form disulfide-linked heterodimers within the virus, with disulfide bonds forming between Cys 9 of M and Cys 48 of GP5 (or Cys 8 and Cys 50 in type 1 strains) (Dea et al., 2000; Mardassi et al., 1996; E. H. Wissink et al., 2005). Notably, the deletion of either of these two open reading frames (ORFs) from an infectious PRRSV clone results in the failure to produce viral particles, whereas the removal of minor envelope proteins does not impact viral production (E. H. Wissink et al., 2005). However, in the case of EAV, co-expression of GP5, M, and N was found to be insufficient for releasing virus-like particles (VLPs) into the culture medium, implying the requirement for other factors, such as non-structural proteins (NSPs) or host proteins, for particle formation and release (Wieringa et al., 2004).

The primary role of both M and GP5 is likely structural, inducing curvature in the viral membrane during the budding process. However, GP5 may also play a role in the initial interactions with the host cell and potentially in the fusion with host membranes (E. H. Wissink et al., 2005; E. H. J. Wissink et al., 2004). Heterodimerization of M with GP5 is essential for the transportation of GP5 and M from the endoplasmic reticulum (ER) to the Golgi apparatus. This process signifies that only properly assembled GP5/M complexes can successfully navigate the ER's quality control system. Consequently, only GP5/M heterodimers are integrated into virus particles, and mutation of cysteine 8 in M leads to a complete cessation of infectious virus particle release (E. J. Snijder, Dobbe, & Spaan, 2003).

Additionally, in PRRSV-1 and PRRSV-2 strains, both GP5 and M undergo palmitoylation, a modification involving cysteine residues. This palmitoylation process has been demonstrated to be crucial for virus rescue and growth. In experiments where all three cysteines in GP5 or both cysteines in M were replaced within a PRRSV-2 strain, neither infectious virus nor genome-containing particles could be successfully rescued. This emphasizes the vital role of acylation in supporting virus growth. In cases where one or two acylation sites in M or GP5 were absent, viruses could be rescued, but they displayed significantly lower titers (M. Zhang, Han, Osterrieder, & Veit, 2021).

1.1.4 The minor envelope proteins GP2, E and GP4 of PRRSV

The GP2 glycoprotein comprises 256 residues in type 2 viruses (253 in type 1). GP2 is characterized by a predicted N-terminal signal sequence spanning residues 1 to 40 (1–37 in type 1). Following the signal sequence, there is an ectodomain of approximately 168 residues, a single transmembrane (TM) helix, and a 20-residue endodomain. Notably, GP2 contains two conserved glycosylation sites, occurring at residues Asn 178 and Asn 184 in PRRSV-2 or Asn 173 and Asn 179 in PRRSV-1 viruses. (Meulenberg et al., 1995; E. H. J. Wissink et al., 2004). Several studies have examined the role of individual glycosylation sites in PRRSV replication and the antigenicity of GP2. It was reported that neither of the two sites significantly impacted

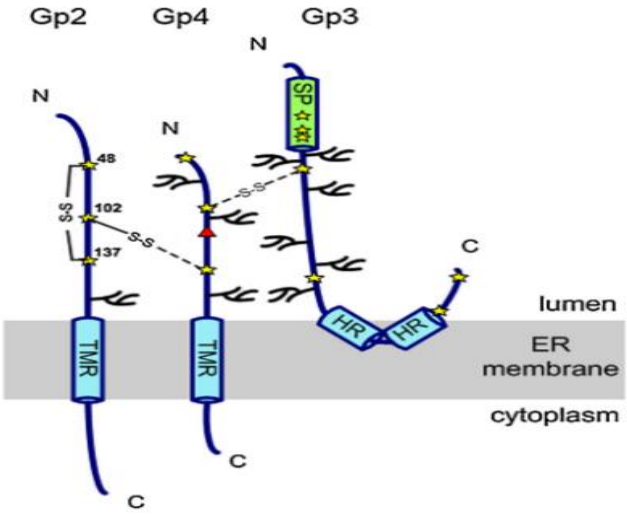

Figure 3 Scheme of the Gp2/3/4 complex of EAV

Cysteine residues within the ectodomains are indicated by stars, and glycosylation sites are represented with branches. The red triangle marks the likely unused glycosylation site NPT in Gp4. "S S" denotes a disulfide bond between cysteine 102 of Gp2 and an unidentified cysteine in Gp4. Gp2 also contains an intramolecular disulfide bond between cysteines 48 and 137. One of the seven cysteines in Gp3 forms a disulfide bond with Gp4. TMR: transmembrane regions; HR: hydrophobic region, refer to(Veit et al., 2014) .

the efficient replication of recombinant viruses. However, another study confirmed that Asn184 was critical for the recovery of the virus but not Asn 178 (Das et al., 2011).

The small E or 2b protein is expressed from ORF2b, which is entirely nested within ORF2a (Wu et al., 2001). The E protein is a non-glycosylated minor envelope protein composed of approximately 70–73 amino acid residues (Wu et al., 2001; Wu et al., 2005). Structurally, it includes an N-terminal domain of about 25 amino acids, predicted not to be a signal peptide, a hydrophobic transmembrane region spanning approximately 20 amino acids, and a hydrophilic, polybasic C-terminal domain consisting of around 25 amino acids, (E. J. Snijder, van Tol, Pedersen, Raamsman, & de Vries, 1999). The hydrophobic domain spans the membrane once. The C-terminus of the E protein faces the lumen of the ER, making it part of the surface of virus particles, while the N-terminus is oriented toward the cytosol, situated inside virus particles (Matczuk, Kunec, & Veit, 2013; Yu et al., 2010). In the case of EAV, this protein was found to be essential for EAV infectivity, but not for particle assembly of EAV (E. J. Snijder et al., 1999; Wieringa et al., 2004). E contains a single predicted transmembrane helix and is believed to form an oligomeric ion channel (Lee & Yoo,

2006). Consequently, this protein is likely involved in the viral fusion and internalization process. However, the conserved cysteine residues found in the C-terminal domain of E are not essential for replication of North American genotype PRRSV, indicating that they do not serve a functional role (Lee & Yoo, 2005).

The GP4 minor envelope protein varies in size, with 178 residues in type 2 and 183 in type 1 (Meulenberg, van Nieuwstadt, van Essen-Zandbergen, & Langeveld, 1997; van Nieuwstadt et al., 1996). GP4 features a predicted signal peptide cleavage site from residues 1 to 21 and is likely to contain a single transmembrane helix spanning residues 156–177 (161–181 for type 1). GP4 possesses four potential glycosylation sites at residues 37, 84, 120, and 130, with at least three of these sites likely to be utilized, as observed in comparison with EAV, which lacks the fourth site (Wieringa, de Vries, Raamsman, & Rottier, 2002). These glycosylation sites are consistently occupied by carbohydrates. In infected cells, these carbohydrates are typically sensitive to Endo-H, but within virus particles, they undergo processing to become Endo-H resistant (Das et al., 2011; de Vries, Raamsman, van Dijk, Horzinek, & Rottier, 1995). Several studies have examined the impact of individual glycosylation sites on PRRS replication and the antigenic properties of GP4. Mutations of individual sequons do not seem to influence virus replication. However, it was observed that double, triple, or quadruple mutants of glycosylation sites result in the inability to produce viable virus. Notably, none of the viable mutants of GP2 or GP4 displayed increased sensitivity to antibody neutralization or elicited higher titers of neutralizing antibodies following infection of piglets (Das et al., 2011; Z. Wei et al., 2012; E. H. J. Wissink et al., 2004). Therefore, it appears that a glycan shielding effect on antibody epitopes, as observed in GP5, does not occur in GP2 and GP4.

It was initially believed that GP3 of PRRSV and LDV was a non-structural protein (Faaberg & Plagemann, 1997; Gonin, Mardassi, Gagnon, Massie, & Dea, 1998) and that it was secreted from infected cells. However, recent findings have demonstrated, for both PRRSV-1 and PRRSV-2, that GP3 is indeed a structural component of virus particles and may be covalently linked to GP2/4 (de Lima et al., 2009; Meulenberg et al., 1995), as shown in figure 3 referring to EAV. The formation of disulfide bonds

between GP3 and GP2/4 is presumed to be a spontaneous process, with acceleration occurring under physiological temperature, oxidizing conditions, and slightly basic pH (Wieringa, de Vries, & Rottier, 2003). Given that the proximity of two cysteine residues is crucial for the formation of a covalent bond, it is plausible that GP3 is non-covalently associated with the GP2/4 dimer during the budding phase of virus particles (Wieringa, de Vries, & Rottier, 2003).

Initially, intramolecular disulfide bonds are formed within GP2 (and likely also in GP4), undergoing rearrangements until a properly folded product is achieved. Subsequently, both proteins associate, and the resulting dimer is stabilized by an intermolecular disulfide bond (Wieringa, De Vries, Post, & Rottier, 2003). Notably, GP3 has the capability to associate with GP2/4 in virus particles and can also interact with GP2 and GP4 in vitro (Kabatek & Veit, 2012). This interaction completes the formation of the GP2/3/4 heterotrimer and finally becomes an essential component of the PRRSV viral particle.

1.1.5 The minor envelope proteins GP3 of PRRSV

Glycoprotein 3, found in Porcine Reproductive and Respiratory Syndrome Virus (PRRSV), GP3 plays a pivotal role in the structure and function of the PRRSV virion. It comprises 265 amino acids, considerably longer than the 163 amino acids in EAV.

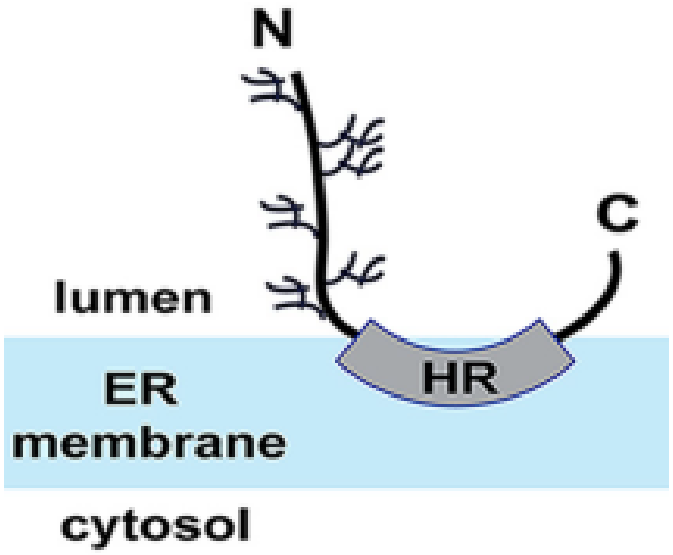

Figure 4 Membrane topology of GP3

HR (Hydrophobic Region): This region attaches Gp3 to the membrane. The branches represent the carbohydrates attached to Gp3 of VR-2332.

GP3 features an N-terminal signal peptide, an ectodomain containing seven potential N-glycosylation sites, a hydrophobic region, and a relatively hydrophilic C-terminal domain. In EAV, GP3 contains six potential N-glycosylation sites, all of which are utilized, including the overlapping sequon(Matczuk et al., 2013). In contrast, GP3 from PRRS-2 possesses seven potential N-glycosylation sites. Compared to EAV-GP3, PRRS-GP3 has just one site located adjacent to the signal peptide. It's worth noting that, except for the last site (N195), which may be shielded by an adjacent hydrophobic region, all of these sites are glycosylated (Das et al., 2011). Mass estimates obtained through SDS-PAGE have indicated that all six sites are utilized, contributing up to 16 kDa to its overall mass(Gonin et al., 1998), a finding consistent with similar observations in EAV (Wieringa et al., 2002). Glycosylation sites N42, N50, and N131 were found to be essential for infectious particle formation in the infectious clone FL12

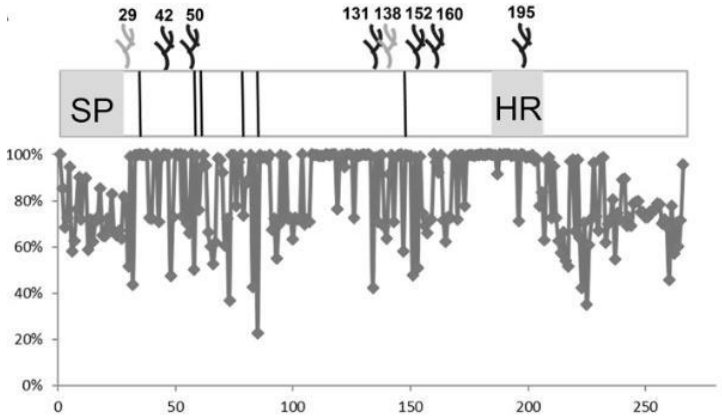

Figure 5 Primary structure of Gp3 with cleavable signal peptide

Primary structure of Gp3 with cleavable signal peptide (SP), hydrophobic region (HR), six conserved cysteines (lines), and glycosylation sites (branches; numbering of sites corresponds to PRRSV-2 strains). The graph shows the percent conservation (y-axis) of amino acids at each position (x-axis) of a consensus sequence compiled from all PRRSV-1 and PRRSV-2 GP3 sequences present in the database.

(PRRSV-2). In contrast, N29, N152, and N160 had little to no impact, and only when these sites were simultaneously exchanged did virus growth become impaired (Das et al., 2011). However, in another study, recombinant viruses could be generated with all GP3 glycosylation mutants, and only the replacement of N42 and N50 resulted in reduced growth kinetics (Z. Wei et al., 2012). Importantly, no significant effects on reactivity with antisera or the induction of neutralizing antibodies were observed for

any of the viruses with hypoglycosylated GP3 (Das et al., 2011; Z. Wei et al., 2012). On a different note, a field isolate lacking the glycosylation site N131 in GP3 triggered a stronger neutralizing antibody response (Vu et al., 2011).

A fraction of the GP3 protein is secreted into the cell medium during PRRSV-2 infections (Gonin et al., 1998; Mardassi, Gonin, Gagnon, Massie, & Dea, 1998; Wieringa et al., 2002). GP3 was also identified as a minor component in both type 1 and 2 viruses (de Lima et al., 2009; van Nieuwstadt et al., 1996; E. H. Wissink et al., 2005). In PRRSV-2, immuno-electron microscopy (immuno-EM) revealed that GP3 is exposed on the viral surface (de Lima et al., 2009).

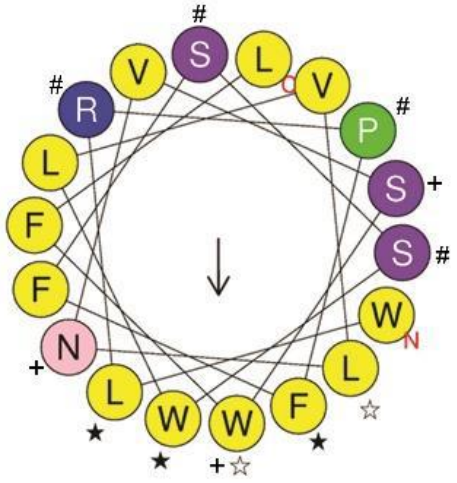

Figure 6 Helical wheel plot of the hydrophobic region

Yellow: Hydrophobic amino acids. Substitution of two and three amino acids with alanine, indicated by white and black asterisks respectively, significantly enhances the secretion of Gp3 and prevents the generation of infectious virus particles. Replacement of the amino acids marked with + and # with hydrophobic ones inhibits the secretion of Gp3. The effect of these substitutions on virus replication was not tested.

Recent studies from my host laboratory identified that Gp3 exhibits an unusual hairpin-like membrane topology: both the N- and C-terminus are oriented towards the lumen of the endoplasmic reticulum (ER), membrane anchoring might occur via an amphipathic helix (Figure 4). Thus, Gp3 from PRRSV and EAV exhibit a similar membrane topology, but only the latter has an un-cleaved signal peptide(Matczuk et al., 2013; M. Zhang, Krabben, Wang, & Veit, 2018; M. Zhang & Veit, 2018). Bioinformatics suggests that the hydrophobic region might form an amphipathic helix

that is highly conserved in all Gp3 proteins (Figure 5). Replacement of three or four hydrophilic by hydrophobic amino acids of the presumed helix prevents secretion of Gp3. Likewise, exchange of only two or three hydrophobic amino acids in the hydrophobic face of the helix by alanine increases secretion of Gp3 by several orders of magnitude (Figure 6). Exchanging the same amino acids in the context of the viral genome did not prevent release of virus particles, but the particles are not infectious confirming a role of Gp2/3/4 for virus entry. It was also observed that a fraction of wild-type Gp3 is secreted, both from transfected and from virus-infected cells, as described before(Mardassi et al., 1998). Interestingly, Gp3 from the PRRSV-1 strains tested is secreted to a greater extent than Gp3 from PRRSV-2 strains. This secretion behavior is reversed after exchange of the between Gp3 proteins highly variable C-terminal domain. The C-terminus of Gp3 from the PRRSV-1 strain is longer, but much more hydrophilic. The rather weak membrane anchoring by an amphiphilic helix (in comparison to a transmembrane region) might explain why a fraction of the protein is secreted. We assume that membrane-bound and soluble Gp3 exist in equilibrium. Wild-type Gp3 is mostly membrane bound in the ER, but some Gp3 molecules detach from the membrane and escape from this organelle by vesicular transport. The hydrophobicity of amino acids anchor determines the strength of membrane binding, which is also influenced by the biophysical properties of the C-terminus (M. Zhang et al., 2018).

1.1.6 Antiviral drug against PRRSV

Due to the variation of PRRSV, current vaccines provide limited protection, and it is thus necessary to identify antiviral drugs. Recently, many effective new strategies were reported, such as adenoviruses mediated short-hairpin RNAs (shRNAs) directed against ORF1b (G. Li et al., 2009), and the siRNAs targeting nonstructural protein (NSP)1a(Shi et al., 2015), NSP9(Xie et al., 2014), and N genes (M. Yang et al., 2014). In addition, Carbon Monoxide (A. Zhang et al., 2017), Glycyrrhiza polysaccharides(Y. Yang et al., 2023), Pyrithione (Guo, Zhu, Wang, Chen, & Liu, 2017) and the antimalaria drug Artesunate (Long et al., 2022) were reported to efficiently inhibit replication of PRRSV by different action mechanisms.

Recently, it was reported that some drugs efficiency inhibited replication of coronavirus by different mechanisms. Such as the RNA-dependent RNA polymerase (RdRp) inhibitors remdesivir and its metabolite active compound GS-441524, Other drugs are the Ribonucleoside analogue molnupiravir (EIDD-2801), Guanosine analogue ribavirin and the protease inhibitor GC376. Since they are commercially available, it is worth to test their effect on PRRSV replication.

Remdesivir functions as a prodrug designed to facilitate the intracellular delivery of GS-441524 monophosphate, which is subsequently transformed into GS-441524 triphosphate, which acts as a ribonucleotide analogue inhibitor targeting viral RNA polymerase. The active metabolite of remdesivir disrupts the activity of viral RNA-dependent RNA polymerase and eludes proofreading by viral exoribonuclease (ExoN), leading to a reduction in viral RNA production (Ferner & Aronson, 2020; Scavone et al., 2020). In certain viruses like the respiratory syncytial virus, it induces RNA-dependent RNA polymerases to pause momentarily, but its primary effect, as seen in Ebola, is to trigger irreversible chain termination. Unlike many other chain terminators, this process doesn't inhibit the addition of the immediately subsequent nucleotide; instead, it's delayed, occurring after the addition of five more bases to the growing RNA chain (Tchesnokov, Feng, Porter, & Götte, 2019). For RNA-Dependent RNA Polymerases of MERS-CoV, SARS-CoV-1, and SARS-CoV-2, synthesis arrest happens after the incorporation of three additional nucleotides (Gordon, Tchesnokov, Feng, Porter, & Götte, 2020; Gordon, Tchesnokov, Woolner, et al., 2020). Consequently, remdesivir is categorized as a direct-acting antiviral agent that operates as a delayed chain terminator (Eastman et al., 2020; Gordon, Tchesnokov, Woolner, et al., 2020).

GS-441524, a potent RdRp inhibitor and the active metabolite of remdesivir, is a 1'-CN-substituted adenine C-nucleoside ribose analogue that demonstrates broad-spectrum activity against various viruses in vitro, including SARS-CoV ([EC50] = 0.18 mM), Middle East respiratory syndrome coronavirus (EC50 = 0.86 mM), feline infectious peritonitis virus (EC50 = 0.78 mM), and SARS-CoV-2 (EC50 = 0.48 mM) (Agostini et al., 2018; Cho et al., 2012; Murphy et al., 2018; D. Wei et al., 2021).

EIDD-2801 inhibits viral reproduction by inducing widespread mutations in viral RNA replication through RNA-directed RNA polymerase (Painter et al.). It is metabolized into a ribonucleoside analog that resembles cytidine, β-D-N4-hydroxycytidine 5′-triphosphate (also known as EIDD-1931 5′-triphosphate or NHC-TP) (Amara et al., 2021; Painter et al., 2021). EIDD-2801 can exist in two forms (tautomers), one mimicking cytidine (C) and the other uridine (U) (Malone & Campbell, 2021). NHC-TP is not recognized as an error by the virus's proofreading exonuclease enzymes, which typically replaces mutated nucleotides with corrected versions. When the viral RNA polymerase attempts to replicate RNA containing EIDD-2801, it may interpret it as either C or U. This results in more mutations in all subsequent copies than the virus can survive, a phenomenon known as viral error catastrophe or lethal mutagenesis (Malone & Campbell, 2021). Initially considered as a potential treatment for influenza viruses and encephalitic alphaviruses such as Venezuelan, Eastern, and Western equine encephalitic viruses due to its significant inhibitory effect in cell cultures (Agostini et al., 2019; Crotty, Cameron, & Andino, 2001), EIDD-2801 has more recently been tested against SARS-CoV-2, exhibiting effective inhibition of virus replication (Rosenke et al., 2021; Wahl et al., 2021).

Ribavirin, a broad-spectrum antiviral drug synthesized in 1972, has been utilized in the treatment of hepatitis C virus (HCV) infections in humans. Additionally, it exhibits antiviral effects against various other viruses (Ramírez-Olivencia, Estébanez, Membrillo, & Ybarra, 2019). The ribavirin molecule is renowned for its diverse antiviral mechanisms, which vary depending on the targeted virus (Graci & Cameron, 2006). In one such mechanism, ribavirin monophosphate demonstrates potent inhibition of guanosine derivatives, including guanosine triphosphate (GTP), thereby reducing nucleotide residues and manifesting an antiviral effect. This effect has been particularly evident in studies involving respiratory syncytial virus (RSV), yellow fever virus, and paramyxovirus (Garcia, Sharma, Johnson, Salgado, & Wille, 2019; Leyssen, De Clercq, & Neyts, 2006; Schleuning, Buxbaum-Conradi, Jäger, & Kolb, 2004; Shah & Chemaly, 2011). Additionally, ribavirin's primary intracellular metabolite, ribavirin triphosphate (RTP), exerts its action through polymerase inhibition. RTP competitively binds with

molecules such as adenosine triphosphate (ATP) or GTP, thereby inducing polymerase inhibition. This mode of action has been observed in studies involving influenza virus, reovirus, and vesicular stomatitis virus (Beigel et al., 2017; Lin et al., 2018; Ramírez-Olivencia et al., 2019). Finally, as a third mechanism, the ribavirin molecule can bind to translation initiation factor 4E (eIF4E), thereby impeding translation initiation or interacting with enzymes responsible for RNA cap synthesis, consequently preventing translation initiation. This mechanism has been elucidated through in silico molecular docking analysis for viruses such as SARS-CoV-2 and Lassa fever (Elfiky, 2020).

GC376 blocks the main protease (M^{pro}), which is common to many single-stranded RNA viruses, thereby hindering the viral polyprotein from maturing into its functional components. Chemically, GC376 is the bisulfite adduct of an aldehyde known as GC373, and it acts as a prodrug for this compound. This aldehyde forms a covalent bond with the cysteine-144 residue at the active site of the protease, resulting in a monothioacetal formation and impeding the enzyme's typical function (Vuong et al., 2020; Ye et al., 2020). GC376 serves as a broad-spectrum antiviral drug that targets the M^{pro} of various viruses, including coronaviruses such as the feline coronavirus (Fu et al., 2020; Pedersen et al., 2018), porcine epidemic diarrhea virus (Ye et al., 2020), Middle East respiratory syndrome coronavirus (Rathnayake et al., 2020), as well as ferret and mink coronaviruses (Perera et al., 2018). As of 2020, GC376 is under investigation as a treatment for SARS-CoV-2 (Fu et al., 2020; Ma et al., 2020). This could be attributed to the highly conserved structure of M^{pro} among these viruses (Perera et al., 2018; Vuong et al., 2020).

1.2 Aims of this study

1.2.1 The first research objective: investigating whether the C-terminus of GP3 is important for virus replication

There are variations in the C-terminus, the C-terminus of GP3 from PRRSV-2 is shorter but more hydrophobic, whereas the C-terminus of GP3 from the PRRSV-1 strain is longer but more hydrophilic(M. Zhang et al., 2018).Exchanging the variable C-terminus

of GP3 from the PRRSV-2 strain XH-GD with the C-terminus of GP3 from the PRRSV-1 strain Lelystad results in a chimeric protein that shows significantly enhanced secretion in transfected cells (Zhang et al., 2018). Based on this work, I will analyze whether the C-terminus of GP3 is indeed crucial for virus replication.

1.2.2 The second research objective: investigating whether the amphiphilic helix of GP3 is essential for virus replication

It has been demonstrated that mutations in the hydrophobic region significantly increased the fraction of secreted GP3 and prevented the generation of infectious virus particles. Only non-infectious particles are released from transfected cells (Zhang et al., 2018). To explain the essential nature of the hydrophobic region, one might speculate that only membrane-bound GP3 can form a complex with GP2 and GP4. Thus, if the percentage of membrane-anchored GP3 decreases, the number of functional GP2/3/4 spikes incorporated into virus particles is too low to catalyze cell entry of viruses. Alternatively, but not exclusively, the exact amino acid sequence (not just the biophysical properties) of the hydrophobic region of GP3 might be essential for virus replication. This sequence is highly conserved across all PRRSV strains, even though amphiphilic helices that can interact with membranes can be formed by very different amino acid sequences.

In this part, I will investigate whether the amphiphilic helix of GP3 is essential for virus replication and requires a specific amino acid sequence.

1.2.3 Screening whether known antiviral drugs inhibit porcine reproductive and respiratory syndrome virus replication

In 2006, a highly pathogenic PRRSV outbreak occurred suddenly in China. The disease resulted in the death of millions of pigs and devastated many swine farms in China (L. Zhou & Yang, 2010; Y. J. Zhou et al., 2008), leading to a dramatic rise in pork prices.

In this study, I will screen five inhibitors known to inhibit coronavirus infections, including protease inhibitors, RNA-dependent RNA polymerase inhibitors, and analog inhibitors. These inhibitors are broadly used to treat coronavirus infections, respiratory syncytial virus infections, hepatitis C, and some hemorrhagic fevers. I will test these

inhibitors on both PRRSV-1 and PRRSV-2 to identify their functions on PRRSV replication and further explore the action mechanism of these drugs.

2 Materials and methods

2.1 Materials

2.1.1 Buffers and solutions

In this study, PBS (phosphate-buffered saline) was prepared using 0.8% (w/v) NaCl, 0.02% (w/v) KCl, 0.02% (w/v) KH2PO4, 0.135% (w/v) Na2HPO4 · 2H2O, and 0.1% Tween-20 was added to PBS to make PBST. TNE buffer was made with 50 mM Tris–HCl pH 7.4, 100 mM NaCl, and 0.1 mM EDTA. The cell culture medium DMEM was composed of 10% (v/v) FCS, penicillin/streptomycin (100 units/mL), while the infection medium DMEM contained 0.1% (v/v) FCS and penicillin/streptomycin (100 units/mL). The fixation solution consisted of 4% PFA (paraformaldehyde) in PBS. The stacking gel (5% (w/v) acrylamide/bisacrylamide) was prepared with 0.1% (w/v) SDS, 125 mM Tris·HCl (pH 6.8), 0.075% (w/v) APS, and 0.15% (v/v) TEMED. The separating gel (12% (w/v) acrylamide/bisacrylamide) included 0.1% (w/v) SDS, 375 mM Tris·HCl (pH 8.8), 0.05% (w/v) APS, and 0.1% (v/v) TEMED. The 1x non-reducing loading buffer comprised 62.5 mM Tris·HCl, 2% (w/v) SDS, 10% (v/v) glycerol, 0.01% (w/v) bromophenol blue, pH 6.8. Additionally, 1x reducing loading buffer was prepared by adding 5% (v/v) β-Mercaptoethanol to the 1x non-reducing buffer. The blocking buffer for Western blotting was 5% skimmed milk powder in PBST, while the blocking buffer for immunofluorescence was 3% BSA in PBST

2.1.2 Consumables

T25, T75, and T175 cell culture flasks with filter caps, 6-, 12-, 24-, and 96-well cell culture plates, 5 mL, 10 mL, and 25 mL pipettes, and 15 mL and 50 mL Falcon tubes were sourced from Sarstedt. PVDF (polyvinylidene difluoride) membranes, microscope slides, and cover slips were obtained from VWR.

2.1.3 Kits and reagents

Phusion DNA Polymerase, dNTP Mix (10 mM each), Turbofect Transfection Reagent, and Lipofectamine® 3000 Transfection Reagent were sourced from Thermo Scientific. Enzymes such as XhoI, BglII, and buffers, as well as T4 DNA ligase, were obtained from NEB. DMEM (Dulbecco’s Modification of Eagle’s Medium), FCS (Fetal Calf

Serum), BSA (Bovine Serum Albumin), Opti-MEM, and EDTA-trypsin were procured from PAN. The GF-1 AmbiClean Kit (PCR & Gel) was supplied by Vivantis. The Invisorb Spin Plasmid Mini Kit was acquired from Stratec Biomedical AG. cOmplete™, EDTA-free Protease Inhibitor Cocktail, and Penicillin/Streptomycin were purchased from Carl Roth. ECLplus reagent was sourced from Pierce/Thermo, and TPCK-trypsin was obtained from Sigma-Aldrich.

2.1.4 Cell and viruses

Cell lines CHO-K1 (Chinese hamster ovary cells; ATCC CCL-61), HEK 293T (human embryonic kidney cells; ATCC CRL-3216), and MARC-145 (simian kidney epithelial cells derived from MA-104; ATCC CRL-6489) were stored in our host laboratory. The PRRSV type 2 XH-GD (Chinese highly pathogenic PRRSV-2 strain, accession number EU624117.1) and PRRSV type 1 Lelystad virus (low-pathogenicity PRRSV-1 prototype strain, GenBank accession number M96262.2) were also stored in our host laboratory.

2.1.5 Apparatuses

In this study, the cell culture incubator is sourced from Heraeus, while the Semidry membrane blotting machine and Fusion SL camera system are provided by Peqlab. The Centrifuge 5417R and Thermo cycler are products of Eppendorf, and the Ultracentrifuge and SW 32Ti Rotor are obtained from Backman company. The Power Pack P25 is supplied by Biometra, and the NanoDrop 1000 Spectrophotometer is acquired from Thermo Scientific. Additionally, the Inverted microscope and Axio Vert A1 fluorescence microscope are procured from MOtic AE30 and Zeiss, respectively.

2.1.6 Plasmid vectors and primers

pCMV-TNT vector, pCAGGS vector, pEGFP vector were stored in our host laboratory, and all primers used in this study are show in following table 1:

Table 1 Primers used in this study

Primer name	Sequences
GD-Gp3-Δ203-F	CTCAGGCGTTAGCCTGCAAGCCATGTTTCAGTTCGAGTCTTTCGGA
GD-Gp3-Δ203-R	CATGGCTTGCAGGCTAACGCCTGAGAAACCACGAAACATTTAAAACC
GD-Gp3-Δ209-F	GCCATGTTTGAGTTCGAGTCTTTCGGACATCAAAACCAACACCACCGC
GD-Gp3-Δ209-R	CGAAAGACTCGAACTCAAACATGGCTTGCAGGCGAACGCCTGAGAAACC
GD-Gp3-Δ227-F	CAGGCTTCGTAGTCCTCCAGGACATCAGCTGCCTTAGGCATGGCGAC
GD-Gp3-Δ227-R	GATGTCCTGGAGGACTACGAAGCCTGATGCTGCGGTGGTGTTGGTTTTGA
GD-Gp3-Δhelix -F	GGTTTCACCTGTGATGGCTGCGCCCTTTCTTTTCCTCTTGGTTGGTTTTAAATG
GD-Gp3-Δhelix-R	GGCGCAGCCATCACAGGTGAAACCAATTGCCGCCGTCGACCTGGTGTTG
P11839 of XH-GD-F	CTGGAAATGGTGAGGACTGGGAGGATTACAATG
P17605 of CMV-R	GTTATGTAACGCGGAACTCCATATATGGGCTATG

GD-Gp3-mut helix-F	GGCTGTCCCCTTTATTTTCCAGGTGGTTGGTTTTCAATGTTTCGTGGTTTCTCAGGCG T
GD-GP3-mut helix-R	CATTGAAAACCAACCACCTGGAAAATAAAGGGGACAGCCATTCCAGGTGAAACCAAT TG
GD-Gp4-4F7L-F	GCCATGTCTCAGTTCGAGTCTTTCGGACATCAAAACCAACACCACCGC
GD-Gp4-4F7L-R	CGAAAGACTCGAACTGAGACATGGCTTGCAGGCGAACGCCTGAGAAACC
GD-Gp3-2A-F	tggttggttgcaaatgtctctgcgtttctcaggcgttcgc
GD-Gp3-2A-R	cctgagaaacgcagagacatttgcaaccaaccacgaggaa
GD-GP3 3H-F	taagtgttttgttgtttctcaggcgttcgcctgcaagccatgtttca
GD-GP3 3H-R	ttgcaggcgaacgcctgagaaacaacaaaacacttaaaaccaaccaa
GD-GP3 4H-F	atggctgctccttttctttttctttggttggttttaaatgtttcgttgt
GD-GP3 4H-R	accaaaagaaaaagaaaaggagcagccattccaggtgaaaccaattg
pEGFP-helix mut-F (Xho I)	ccgCTCGAGgaTGGCTGTCCCCTTTATT
pEGFP-helix mut- R (BamH I)	cgcGGATCCGAGAAACCACGAAACA
pCAGGS-Gp4(XhoI)-F	ccCTCGAGggATGGCTGCGCCCTTTCTTT
pCAGGS-Gp4-2A(XhoI)-F	ccCTCGAGggATGGCTGCGCCCTTTCTTTTCCTCTtggttggttgcaaatgtCtctgcgtttctcag
pCAGGS-Gp4-helix mut (XhoI)-F	ccCTCGAGggATGGCTGTCCCCTTTATTT
pCAGGS-Gp4(Bgl II)-Myc-R	gaAGATCTtcTCACAGATCCTCTTCAGAGATGAGTTTCTGCTCcaccggAATTGCCAGTAG GATGGCAAA

2.1.7 Antibodies

The Anti-GP5 primary antibody was stored by our host laboratory. The mouse anti-Myc-tag (9B11) monoclonal antibody was purchased from Cell Signal company, while the mouse anti-GFP monoclonal IgG2a (B-2) was obtained from Santa Cruz company. Additionally, the goat anti-mouse IgG-HRP was purchased from Sigma-Aldrich.

2.2 Methods

2.2.1 Cell culture

Cultures of 293T cells (human embryonic kidney cells; ATCC CRL-3216), MARC-145 cells (simian kidney epithelial cells derived from MA-104; ATCC CRL-6489), and CHO-K1 cells (Chinese hamster ovary cells; ATCC CCL-61) were maintained in Dulbecco's modified Eagle's medium (DMEM; PAN, Aidenbach, Germany) supplemented with 10% fetal calf serum (FCS) (Perbio, Bonn, Germany), 100 U/ml penicillin, and 100 mg/ml streptomycin. These cultures were incubated at 37°C with 5% CO2 and 95% humidity.

2.2.2 Reverse genetics and mutagenesis

To generate three full-length mutants (ΔC203, ΔC209, and ΔC227) with deletions in the C-terminus of GP3, I targeted three specific amino acid positions (203, 209, and 227) for the insertion of a "stop codon," thus mutating the relevant nucleotides. For the mutant with a deletion in the hydrophobic region of GP3 (ΔHelix), I introduced a "stop codon" at the start codon position of the GP4 nucleotide sequence by mutating only one nucleotide. In the case of the helix mutant, I exchanged position 185 with position

190 and position 187 with position 194 within the predicted amphiphilic helix of GP3. The nucleotide sequences of GP3 from XH-GD (Chinese highly pathogenic PRRSV-2 strain, accession number EU624117.1) were utilized to design mutagenesis primers, and the XH-GD reverse genetic full-length clone served as a template for site-directed mutagenesis via overlap extension PCR amplification, employing Asc I and Not I restriction enzyme sites in accordance with standard molecular biology techniques.

To generate mutant variants of XH-GD GP3 featuring hydrophilic or hydrophobic amino acid substitutions within the predicted amphipathic helix, I employed site-directed mutagenesis via overlap extension PCR. Specifically, I created four mutants with multiple substitutions (GP3-3H [N195S S197L W198L], GP3-4H [R185L P186L S189F S190F], GP3-7H [R185L P186L S189F S190F N195S S197L W198L]), as well as single-substitution mutants (GP3-2A [L194A W198A], all targeted to the predicted amphipathic helix. The same strategy as described above was employed to construct these mutants.

To create expression plasmids of GP4-myc, GP4-2A-myc and GP4-mutant-myc, the nucleotide sequences of XH-GD, GP3-2A and mutant helix full-length clones were utilized for PCR using forward primers encoding XhoI restriction enzyme sites and reverse primers equipped with Bgl II restriction enzyme sites and a myc tag (amino acids: EQKLISEEDL), along with a small linker (PV). The resulting PCR products were then cloned into the corresponding sites in the pCAGGS vector.

To fuse the hydrophobic regions from GP3 of XH-GD and the hydrophobic regions with amino acids exchanged from GP3 of mutant helix full-length to the C-terminus of GFP, nucleotides encoding amino acids 183 to 200 (hydrophobic region only) were amplified by PCR (using primers with XhoI or BamHI sites) and subsequently cloned into the corresponding sites in pEGFP-C1 (Clontech, Saint-Germain-en-Laye, France). The resulting constructs were named GFP-HR and GFP-mut-HR, respectively.

2.2.3 Virus rescue and reproductive

293T cells, cultured in 6-well plates until reaching 70-90% confluence, were transfected with 2.5 μg of infectious full-length plasmid DNA per well using Lipofectamine 3000 (Thermo Fisher Scientific, Carlsbad, CA) following the

manufacturer's protocol. After 72 hours post-transfection, the supernatant was collected from thawed and centrifuged cells at 5000 rpm. Subsequently, Marc-145 cells were infected with the virus obtained from the transfected 293T cells, as described previously. Following 72 hours of infection, the supernatant was harvested by centrifugation of thawed Marc-145 cells at 5000 rpm/min for 5 minutes, in preparation for subsequent passages.

2.2.4 Viral genome extraction

To ensure the stability of the rescued viruses, they were harvested from repeatedly frozen and thawed samples, then centrifuged at a speed of 5000 rpm/min for 5 minutes. Subsequently, 200μL of virus per sample was used to extract the viral genome for RT-PCR to cDNA, followed by sequencing. For each sample, 200μL of lysis solution CBV, 10μL of carrier RNA, and 10μL of proteinase K were employed to release viral RNA. The mixture was incubated at 70℃ for 10 minutes. Next, 400μL of isopropanol was added to the lysed sample, and the resulting mixture was applied to the Spin Filter and centrifuged at 11,000g for 1 minute. After washing with 650μL of washing solution and 80% ethanol, the viral RNA was eluted by adding 30μL of pre-heated RNase-free water and centrifuging at 11,000g for 1 minute.

2.2.5 RT-PCR and sequencing

RNA was extracted using the PureLink Viral RNA/DNA Minikit (Invitrogen, Carlsbad, CA) following the provided protocol. Subsequently, the viral RNA underwent reverse transcription into cDNA employing the High-Capacity cDNA Reverse Transcription Kit (Applied Biosystems, Carlsbad, CA) according to standard procedures (refer to Table 2 and Table 3). The resulting cDNA was obtained post-agarose gel electrophoresis and subsequently sent for sequencing to LGC Genomics (Berlin, Germany).

Table 2 RT-PCR reaction system

Reagents	Volume(μL)
10×RT Buffer	2.0
25×dNTP Mix (100mM)	0.8
10×RT Random Primers	2.0
Multiscribe Reverse Transcriptase	1.0
RNase Inhibitor	1.0
Nuclease free water	3.2

Totally per reaction	10

Table 3 RT-PCR reaction program

Steps	Step1	Step2	Step3	Step4
Temperature (℃)	25	37	85	4
Time (minutes)	10	120	5	∞

2.2.6 Determining virus titer ($TCID_{50}$) and growth kinetics

To determine the virus titer, Marc-145 cells were prepared in a 96-well plate for 24 hours. Subsequently, 100μL of virus from the prepared stock was used to perform a 10-fold serial dilution ranging from 10^-1 to 10^-12. The cells were washed once with PBS, and the diluted viruses were added to the respective wells of the 96-well plate. The plate was then placed in an incubator at 37°C with 5% CO2 and 95% humidity. Following a one-hour infection period, the culture supernatant was discarded, and the wells were washed twice with PBS buffer. Next, 300μL of fresh culture medium supplemented with 2% FCS, 100 U/ml penicillin, and 100 mg/ml streptomycin was added to each well. After four days, the wells exhibiting cytopathic effects (CPE) at different dilutions were counted, and the virus titer (TCID50) was calculated using either the Karber or Reed-Muench method.

For the determination of virus growth kinetics, Marc-145 cells were cultured in 24-well plates for 24 hours and subsequently infected with the relevant viruses at a multiplicity of infection (MOI) of 0.001. Following a one-hour infection period, the culture supernatant was discarded, and the wells were washed twice with PBS buffer. Subsequently, 300μL of fresh culture medium supplemented with 2% FCS, 100 U/ml penicillin, and 100 mg/ml streptomycin was added to each well. The culture supernatants were collected at specific time points (12, 24, 48, 72, and 96 hours) and subjected to a 10-fold dilution for TCID50 testing. The TCID50 titer was calculated using the Reed and Muench method, and two-way ANOVA was used for the analysis of differences. All experiments were independently performed two or three times, and the results are presented as means with standard deviations.

2.2.7 Indirect immunofluorescence assay

MARC-145 cells were cultured in 6-well plates and infected with supernatant from 293T cells transfected with infectious full-length virus. After 48 hours of growth, cells were fixed with 4% paraformaldehyde in PBS for 20 minutes at 4°C, followed by two washes with PBS. Subsequently, the cells were permeabilized with 0.2% Triton in PBS for 10 minutes at room temperature and again washed twice with PBS. Blocking was performed using a solution containing 3% bovine serum albumin (BSA) in PBST for 30 minutes at room temperature, followed by incubation with a mouse monoclonal anti-GP5 antibody (reactive against PRRSV-2 strains) diluted in blocking solution (1:100) at room temperature for 1 hour. After three washes with PBS, cells were incubated with a secondary antibody (Alexa Fluor 568 goat anti-mouse IgG(H&L); Invitrogen, Darmstadt, Germany) at a dilution of 1:1,000. Images were acquired using a Zeiss Axio Vert A1 inverse epifluorescence microscope.

2.2.8 Prediction of Signal Peptide Cleavage Sites in Gp4 of virus

To predict the signal peptide cleavage site of Gp4, I utilized SignalP 5.0, a deep neural network-based approach (Almagro Armenteros et al., 2019). SignalP, supplied with the full-length protein sequence, provided information on whether the N-terminus of Gp4 acted as a signal peptide and the position at which it was cleaved. The resulting summary sheets listed the UniProt ID for each queried Gp4 protein, the prediction of whether the N-terminus is a eukaryotic signal peptide, the prediction of the cleavage site, the five amino acids surrounding the site, and the probabilities for each prediction ranging between 0 and 1. Mean and standard deviation of the probabilities, along with the highest and lowest probabilities for each cleavage site, were calculated. Additionally, for each predicted sequence, a graphical representation was provided, indicating the probability that each of the approximately 70 N-terminal amino acids were or were not part of a eukaryotic signal peptide, and whether it functioned as a cleavage site. This method enables the identification of additional putative cleavage sites with lower probabilities than the main cleavage site.

2.2.9 Prediction of biophysical property of amphiphilic helix and its mutants

I utilized the Heliquest tool (https://heliquest.ipmc.cnrs.fr/, accessed on 1 April 2023) to compute the physicochemical properties of the amphiphilic helix of GP3, comprising 18 amino acid residues. The tool assesses two parameters: the hydrophobic moment (<μH>) and the average hydrophobicity (<H>) of a helix. The hydrophobic moment quantifies amphipathicity by calculating the mean vector sum of the hydrophobicities of the side chains if this region adopts an α-helix conformation, while hydrophobicity denotes the affinity of the helix for lipids (Eisenberg, Weiss, & Terwilliger, 1982). The software generates a helical wheel diagram with an arrow inside, indicating the hydrophobic side of the helix, with its length corresponding to the hydrophobic moment(Gautier, Douguet, Antonny, & Drin, 2008).

2.2.10 Signal peptide cleavage assay

To analyze if the signal peptide cleavage of GP4 is affected by the exchange of amino acids in the amphiphilic helix of GP3 in the mutant helix full-length, Marc-145 cells were grown in 6-well plates for 24 hours and then subjected to transfection with 2.5μg of GP4-myc and GP4-mutant-myc plasmids, respectively, using Lipofectamine 3000 (Thermo Fisher Scientific, Carlsbad, CA) according to the protocol. After transfection for 48 hours, the cells were washed twice with pre-cold PBS and lysed for 1 hour with 10% NP-40 lysis buffer. The cell lysate supernatant was collected by centrifugation at a speed of 16,000g/min for 10 minutes, and the samples were then digested with peptide-N-glycosidase (PNGase F; 2.5 to 5 U/ l, 1 h at 37°C) according to the manufacturer's instructions (New England BioLabs, Frankfurt am Main, Germany). The deglycosylated or untreated samples were supplemented with reducing SDS-PAGE loading buffer and subjected to SDS-PAGE and Western blotting.

2.2.11 Confocal microscopy

To detect the distribution of green fluorescence signals from GFP and GFP chimeras, CHO cells were seeded at 50% confluency one day prior to transfection onto glass coverslips in 24-well cell culture plates. The cells were transfected with 0.6 μg of GFP and GFP chimera plasmid DNA per well using Lipofectamine 3000 (Thermo Fisher Scientific, Carlsbad, CA) following the protocol. After 24 hours, the cells were fixed with 4% paraformaldehyde (PFA) for 20 minutes at room temperature, followed by two

washes with PBS. Subsequently, they were permeabilized with 0.1% Triton X-100 in PBS for 10 minutes and again washed twice with PBS. Fluorescence signals were visualized using the VisiScope confocal FRAP System (VisiTron Systems GmbH), equipped with an iXon Ultra 888 EMCCD camera and a 100X objective. The acquired images were processed using Fiji software.

2.2.12 Membrane separation assay

Transfection of CHO cells with 2.5 µg of plasmids per well in a 6-well plate was conducted. After transfection for 24 hours, cellular supernatants were discarded, and the cells were then washed twice with ice-cold PBS. Subsequently, the cells were treated with digitonin (30 µM) for 25 minutes on ice to allow for permeabilization. Cell debris was subsequently removed by centrifugation at a speed of 700g for 3 minutes using an Eppendorf centrifuge. The microsomes (ER and Golgi membrane) were then recovered from the supernatant by high-speed centrifugation (100,000g, 1 hour, 4°C, 60 min; Beckman TL100 centrifuge, rotor TLA100.3). The resulting precipitation was washed twice with absolute ethanol. The supernatant of this centrifugation contained cytosolic proteins, which were precipitated with 20% TCA. Finally, the proteins from both the precipitation and supernatant were dissolved using protein loading buffer for Western blotting analysis.

2.2.13 SDS-PAGE and western bolting

Following SDS-PAGE using a 12% polyacrylamide gel, the gels were transferred onto polyvinylidene difluoride (PVDF) membranes (GE Healthcare, Freiburg im Breisgau, Germany). Subsequently, the membranes were blocked with a 5% skim milk powder solution in PBS with 0.1% Tween 20 (PBST) for 1 hour at room temperature before being incubated overnight at 4°C with antibodies in the blocking solution. The mouse anti-Myc tag antibody (9B11; Cell Signaling, Leiden, The Netherlands) and the mouse anti-GFP antibody (B-2, Santa Cruz, Heidelberg, Germany) were utilized to detect GP4 with Myc tag and the hydrophobic region with GFP, respectively. After washing the membranes three times for 10 minutes each with PBST, a suitable horseradish peroxidase-coupled secondary antibody (1:5,000; anti-mouse; Sigma-Aldrich, Taufkirchen, Germany) was applied for 1 hour at room temperature. Finally, the signals

were detected by chemiluminescence using the ECL Plus reagent (Pierce/Thermo, Bonn, Germany) and a Fusion SL camera system (Peqlab, Erlangen, Germany).

2.2.14 Cytotoxicity assay

The stock solutions of the 3CLpro inhibitor GC376 (BPS Bioscience), the ribonucleoside analog molnupiravir (EIDD-2801; MedChem Express), the ribonucleotide analogue inhibitor of viral RNA polymerase remdesivir, and its active molecular form GS-441524 (MedChem Express), as well as the guanosine analog ribavirin, were prepared in 100% dimethyl sulfoxide (DMSO). The cytotoxicity of these inhibitors to Marc-145 cells was determined using the colorimetric assay Cell Counting Kit 8 (Merck). The number of viable cells was determined by measuring the absorbance at 450 nm with a microplate reader (BMG Labtech).

2.2.15 Antiviral assay

The inhibitory effects of antivirals GC376, EIDD-2801, remdesivir, GS-441524, and ribavirin on the replication of type-1 and type-2 PRRSV were determined through flow cytometry and virus titer analysis. Marc-145 cells were cultured in a 24-well plate with medium containing 10% FBS and 1% penicillin & streptomycin for 24 hours. After removing the medium, the cells underwent a single wash with PBS buffer. The viruses were used to infect the cells at an MOI of 0.1, and the plate was gently shaken every 15 minutes to ensure complete virus adsorption. Following 1.5 hours of infection, the medium was discarded, and the cells were again washed with PBS buffer. Subsequently, medium with 2% FBS and the inhibitor at various concentrations was added. The plate was then placed in a 37℃ and 5% CO2 incubator for 24 hours. Supernatant containing released viruses from intracellular spaces was collected, and the virus titer was determined by TCID50. Cells were harvested by digestion with trypsin and resuspended in PBS after a single wash with PBS buffer. Fluorescent cells were quantified by flow cytometry using the CytoFlex flow cytometer from Beckman Coulter. The IC50 value was defined as the concentration resulting in a 50% reduction of fluorescent cells in infected cells compared to the wild type. IC50 values were determined through nonlinear regression analysis using the dose-response (variable slope) equation with GraphPad Prism 8.0 software (Dotmatics).

2.2.16 FACS

To determine the inhibitor's effect on PRRSV replication, Marc-145 cells were infected with viruses. After the addition of inhibitors at different concentrations for 24 hours, the supernatant was harvested for virus titer determination. Cells were then washed once with PBS and harvested in 1.5mL centrifuge tubes after trypsin digestion. The cells were centrifuged at a speed of 1200rpm/min for 5 minutes, and the supernatant was discarded. The cells were resuspended in PBS, and fluorescent cells were quantitated using flow cytometry with the CytoFlex flow cytometer from Beckman Coulter. The inhibition rate of the inhibitor on virus replication was calculated using the formula (Sample-NC) ×(100/(PC-NC)), where NC and PC represent negative and positive controls, respectively.

2.2.17 Alphafold2 predicts structure of RNA polymerase of PRRSV

To compare the differences between the RNA-dependent RNA polymerase (RdRp) of PRRSV and SARS-CoV-2, I employed the AlphaFold2 online software to predict the crystal structure of RdRp (Nsp9) of PRRSV. I utilized ColabFold: AlphaFold2 using MMseqs2notebook(https://colab.research.google.com/github/sokrypton/ColabFold/blob/main/AlphaFold2.ipynb#scrollTo=kOblAo-xetgx), accessed on December 10, 2023, with the following settings: msa_method = mmseqs2, homooligomer = 1:1, pair_mode = unpaired_Paired, num_relax = 1, template_mode = none, mas_mode = mmseqs2_uniref_env, model_type = auto, num_recycles = 3, recycle_early_stop_tolerance = auto, relax_max_iterations = 200, pairing_strategy = greedy, max_msa = 512:1024, num_seeds = 1, dpi = 200, rank_num = 1, color = IDDT, num_samples = 1, num_ensemble = 1, max_recycles = 3, tol = 0, is_training = False, and use_templates = False.

2.2.18 Data statistics and analysis

In this study, EditSeq and ApE software were employed for sequence alignment. GraphPad Prism software was used for data analysis, while Adobe Illustrator was utilized for arranging figures. PyMol software was employed to align the crystal structures of RdRp of PRRSV and SARS-CoV-2.

3 Results

3.1 Testing the function of the amphiphilic helix of GP3 and its C-terminus for replication of porcine reproductive and respiratory syndrome virus

3.1.1 Deletion of the C-terminus of Gp3

3.1.1.1 Removal of C-terminus of GP3 affects virus growth

To investigate the effect of the C-terminus of GP3 on virus replication, three mutants with a deletion of parts of the C-terminus of GP3 (Δ203, Δ209, and Δ227) were

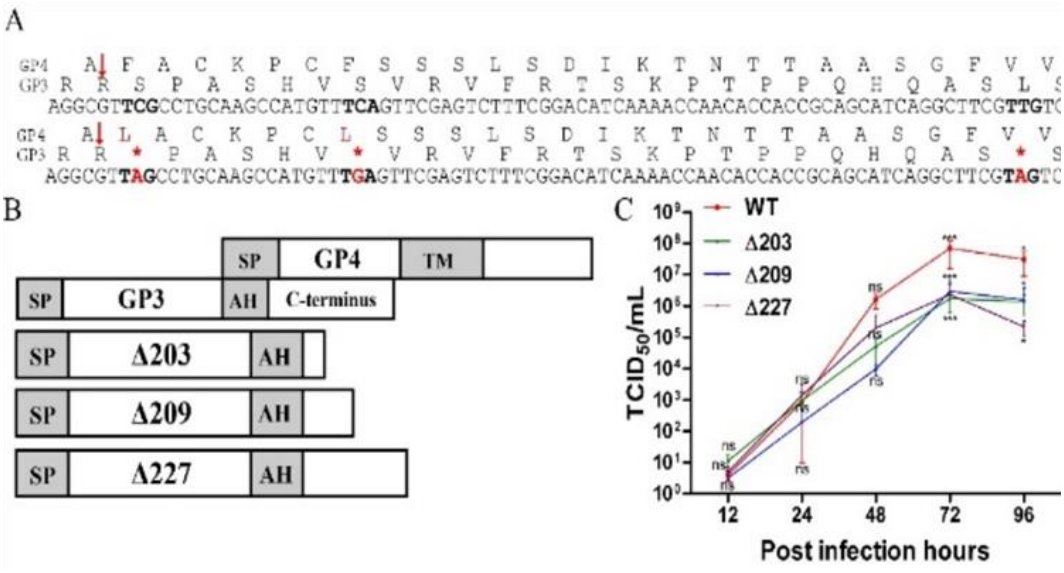

Figure 7 Removal of C-terminus of GP3 reduces virus titers

(A)The schematic representation for constructing infectious full-length PRRSV clones involves introducing stop codons at specific positions in GP3 to create three different deletions at the C-terminus: ΔC203 (at position 203), ΔC209 (at position 209), and ΔC227 (at position 227). The first row shows the amino acids of GP4, the second row shows the amino acids of GP3 at the C-terminus, and the third row shows the nucleotides shared by GP3 and GP4. The nucleotides in bold in the third row indicate the sites where stop codons were introduced (marked with red asterisks in the fifth row) to delete the C-terminus. The amino acids of GP4 that were changed due to the introduction of the stop codon in GP3 are marked in red in the fourth row, and the corresponding changed nucleotides are marked in bold red in the sixth row. The red downward-pointing arrows indicate the sites of signal peptide cleavage in GP4. (B) A sketch of the overlapping genes of GP3 and GP4 shows that the C-terminus of GP3 overlaps with the N-terminus of GP4. SP stands for signal peptide, AH for amphiphilic helix, and TM for the transmembrane region.(C) The growth kinetics of ΔC203, ΔC209, and ΔC227 were compared to the wild-type virus. Marc-145 cells were grown in 24-well plates for 24 hours and then infected with the relevant viruses at a multiplicity of infection (MOI) of 0.001. Culture supernatants were harvested at specific time points, and the titer was determined using the TCID50 assay. The experiments were performed in triplicate, and the results are presented as means with standard deviations. Differences between the three mutants and the wild type were analyzed by two-way ANOVA, with significance levels indicated as follows: "**" ($P < 0.001$), "*" ($P < 0.05$), and "ns" (non-significant).

constructed. Three amino acids (Figure 7A) were selected for insertion of stop codons (TAG or TGA) by changing a single nucleotide. The mutants were named Δ203, Δ209, and Δ227 respectively, indicating the deletion of a part of the C-terminus of GP3 at this specific position (Figure 7B). Due to the overlap of the N-terminus of GP4 with the C-terminus of GP3, altering the nucleotides to introduce stop codons resulted in changes to the amino acids of GP4 in two of the mutants (Figure 7A) and a possible effect has to be investigated.

For the Δ203 variant, inserting a stop codon at position 203 of GP3 resulted in the mutation of the first amino acid in mature GP4 (from Phe to Leu). In Δ209, the insertion of the stop codon caused a mutation in one amino acid further downstream in the ectodomain of GP4 (from Phe to Leu). Whether this amino acid change affects the function of GP4 remains to be investigated in subsequent research. In Δ227, the amino acid of GP4 was not affected when the stop codon was inserted at the 227th amino acid position of GP3. Although one nucleotide of GP3 was altered, resulting in one nucleotide mutation in GP4, the mutated codon codes for the same amino acid as the original codon, thus not affecting the amino acid of GP4.

Using a reverse genetics system as described in the methods section I could rescue recombinant infectious virus particles with the described mutations. To further investigate the influence of the C-terminus of GP3 on virus replication, I compared the growth kinetics (TCID50/mL) of the three mutants. Marc-145 cells were infected with the three mutant viruses at a multiplicity of infection (MOI) of 0.001, the medium was harvested at different time points, and then the virus titers were tested by TCID50 assay. If the C-terminus of GP3 is important for virus replication, viruses with a deletion in the C-terminus would show slower growth compared to the wild type. However, if the C-terminus does not affect virus replication, viruses with a deletion in the C-terminus would display no significant differences in virus titer. No significant differences were observed from 12 to 48 hours; however, the virus titer of the three mutants significantly decreased at 72 and 96 hours, indicating that the mutated viruses grew to lower titers than the wild type after 72 hours (Figure 7C).

3.1.1.2 Virus re-gains the C-terminus of GP3 after passage in cell culture

To further explore the influence of the C-terminus of GP3 on the virus, I conducted tests to determine whether the three mutants remained stable. Our hypothesis was

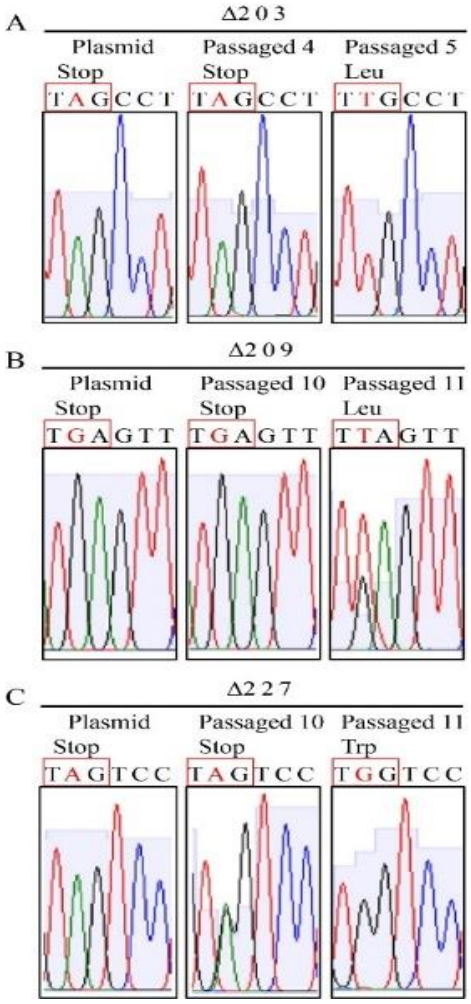

Figure 8 Virus re-gains the C-terminus of GP3 after passage in cell culture
(A, B, and C) Sequencing chromatograms of cDNA from Δ203, Δ209, and Δ227. The virus was passaged in Marc-145 cells, and viruses were collected from the different supernatants. The viral RNA was isolated, subjected to RT-PCR, and then sequenced. The nucleotide sequences of both the wild type (WT) and mutants are listed above the chromatograms, with nucleotides in red indicating the mutation sites identified in this experiment.

that if the C-terminus is not crucial for virus growth, the viral genome would remain stable during passage in cell culture. I passaged the three mutant viruses in Marc-145 cells, and viral RNA was extracted for use as a template for cDNA production and subsequently the cDNA encompassing GP3 was sequenced.

For the Δ203 virus, the GP3 genes from passages 3 to 10 were sequenced. The results revealed that the stop codon at the 203rd amino acid position of GP3 is still present at

passage four, but it disappeared completely by the 5th passage (Figure 8A). The amino acid changed from serine to leucine. Additionally, the corresponding amino acid of GP4 reverted back to its original phenylalanine residue (Table 4).

Regarding the Δ209 virus, sequencing of GP3 genes from passage 10 to 15 showed that the stop codon is still present at passage 10. However, this stop codon changed to leucine, which is distinct from the original serine. Notably, sequencing chromatograms at passage 11 displayed two peaks, indicating the presence of mixed viruses, which persisted until passage 11 (Figure 8B). The amino acid of GP4 at this site returned to its original phenylalanine state (Table 4).

As for the Δ227 virus, sequencing of genes from passages 10 to 13 revealed that the inserted stop codon is still present at passage 10 (Figure 8C). However, by passage 11, the stop codon was completely replaced by tryptophan, which is different from the leucine present in the wild type virus. Notably, the amino acid of GP4 at this position remained valine throughout the process (Table 4).

Table 4 Amino acids change of mutants

	Wild type	**mutation**	**Passaged 5**
Nucleotides	TCGCCT TTCGCC	TAGCCT TTAGCC	TTGCCT TTTGCC
Δ203	Ser	Stop	Leu
GP4	Phe	Leu	Phe
	Wild type	**mutation**	**Passaged 11**
Nucleotides	TCAGTT TTCAGT	TGAGTT TTGAGT	TTAGTT TTTAGT
Δ209	Ser	Stop	Leu
GP4	Phe	Leu	Phe
	Wild type	**mutation**	**Passaged 11**
Nucleotides	TTGTCC GTTGTC	TAGTCC GTAGTC	TGGTCC GTGGTC
Δ227	Leu	Stop	Trp
GP4	Val	Val	Val

Table 4 shows the amino acid changes observed in the mutants. Red nucleotides from the GP3 sequence indicate substitutions that lead to the insertion of a stop codon, along with their subsequent alterations after passages in cell culture. Blue nucleotides from the GP4 sequence indicate changes resulting from the insertion of a stop codon in the GP3 sequence, followed by their modifications after passages in cell culture.

3.1.1.3 Investigating the corresponding amino acid exchanges in GP4

The insertion of the stop codons at position 203 and 209 in Gp3 also changed the corresponding amino acid in Gp4. For Δ203, the insertion of the stop codon in GP3 led to a conservative exchange of the first amino acid of mature GP4 (from Phe to Leu).

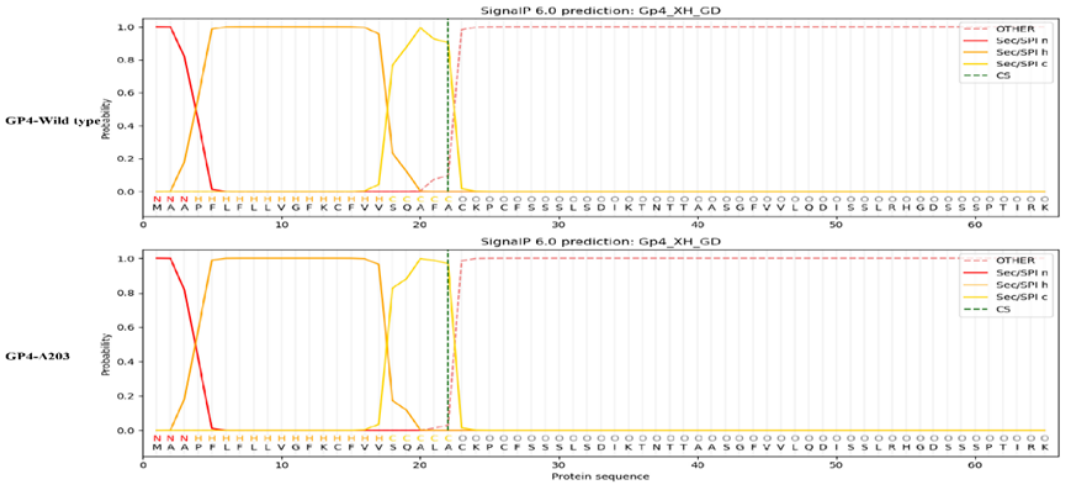

Figure 9 Prediction of signal peptides cleavage site of GP4 wild type and GP4-Δ203 by Signal IP 6.0 online software

The Y-axis represents the probability that a region in GP4 functions as signal peptide, while the X-axis denotes the positions of amino acids along the sequence. The green dotted line indicates the signal peptide cleavage site within the amino acid sequence. Additionally, the yellow and red lines depict the probability of a signal peptide for each amino acid. The labels 'N', 'H', and 'C' denote regions within the signal peptides, while 'O' signifies other regions.

I predicted the signal peptide cleavage site for both wild-type GP4 and GP4-Δ203 (where the stop codon was inserted at position 203 of GP3), both results show that those amino acids before green dotted line (cleavage site) were identified as signal peptide (The labels 'N', 'H', and 'C' denote regions with signal peptides), and those amino acids after dotted line were identified as other (The 'O' signifies other regions). Revealing that the cleavage sites were identical, with both located between positions 22 and 23, with a probability of 96.99 percent (Figure 9). This suggests that this change does not affect signal peptide cleavage and probably does not impact the function of GP4 since only the first amino acid was altered by a conservative exchange.

Introducing a stop codon into Δ209 changed the amino acid at position 7 of mature GP4 from the original phenylalanine to leucine, but the changed leucine reverted back to phenylalanine after passages in cell culture, suggesting that phenylalanine may be important for the virus. Therefore, I constructed the GP4F7L mutant which exchanged the amino acid at position 7 in the mature protein from phenylalanine to leucine, without altering the amino acid sequence of GP3.

After constructing the full-length GP4F7L clone, I transfected it into 293T cells for virus rescue and passaged the virus in Marc-145 cells. The growth kinetics of GP4F7L were determined, and the results showed that the titers of the GP4F7L mutant is lower at each time point, but a statistical analysis revealed no significant difference compared

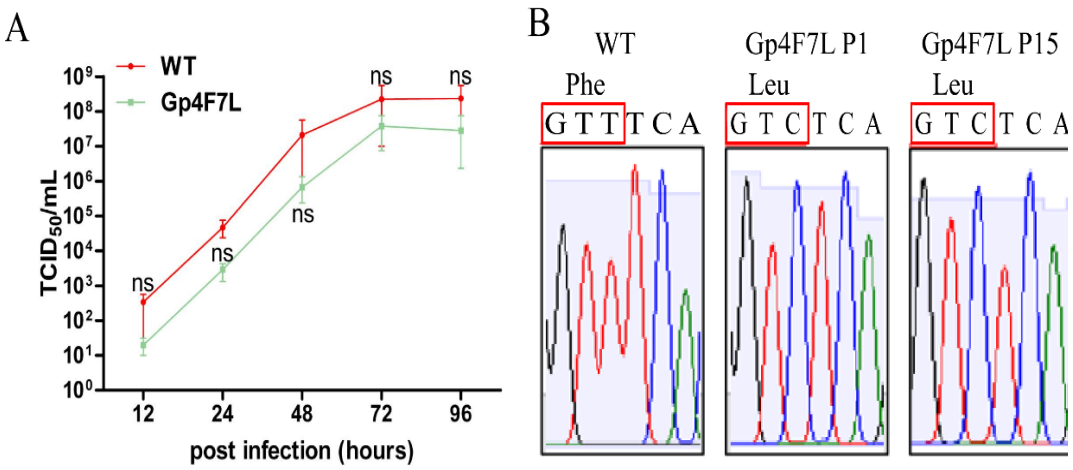

Figure 10 Amino acid change of GP4 does not affect virus growth

(A) The growth kinetics of GP4F7L were compared to those of the wild-type virus. Marc-145 cells were cultured in 24-well plates for 24 hours and then infected with the virus at a multiplicity of infection (MOI) of 0.001. Culture supernatants were harvested at specific time points, and virus titers were determined using a TCID50 assay. The experiments were performed in triplicate, with results presented as means with standard deviations (SD). Differences between the mutant and wild-type viruses were analyzed using a two-way ANOVA. "ns" indicates non-significant differences. (B) Sequencing chromatograms demonstrate that GP4F7L remained stable through at least 15 passages. The virus was passaged in Marc-145 cells, with samples collected from various passages following repeated cell freezing. Viral RNA was isolated and subjected to RT-PCR and sequencing. Nucleotide sequences and amino acid residues of both the wild-type and GP4F7L viruses are shown above the chromatogram. Mutated nucleotides are highlighted with a red rectangle. "P" denotes passage number.

to the wild type (Figure 10A).

The mutant virus was passaged in cell culture up to passage 15, and viral RNA from passages 1 and 15 was extracted and reverse-transcribed to cDNA for sequencing. Sequencing chromatograms showed that GP4F7L remained stable up to at least passage 15 (Figure 10B). This suggests that the GP4F7L mutation has a small, but statistically not significant effect on virus growth, but it is probably less important than the insertion of the stop codon at position 203 of Gp3 since the substitution of phenylalanine with leucine is stable.

3.1.2 Mutations in the amphiphilic helix of Gp3

3.1.2.1 Replacement of amino acids in the hydrophobic face of the amphiphilic helix by alanine prevent virus rescue.

To investigate the importance of the amphiphilic helix in Gp3 for virus growth, one full-length mutant was constructed. Alanine was used to replace two amino acids (Leu, Trp) on the hydrophobic face of the helix, resulting in the construction of the mutant

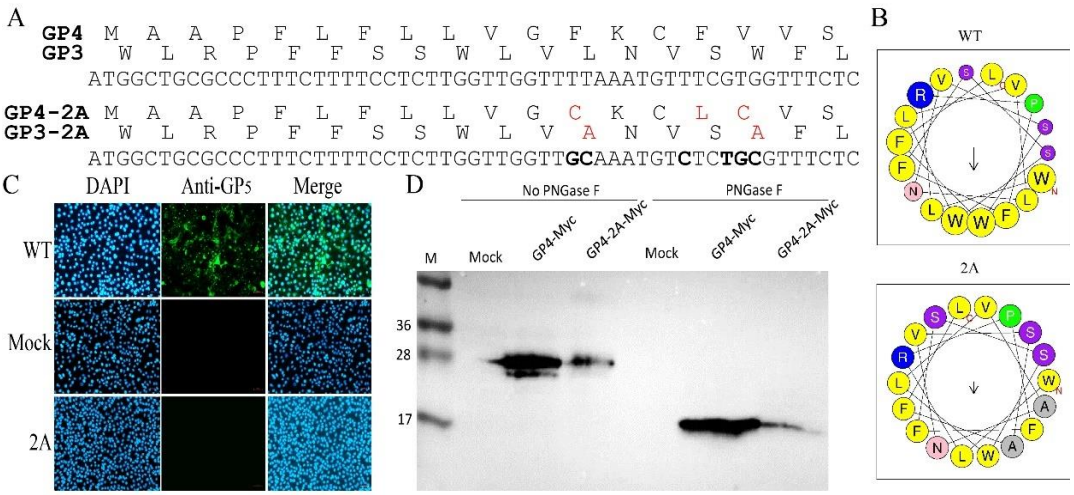

Figure 11 Replacement of amino acids in the hydrophobic face by alanine in amphiphilic helix affect virus replication

(A) The scheme for constructing an infectious full-length PRRSV clone involved creating a mutant (GP3-2A), in which two hydrophobic amino acids were replaced with alanine in the predicted amphiphilic helix. The replaced amino acids in GP3-2A and the altered amino acids in GP4-2A are marked in red, with the changed nucleotides marked in bold. (B) The biophysical properties of the amphiphilic helix of the wildtype and 2A mutant were predicted using a helical wheel plot. The bioinformatics tool HeliQuest (http://heliquest.ipmc.cnrs.fr/) predicts that the hydrophobic region of GP3 forms an amphiphilic helix with a mean hydrophobicity (<H>) of 1.131 and a hydrophobic moment (<μH>) of 0.302. Hydrophobic amino acids are shown in yellow. Replacing two amino acids in the amphiphilic helix with alanine results in a mean hydrophobicity (<H>) of 0.946 and a hydrophobic moment (<μH>) of 0.155. (C) To confirm the rescue of the viruses, 293T cells were transfected with the full-length wildtype (WT) and relevant mutants. After 48 hours, the cell culture supernatant was collected and used to infect Marc-145 cells. Indirect immunofluorescence was performed using an anti-GP5 antibody, and images were captured using an epifluorescence microscope. Mock refers to untransfected cells. (D) Replacement of amino acids does not affect the cleavage of GP4's signal peptide. Expression of GP4-myc and GP4-2A-myc, with or without PNGase F digestion, was assessed. CHO cells grown in a 6-well plate for 24 hours were transfected with GP4 and GP4-2A-myc (amino acids in the signal peptide domain of GP4 were affected by the exchange of amino acid positions in the amphiphilic helix of GP3). Cell lysates were either digested or not digested with PNGase F prior to Western blotting with anti-myc antibodies. M indicates the mobilities of molecular weight markers.

GP3-2A (Figure 11A). I utilized the bioinformatics tool HeliQuest (http://heliquest.ipmc.cnrs.fr/) to predict the biophysical properties of the amphiphilic helix of the wildtype and GP3-2A mutant helix, and displayed them using a helical wheel plot (Figure 11B). It shows that the wild type helix has a mean hydrophobicity, <H>, of 1.131, and a hydrophobic moment, <μH>, of 0.302, whereas the mutant helix displays a lower mean hydrophobicity, <H>, of 0.946, and also a lower hydrophobic moment, <μH>, of 0.155.

The full-length clones were transfected into 293T cells for infectious virus rescue. The cells and supernatant were harvested to infect Marc-145 cells. At 24 hours post-infection, an indirect immunofluorescence assay was performed on the Marc-145 cells using PRRSV GP5 antibody to confirm the success of virus rescue. Immunofluorescence showed cells infected by wild-type virus but not by the GP3-2A mutant suggesting that this virus could not be rescued (Figure 11C).

This failure could potentially be attributed to the fact that the N-terminus of GP4 overlaps with the C-terminus of GP3, resulting in the replacement of amino acids within the signal peptide of GP4. It is plausible to suspect that these amino acid substitutions in GP4 hindered the cleavage of its signal peptide, thus leading to the failure of virus rescue. To test this hypothesis, I predicted the signal peptide cleavage site of GP4. The results show that the cleavage site is located between positions 20 and 21 with a probability of 95.82% (Figure 12). It has shifted upstream by one site compared to the wild-type GP4, where the cleavage site is between positions 22 and 23. However, this alteration still does not affect the cleavage of the signal peptide of GP4-2A (in which amino acids of GP4 have been changed by replacing amino acids in the amphiphilic helix of GP3, referred to as GP4-2A).

Next. I constructed wild-type GP4 and GP4-2A expression plasmids fused with a myc-tag. GP4-2A contained the same amino acid substitutions as GP4 in the full-length GP3-2A construct. These constructs were then transfected into Marc-145 cells, and cell lysates were collected after 48 hours. As both a signal peptide and a carbohydrate chain have similar molecular weights (~3 kDa), any observed reduction in molecular mobility could be due to either the cleavage of the signal peptide, loss of the

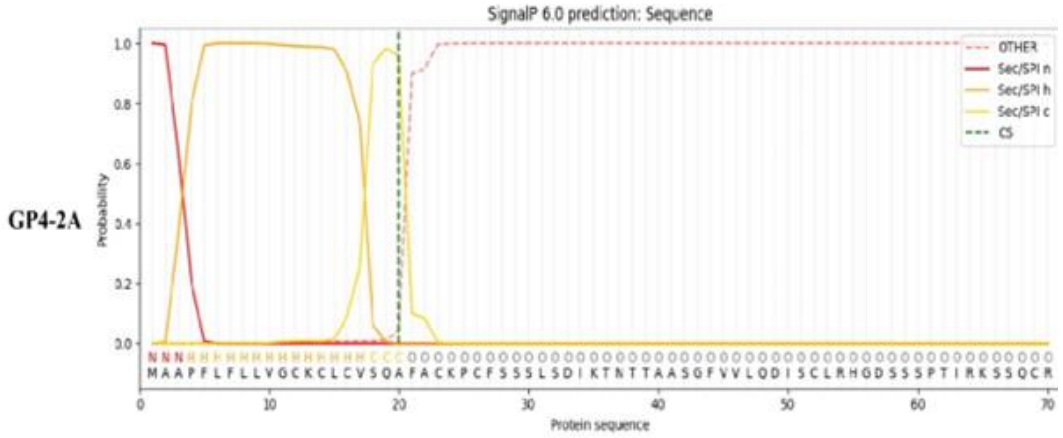

Figure 12 Prediction of signal peptides cleavage site of GP4-2A by Signal IP 6.0 online software
The X-axis represents the probability of a signal peptide, while the Y-axis represents amino acids. The green dotted line indicates the predicted signal peptide cleavage site within the amino acid sequence. Additionally, the yellow and red lines illustrate the probability of a signal peptide for each amino acid. The labels 'N', 'H', and 'C' denote regions containing signal peptides, whereas 'O' signifies other regions.

carbohydrate, or a combination of both. To distinguish between these possibilities, all carbohydrates were removed by digestion with PNGase F prior to SDS-PAGE and western blotting. PNGase F is known for effectively removing all N-linked oligosaccharides from glycoproteins. It was used to digest both GP4 and GP4-2A proteins. Generally, the cleavage of the signal peptide of GP4 would result in a lower molecular weight for the naked protein after PNGase F digestion compared to the undigested protein. If the naked protein of GP4-2A exhibited a higher molecular weight than wild-type GP4 under PNGase F digestion, it would indicate that the signal peptide of GP4-2A was not cleaved. Conversely, if both proteins showed the same molecular weight without PNGase F digestion, it would indicate signal peptide cleavage. The presence of two bands of GP4 and GP4-2A with the same molecular weight under PNGase F digestion suggests that the signal peptide had already been cleaved (Figure 11D), implying that the inability to rescue the virus is not solely due to amino acid substitutions in the signal peptide of GP4. Note, however, that the expression level of the GP4-2A mutant is lower, which might contribute to the failure in virus rescue. Since amino acid substitutions in the helix led to a reduction in hydrophobicity and changes in the amino acid sequence, the inability to rescue the virus could be attributed to either or both of these factors. This will be further explored in the following sections.

3.1.2.2 Exchange of hydrophilic by hydrophobic amino acids in the amphiphilic helix affect virus replication

In the next mutants I substituted amino acids in the hydrophilic face of the helix with more hydrophobic ones. Three (Asn, Ser, Trp), four (Arg, Pro, Ser, Ser), or all seven hydrophilic amino acids, respectively were replaced by leucine, phenylalanine and/or serine to produce the GP3-3H, GP3-4H, and GP3-7H mutants (Figure 13A). These exchanges were chosen since none of these exchanges altered the amino acid sequence of Gp4. Analysis using the bioinformatics tool HeliQuest

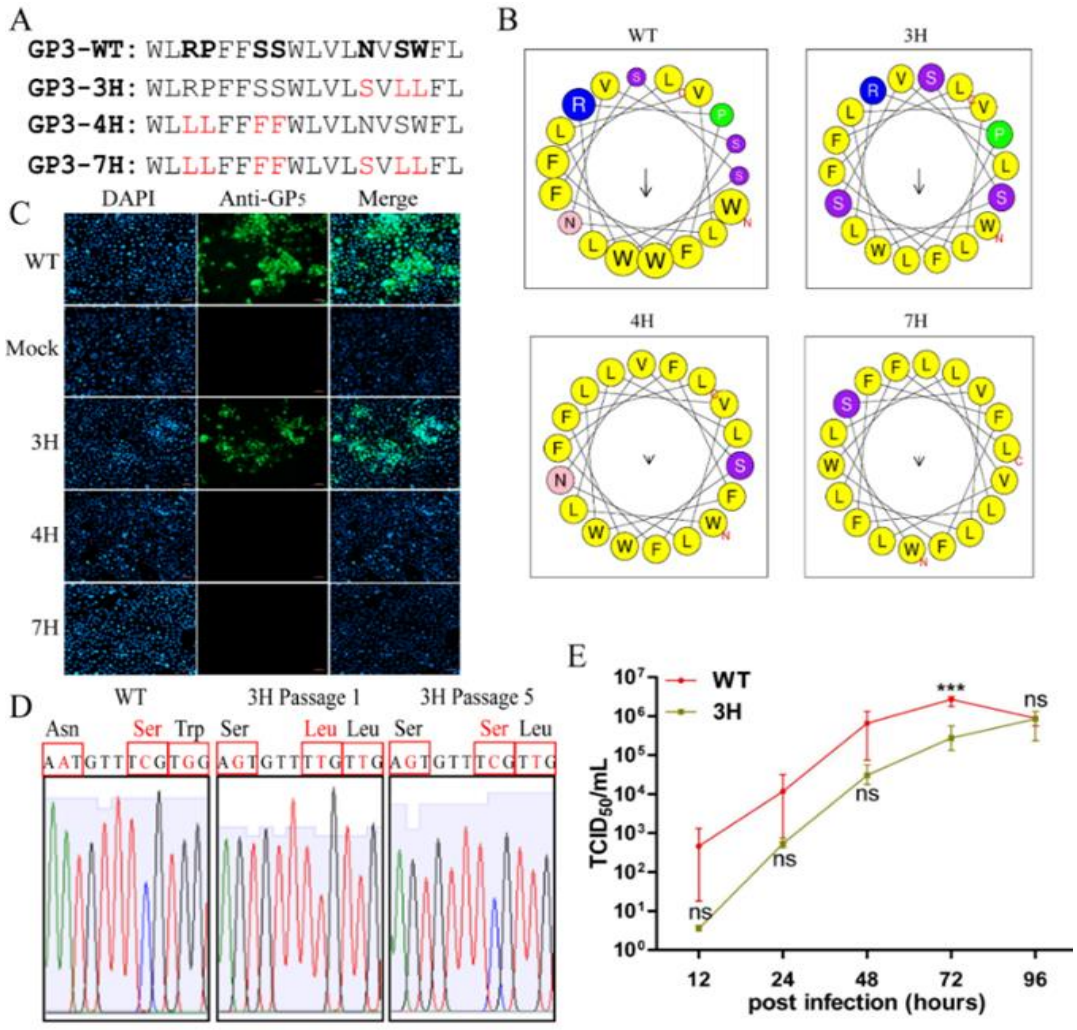

Figure 13 Exchange of hydrophilic amino acids by the more hydrophobic amino acids affect virus replication

(A) Amino Acids of Mutants in this Experiment: To create these mutants (3H, 4H, 7H: indicating that 3, 4, or 7 hydrophilic amino acids were exchanged), hydrophobic amino acids were replaced by alanine in the predicted amphiphilic helix. The amino acids in red indicate the relevant replacement positions, and the changed nucleotides are marked in bold. (B) Prediction of Biophysical Properties of Amphiphilic Helix in Wildtype and Mutants: Using the bioinformatics tool HeliQuest (http://heliquest.ipmc.cnrs.fr/), the

hydrophobic region of GP3 is predicted to form an amphiphilic helix with a mean hydrophobicity (<H>) of 1.131 and a hydrophobic moment (<μH>) of 0.302. Hydrophobic amino acids are highlighted in yellow. Replacing three amino acids in the amphiphilic helix with hydrophobic amino acids (3H) results in a mean hydrophobicity (<H>) of 1.228 and a hydrophobic moment (<μH>) of 0.271. Replacing four amino acids (4H) results in a mean hydrophobicity (<H>) of 1.539 and a hydrophobic moment (<μH>) of 0.076. Replacing seven amino acids (7H) results in a mean hydrophobicity (<H>) of 1.636 and a hydrophobic moment (<μH>) of 0.098. (C) Confirmation of Virus Rescue: 293T cells were transfected with the full-length wildtype (WT) and relevant mutants. After 48 hours, the cell culture supernatant was collected and used to infect Marc-145 cells. Indirect immunofluorescence was performed with an anti-GP5 antibody, and images were captured using an epifluorescence microscope. "Mock" refers to untransfected cells. (D) Sequencing Chromatograms: Sequencing chromatograms showed that one amino acid of 3H reverted to wildtype after passage 5 in cell culture. The virus was passaged in Marc-145 cells, and the virus was collected from different passages after repeated freezing of cells. The viral RNA was isolated, subjected to RT-PCR, and sequenced. The nucleotide sequences and amino acids are listed above the chromatogram, indicating the mutation sites in this experiment. (E) Growth Kinetics of 3H: Marc-145 cells were grown in 24-well plates for 24 hours and then infected with the virus at an MOI of 0.001. Culture supernatants were harvested at specific time intervals, and virus titers were tested using the TCID50 assay. The experiments were performed in triplicate, and the results are presented as means with standard deviations. The difference between the mutant and wild type was analyzed by two-way ANOVA. Asterisks indicate statistically significant differences (***, $P < 0.001$), and "ns" indicates non-significant differences

(http://heliquest.ipmc.cnrs.fr/) predicted that all mutants form helices with a higher hydrophobicity, but lower hydrophobic moment after amino acid substitutions. Specifically, replacing three amino acids in an amphiphilic helix with hydrophobic amino acids (3H) resulted in a mean hydrophobicity, <H>, of 1.228 and a hydrophobic moment, <μH>, of 0.271. Replacing four amino acids (4H) led to a mean hydrophobicity of 1.539 and a hydrophobic moment of 0.076, while replacing seven amino acids (7H) resulted in a mean hydrophobicity of 1.636 and a hydrophobic moment of 0.098 (Figure 13B).

The full-length constructs were transfected into 293T cells for infectious virus rescue, the results of the indirect immunofluorescence assay performed on infected Marc-145 cells revealed that only GP3-3H could be rescued (Figure 13C), while GP3-4H and GP3-7H could not. GP3-3H was passaged in Marc-145 cells, and viruses from different passages were sequenced. Analysis of the sequencing chromatograms of GP3-3H showed that one of the amino acids (Leu) reverted back to the wild type (Ser) after the fifth passage in cell culture (Figure 13D), while the other two remained unchanged. Growth kinetics analysis of GP3-3H demonstrated a significant decrease in virus titer

compared to the wild type (Figure 13E), indicating that increased hydrophobicity could impede virus growth.

3.1.2.3 The amphiphilic helix of Gp3 cannot be replaced by another amphiphilic helix with the same biophysical properties

In the preceding sections, I established that alterations in the hydrophobicity of the helix could lead to either the failure of virus rescue or the rescue of viruses with reduced virus titers. To delve deeper into the role of the amphiphilic helix in virus function, I

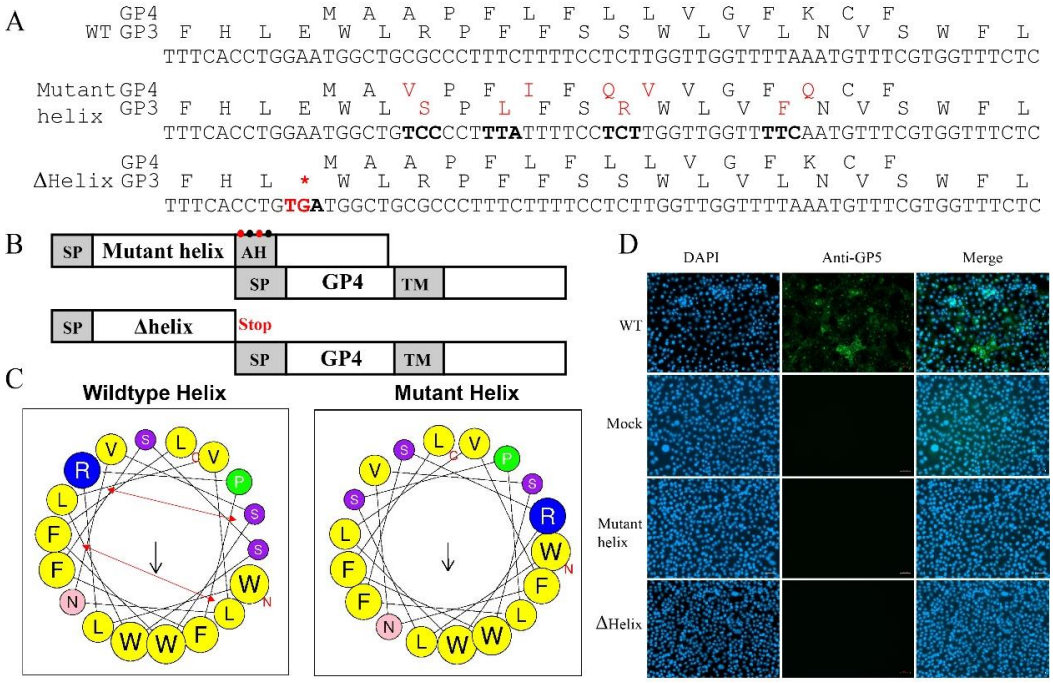

Figure 14 Amphiphilic helix cannot be replaced by amphiphilic helix with same biophysical properties (A) Amino acids and nucleotides of mutants in this experiment. The mutated amino acids of GP3 and GP4 are marked in red, while the mutated nucleotides are marked in bold or red. The red "*" indicates a stop codon. (B) Schematic constructs of mutant helix and Δhelix. The red and black dots indicate two pairs of amino acids that were exchanged in the amphiphilic helix of GP3. The "stop" indicates a stop codon inserted at the start codon site of GP4 to delete the entire amphiphilic helix. (C) Predicted biophysical properties of the amphiphilic helix of wild-type and mutant helix displayed by helical wheel plot. The bioinformatics tool HeliQuest (http://heliquest.ipmc.cnrs.fr/) predicts that the hydrophobic region of GP3 forms an amphiphilic helix with a mean hydrophobicity (<H>) of 1.131 and a hydrophobic moment (<μH>) of 0.302. Yellow amino acids represent hydrophobic amino acids. The red arrows indicate the positions of amino acids that will be exchanged to create the mutant helix, which has a mean hydrophobicity (<H>) of 1.131 and a hydrophobic moment (<μH>) of 0.274. (D) To confirm the rescue of the viruses, 293T cells were transfected with the full-length mutant helix, Δhelix, and wild-type constructs. After 48 hours, the cell culture supernatant was collected and used to infect Marc-145 cells. Indirect immunofluorescence was performed with an anti-GP5 antibody, and images were captured using an epifluorescence microscope. Mock refers to un-transfected cells.

conducted an experiment wherein I swapped the positions of two pairs of amino acids within the helix (Figure 14A and B). This mutation did not alter the specific amino acid composition, but it disrupted the sequence within the helix. I analyzed the biophysical properties of the mutant helix using a helical wheel plot (Figure 14C). The analysis revealed that the mutant helix exhibited the same biophysical properties as the wild type, with a mean hydrophobicity, <H>, of 1.131, and a hydrophobic moment, <μH>, of 0.274.

However, virus with a mutant helix could not be rescued, as confirmed by indirect immunofluorescence assay (Figure 14D), indicating that the altered amino acid sequence was lethal to the virus.

Additionally, I constructed another mutant, termed Δhelix, wherein a stop codon was inserted (Figure 14A and B). This mutation resulted in the deletion of the entire C-terminus (including the helix) of GP3 but did not affect the amino acid sequence of GP4. Similar to the mutant helix, Δhelix also could not be rescued (Figure 14D), further underscoring the importance of the C-terminus and the amphiphilic helix of GP3 in virus replication.

3.1.2.4 Exchange of amino acids does not affect cleavage of GP4's signal peptide

Since I exchanged the positions of amino acids in the helix of GP3, which induced changes in the amino acids of GP4 in the signal peptide domain, it remains uncertain

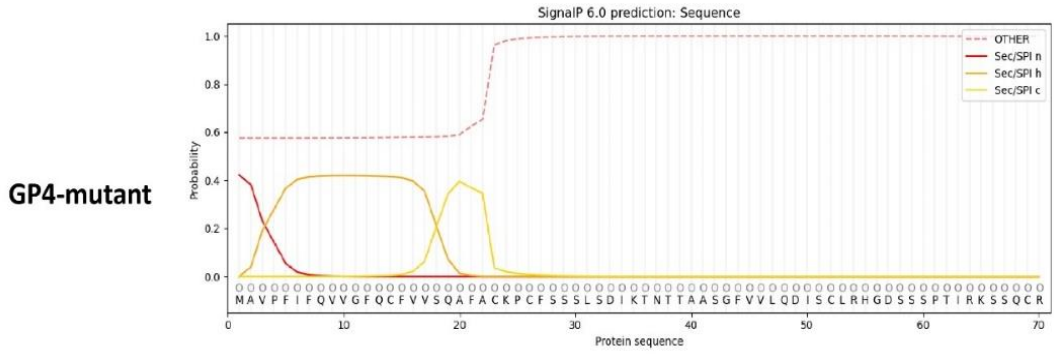

Figure 15 Prediction of signal peptides cleavage site of and GP4-mutant by Signal IP 6.0 online software

The Y-axis represents the probability of a signal peptide, while the X-axis represents amino acids. The yellow and red lines depict the probability of a signal peptide for each amino acid. The label 'O' signifies other regions.

whether the altered amino acids in the signal peptide domain of GP4 affect the cleavage of GP4's signal peptide, potentially preventing virus rescue. To investigate this, I predicted the signal peptide cleavage site of GP4-mutant (wherein amino acids of GP4 had undergone the exchange of positions of two pairs of amino acids in the amphiphilic helix of GP3, named as GP4-mutant) using the Signal IP 6.0 online software. The results indicated that the probability that the N-terminus functions as a signal peptide was largely decreased (Figure 15). To confirm whether the signal

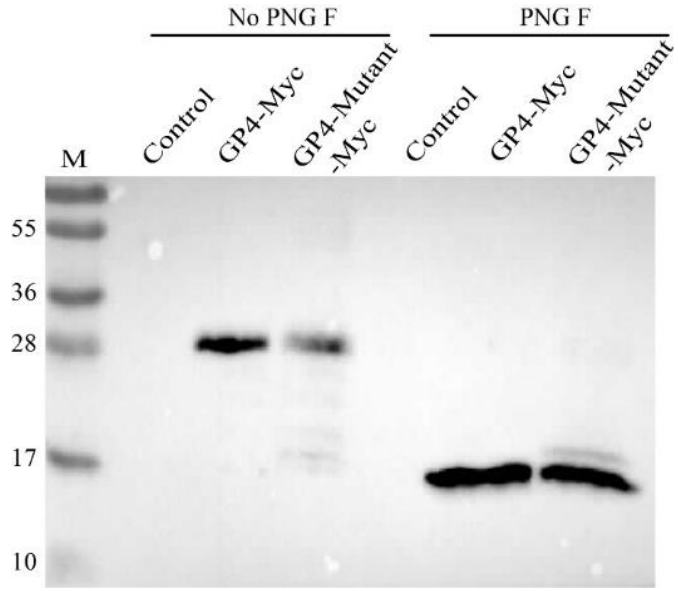

Figure 16 Exchange of amino acids does not affect cleavage of GP4's signal peptide
Expression of Gp4-myc and GP4-mutant-myc, followed by digestion with PNG F, was conducted on CHO cells cultured in 6-well plates for 24 hours after transfection with GP4 and GP4-mutant-myc constructs. Subsequently, cell lysates were either subjected to PNG F digestion or left untreated prior to Western blot analysis using anti-myc antibodies. Molecular weight markers (M) were utilized to determine protein mobilities.

peptide of GP4 was indeed affected by the exchange of positions of two pairs of amino acids in the amphiphilic helix of GP3, I constructed a GP4-mutant expression plasmid fused with a myc tag. The GP4-mutant-myc contains the same amino acid changes as the GP4 full-length mutant helix. Both proteins exhibit the same molecular weight under conditions without PNGase F digestion. Furthermore, both GP4 and GP4-mutant exhibit identical molecular weights upon PNGase F digestion, demonstrating that the signal peptide has been cleaved (Figure 16).

Therefore, the altered amino acids in the signal peptide domain of GP4 are not the cause of the virus's inability to be rescued, as cleavage occurs normally. This further confirms the lethal nature of certain sequences within the helix of GP3 for virus replication.

3.1.2.5 Amphiphilic helix with replaced amino acids still binds to membranes.

GP3 forms a hairpin-like structure, with an amphiphilic helix attaching the entire GP3 to the lumen of the endoplasmic reticulum. Since I exchanged the positions of amino acids in the helix, it might affect its binding to the endoplasmic reticulum membrane.

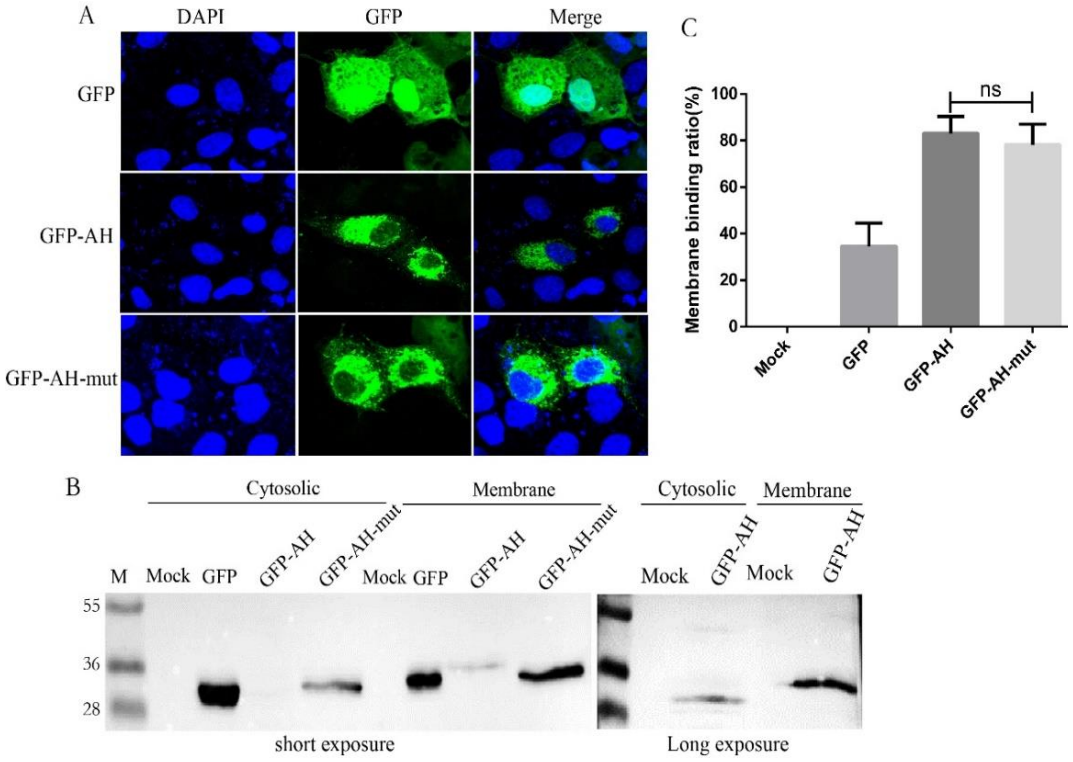

Figure 17 Amphiphilic helix with replaced amino acids still bind to membranes

(A) The fluorescence signal of GFP exhibits distribution differences after fusion with the amphiphilic helix of GP3. CHO cells were transfected with GFP and GFP chimeras. After 24 hours of transfection, cells were fixed with 4% paraformaldehyde (PFA), stained with DAPI for nuclear visualization, and then subjected to confocal microscopy to visualize the localization of GFP and GFP chimeras in transfected CHO cells. (B) Membrane separation experiment: GFP, GFP-AH, and GFP-AH-mut were expressed in CHO cells. The cells were lysed and separated into cytosolic and membranous fractions, which were then blotted with anti-GFP antibodies. GFP-AH was exposed for a longer duration since it exhibited a low amount in the short exposure. (C) Quantification of this and two other independent experiments: The ratio of membrane binding was calculated using the formula ((membrane density / (membrane density + cytosolic density)) × 100%). The mean ± SD and the results from the three independent experiments are presented. One-way ANOVA followed by the Dunnett test for multiple comparisons was applied for statistical analysis. "ns" indicates nonsignificant differences.

To investigate this, I constructed plasmids which express the wild-type amphiphilic helix (AH) and a mutant form of the amphiphilic helix (AH-mut), both fused at the C-terminus with a GFP tag. These plasmids were transfected into CHO cells to observe the distribution of proteins within the cell. The GFP protein expressed alone is present in the cytoplasm and can also penetrate the nucleus via passive transport. GFP-AH only appeared in the cytoplasm and could not penetrate the nucleus as described previously(M. Zhang et al., 2018), presumably because it is at least partly attached to membranes. I hypothesized that if the AH-mut loses its ability to bind to the membrane, it will show the same distribution within the cell as the wild-type GFP. However, this was not the case, both GFP-AH and GFP-AH-mut had the same intracellular distribution (see Figure 17A). This suggests that exchanging the positions of two pairs of amino acids in the helix does not alter its ability to bind to the membrane.

To confirm that the membrane binding characteristic of GFP-AH-mut remains unchanged, I separated proteins present in membranes (including ER and Golgi membranes) from cytosolic proteins through high-speed centrifugation. Results indicate that, upon brief exposure of the western blot, the majority of wild-type GFP is present in the cytosol, with a smaller portion in the membrane. Conversely, GFP-AH predominantly localized to the membrane, with minimal cytosolic expression.

The GFP-AH mutant is, due to its lower expression levels only barely visible in the blot. However, when more of the samples are loaded and the blot is exposed for longer, it becomes obvious that it is also predominantly membrane localized, with minimal cytosolic presence (Figure 17B). Quantification of three independent experiments revealed membrane binding ratios of 34.66% for wild-type GFP, and 83.14% and 78.19% for GFP-AH and GFP-AH-mut, respectively. There was no significant difference observed between GFP-AH and GFP-AH-mut membrane binding ratios (Figure 17C), indicating that GFP-AH-mut maintains similar membrane binding properties despite the exchange of two pairs of amino acids.

3.2 Screening of putative inhibitors of porcine reproductive and respiratory syndrome virus replication

3.2.1 Constructing infectious clones by inserting GFP tag in PRRSV-1 and PRRSV-2

To screen for inhibitors of PRRSV replication, infectious clones of PRRSV-1 and PRRSV-2 were constructed in my host laboratory and utilized for the antiviral assay.

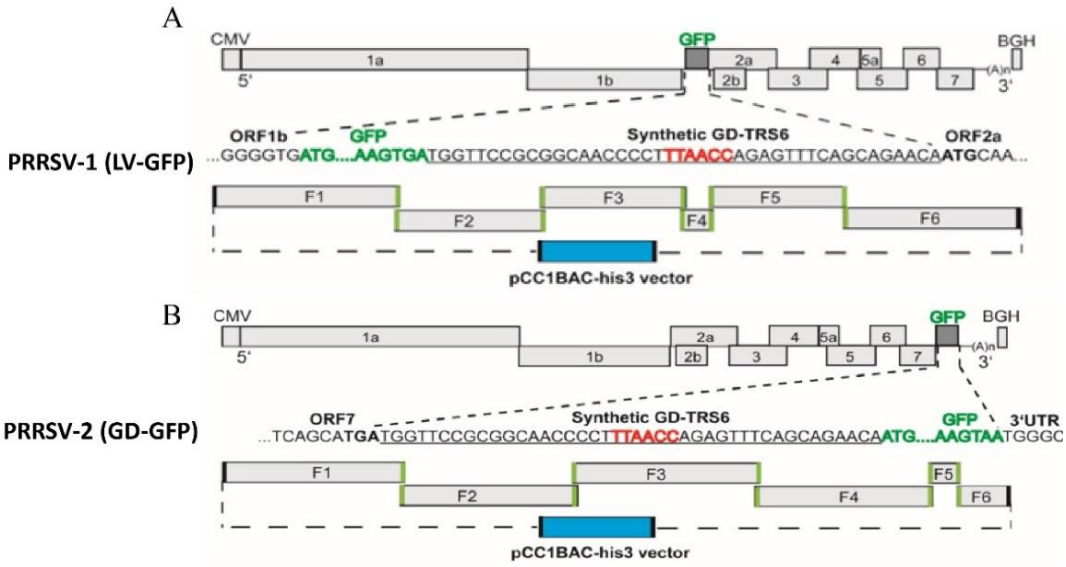

Figure 18 Construction scheme of infectious clone in PRRSV-1 and PRRSV-2
(A) The GFP tag is inserted between ORF1 and ORF2 to construct the PRRSV-1 infectious clone. LV-GFP, a fusion of the Lelystad strain with the GFP tag. (B) The GFP tag is inserted between ORF7 and the 3' terminal UTR to construct the PRRSV-2 infectious clone. GD-GFP, a fusion of the XH-GD strain with the GFP tag.

For PRRSV-1, one GFP tag is inserted between ORF1 and ORF2 (Figure 18A) and for PRRSV-2 one GFP tag is inserted between ORF7 and 3' terminal UTR to construct infectious clone (Figure 18B).

3.2.2 Remdesivir inhibits the replication of PRRSV

Remdesivir was tested against PRRSV-1 (Lelystad) and PRRSV-2 (XH-GD) to investigate its potential to inhibit PRRSV replication. The cytotoxicity of remdesivir to Marc-145 cells was determined by evaluating the number of living cells. Marc-145 cells were infected by the indicated viruses, fluorescent cells were quantitated and the virus titer in supernatant was determined, and the half maximal inhibitory concentration (IC50) value of inhibitor was calculated. Results indicate that all the concentrations (10^{-}

^{3}, 10^{-2}, 10^{-1}, 10^{0}, 10^{1}, or 10^{2} μM) of remdesivir tested had no significant effect on the viability of Marc-145 cells (Blue dots in figure 19A and B). However, higher

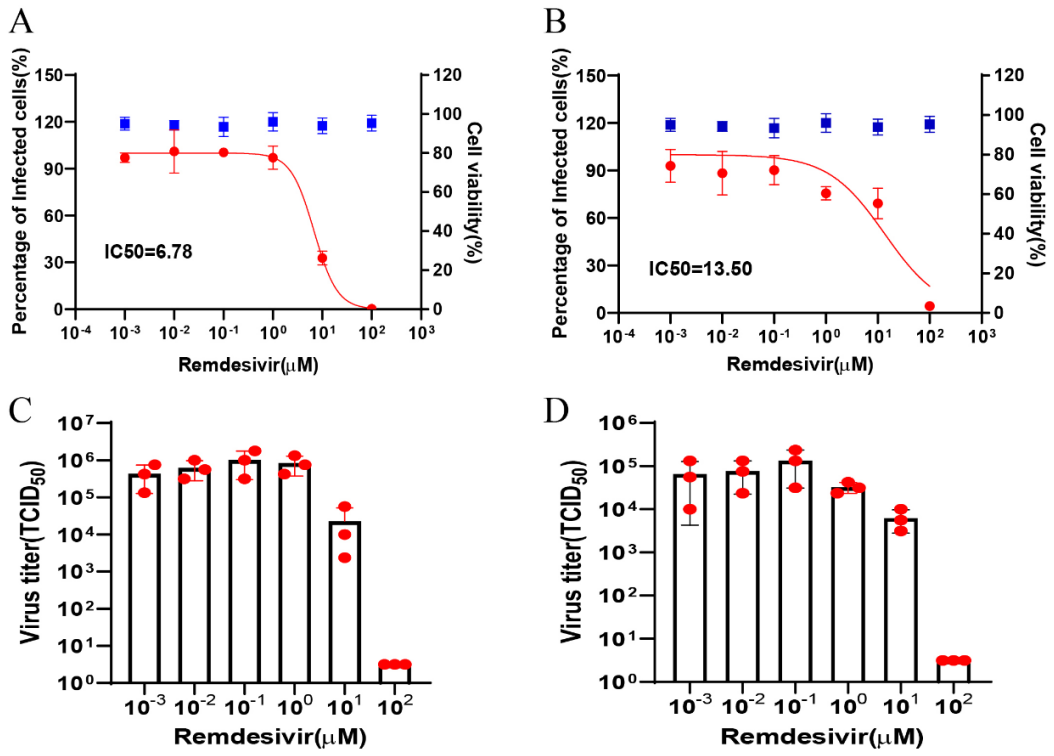

Figure 19 The inhibitory effects of remdesivir were tested on PRRSV-1 and PRRSV-2 in Marc-145 cells

The cytotoxicity and inhibitory effects of remdesivir on the replication of PRRSV-1 and PRRSV-2 were evaluated in Marc-145 cells. Marc-145 cells were infected with the two viruses in triplicate at a multiplicity of infection (MOI) of 0.1, while being exposed to various concentrations of remdesivir (10^-3, 10^-2, 10^-1, 100, 10^1, or 10^2 μM). Replication of PRRSV-1 (panels A and C) and PRRSV-2 (panels B and D) was assessed after 24 hours by measuring EGFP cell production through flow cytometry (red curve) or by determining the released virus titer in the supernatant (bar diagram). The cytotoxicity of remdesivir on Marc-145 cells was evaluated in uninfected cells using a colorimetric assay (Cell Counting Kit 8; blue scattergram). Relative EGFP production is presented as the mean ± standard deviation with a nonlinear fit curve (n = 3).

concentrations (10^{1}, or 10^{2} μM on PRRSV-1 and 10^{0}, 10^{1}, or 10^{2} μM on PRRSV-2) demonstrated a significant inhibitory effect on both PRRSV-1 (Figure 19A) and PRRSV-2 (Figure 19B). The IC50 for remdesivir against PRRSV-1 and PRRSV-2 was found to be 6.78μM and 13.50μM, respectively. Furthermore, the viral titers in the medium were tested, revealing a significant reduction at higher concentrations of remdesivir for both PRRSV-1 (Figure 19C) and PRRSV-2 (Figure 19D). These results demonstrate that remdesivir effectively inhibits the replication of PRRSV. Previous

studies on coronavirus have shown a half-maximal IC50 of 0.77μM for remdesivir (Wang et al., 2020).

3.2.3 GS-441524 inhibits the replication of PRRSV

Next, using the same type of experiments I tested whether GS-441524 inhibits replication of PRRSV-1 and PRRSV-2. Our results demonstrate that all the tested concentrations (10^{-3}, 10^{-2}, 10^{-1}, 10^{0}, 10^{1}, or 10^{2}μM) of GS-441524 had no significant effect on the viability of Marc-145 cells. However, at higher concentrations (10^{0}, 10^{1}, or 10^{2}μM on PRRSV-1 and PRRSV-2) significant inhibitory effect on both PRRSV-1 (Figure 20A) and PRRSV-2 (Figure 20B) replication was observed. The half-maximal inhibitory concentration (IC50) obtained with GS-441524 for PRRSV-1 and PRRSV-2

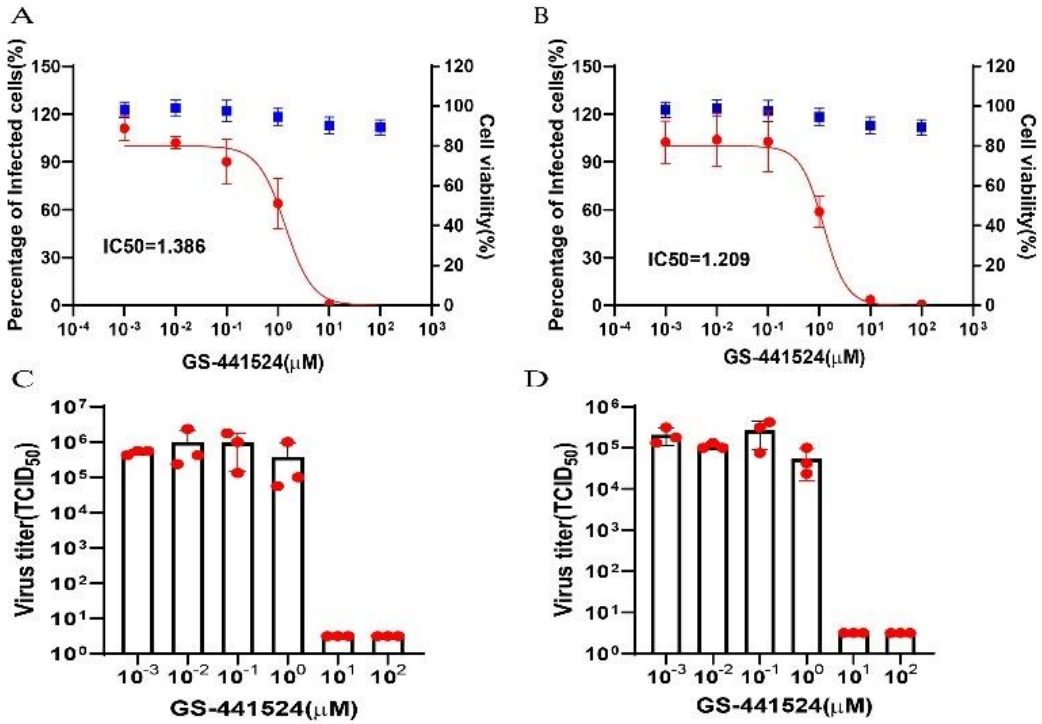

Figure 20 The inhibitory effects of GS-441524 were tested on PRRSV-1 and PRRSV-2 in Marc-145 cells

The cytotoxicity and inhibitory effects of GS-441524 on the replication of PRRSV-1 and PRRSV-2 were assessed in Marc-145 cells. Marc-145 cells were infected with the two viruses in triplicate at a multiplicity of infection (MOI) of 0.1, in the presence of varying concentrations of GS-441524 (ranging from 10^-3 to 10^2 μM). Replication of PRRSV-1 (panels A and C) and PRRSV-2 (panels B and D) was evaluated after 24 hours by quantifying EGFP cell production via flow cytometry (depicted by the red curve) or by measuring the released virus titer in the supernatant (shown in the bar diagram). The cytotoxicity of GS-441524 to Marc-145 cells was determined in uninfected cells using a colorimetric assay (Cell Counting Kit 8; represented by the blue scattergram). Relative EGFP production is presented as the mean ± standard deviation with a nonlinear fit curve (n = 3).

is 1.386μM and 1.209μM, respectively. Additionally, I tested the titer of released virus in the medium, which showed a significant reduction at higher concentrations of GS-441524 for both PRRSV-1 (Figure 20C) and PRRSV-2 (Figure 20D). These findings demonstrate that GS-441524 effectively inhibits the replication of PRRSV.

3.2.4 Molnupiravir (EIDD-2801) inhibits the replication of PRRSV

Here, I evaluated its efficacy against PRRSV-1 and PRRSV-2 to determine whether it

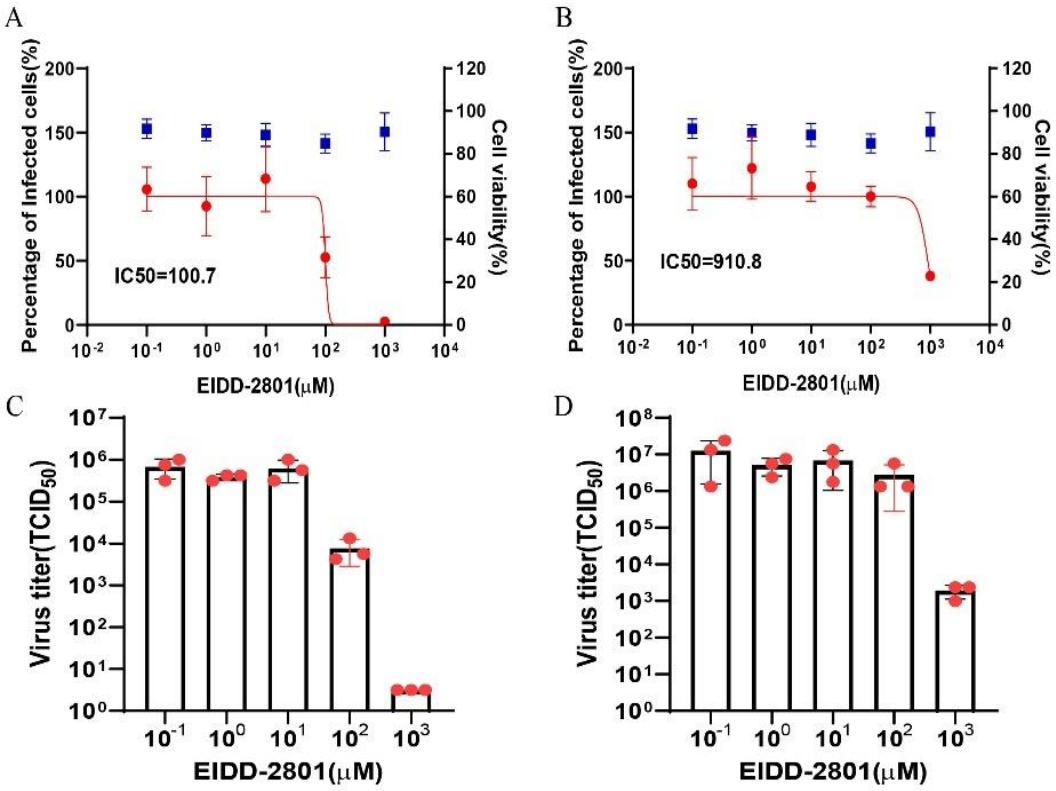

Figure 21 The inhibitory effects of EIDD-2801 were tested on PRRSV-1 and PRRSV-2 in Marc-145 cells

The cytotoxicity and inhibitory effects of EIDD-2801 on the replication of PRRSV-1 and PRRSV-2 were assessed in Marc-145 cells. Marc-145 cells were infected in triplicate with the two viruses at an MOI of 0.1 in the presence of various concentrations of EIDD-2801 (10^-1, 100, 10^1, 10^2, or 10^3 μM). Replication of PRRSV-1 (A and C) and PRRSV-2 (B and D) was evaluated after 24 hours by quantifying EGFP cell production through flow cytometry (depicted by the red curve) or by measuring the released virus titer in the supernatant (represented by the bar diagram). The cytotoxicity of EIDD-2801 on Marc-145 cells was determined in uninfected cells using a colorimetric cell counting assay (depicted in the blue scattergram). Relative EGFP production is expressed as mean ± standard deviation with a nonlinear fit curve (n = 3).

can inhibit their replication. antiviral experiments of EIDD-2801 were performed as like as tested on remdesivir. Results indicate that the tested concentrations (10^{-1}, 10^{0}, 10^{1},

10^2, or 10^3 μM) of EIDD-2801 had no significant effect on the viability of Marc-145 cells, and while lower concentrations (10^{-1}, 10^0, 10^1μM on PRRSV-1 and 10^{-1}, 10^0, 10^1, 10^2μM on PRRSV-2) of EIDD-2801 did not significantly reduce replication, higher concentrations (10^2, or 10^3 μM on PRRSV-1 and 10^3 μM on PRRSV-2) showed significant inhibitory effects on both PRRSV-1 (Figure 21A) and PRRSV-2 (Figure 21B). The half maximal inhibitory concentration (IC50) obtained with EIDD-2801 for PRRSV-1 and PRRSV-2 are 100.7μM and 910.8μM respectively. Additionally, the titers of released virus in the medium were tested, revealing a significant reduction at higher concentrations of EIDD-2801 for both PRRSV-1 (Figure 21C) and PRRSV-2 (Figure 21D). These results demonstrate that EIDD-2801 effectively inhibits the replication of PRRSV.

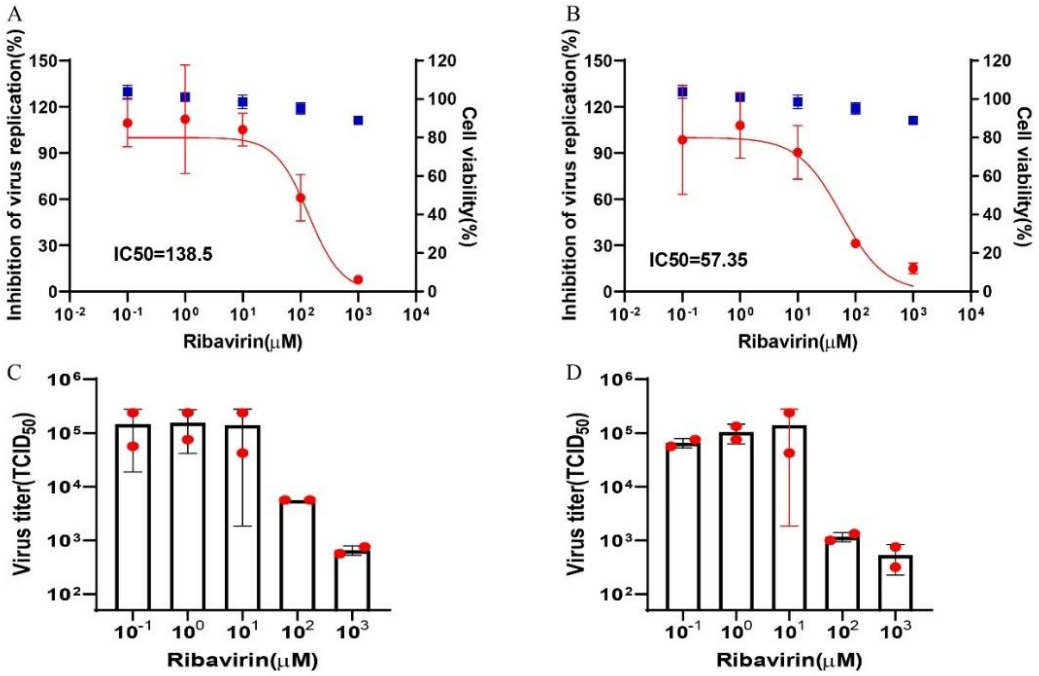

Figure 22 The inhibitory effects of ribavirin were tested on PRRSV-1 and PRRSV-2 in Marc-145 cells The cytotoxicity and inhibitory effects of ribavirin on the replication of PRRSV-1 and PRRSV-2 were assessed in Marc-145 cells. Marc-145 cells were infected with the two viruses in triplicate at a multiplicity of infection (MOI) of 0.1, while exposed to varying concentrations of remdesivir (10^-1, 100, 10^1, 10^2, or 10^3 μM). Replication of PRRSV-1 (A and C) and PRRSV-2 (B and D) was evaluated after 24 hours by measuring EGFP expression through flow cytometry (represented by the red curve) or by determining the released virus titer in the supernatant (illustrated in the bar diagram). The cytotoxicity of remdesivir on Marc-145 cells was assessed in uninfected cells using a colorimetric assay (Cell Counting Kit 8; depicted in the blue scattergram). Relative EGFP expression is presented as mean ± standard deviation with a nonlinear fit curve (n = 2).

3.2.5 Ribavirin inhibits the replication of PRRSV

Ribavirin has been tested as a potential candidate against SARS-CoV-2 with an EC50 of 109.5μM (Wang et al., 2020). Based on its broad spectrum of antiviral activity and diverse antiviral mechanisms, I hypothesized that ribavirin could also play an inhibitory role in the replication of PRRSV. Results showed that all the tested concentrations (10^{-1}, 10^{0}, 10^{1}, 10^{2} or 10^{3} μM) of ribavirin had no significant effect on the viability of Marc-145 cells. However higher concentrations (10^{2} or 10^{3} μM on both PRRSV-1 and PRRSV-2) exhibited a significant inhibitory effect on both PRRSV-1 (Figure 22A) and PRRSV-2 (Figure 22B). The half-maximal inhibitory concentration (IC50) obtained with remdesivir for PRRSV-1 and PRRSV-2 was 138.5μM and 57.35μM, respectively. Additionally, the titer of released virus in the medium is significantly reduced at higher

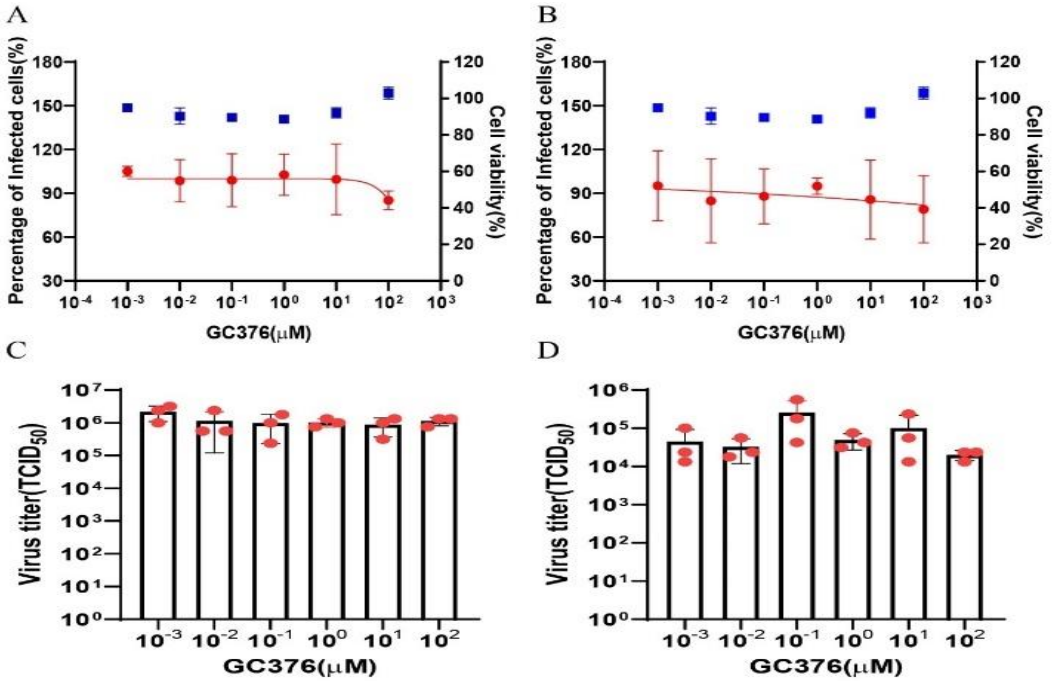

Figure 23 The inhibitory effects of GC376 were tested on PRRSV-1 and PRRSV-2 in Marc-145 cells The cytotoxicity and inhibitory effects of GC376 on the replication of PRRSV-1 and PRRSV-2 were assessed in Marc-145 cells. Marc-145 cells were triplicate-infected with the two viruses at a multiplicity of infection (MOI) of 0.1, in the presence of various concentrations of GC376 (10^-3, 10^-2, 10^-1, 100, 10^1, or 10^2 μM). Replication of PRRSV-1 (A and C) and PRRSV-2 (B and D) was evaluated after 24 hours by quantifying EGFP cell production via flow cytometry (red curve) or by measuring the released virus titer in the supernatant (bar diagram). Cytotoxicity of GC376 to Marc-145 cells was determined in uninfected cells using a colorimetric assay (Cell Counting Kit 8; blue scattergram). Relative EGFP production is presented as mean ± standard deviation with a nonlinear fit curve (n = 3).

concentrations of ribavirin for both PRRSV-1 (Figure 22C) and PRRSV-2 (Figure 22D), demonstrating that ribavirin can effectively inhibit the replication of PRRSV.

3.2.6 GC376 does not inhibit the replication of PRRSV

Given that the porcine reproductive and respiratory syndrome virus (PRRSV) also contains M^{pro} (Nsp4), I hypothesized that GC376 could potentially interact with the ^{Mpro} of PRRSV and inhibit its function. Therefore, GC376 was tested on PRRSV-1 and PRRSV-2 at various concentrations (10^{-3}, 10^{-2}, 10^{-1}, 10^{0}, 10^{1}, or 10^{2} μM), and the number of fluorescent cells and the titer of released virus in the medium were calculated to evaluate whether GC376 inhibits the replication of PRRSV. The results indicate that at all the tested concentrations, GC376 had no significant effect on the viability of Marc-145 cells. Moreover, GC376 neither reduced the production of fluorescent cells for both PRRSV-1 (Figure 23A) and PRRSV-2 (Figure 23B) nor caused a decrease in the virus titer of PRRSV-1 (Figure 23C) and PRRSV-2 (Figure 23D). This suggests that GC376 does not exhibit inhibitory effects on the replication of PRRSV.

4 Discussion

4.1 The C-terminus of Gp3 has a positive effect on replication of PRRSV

In this study, I showed that the deletion of the C-terminus of GP3 by introducing stop codons at three positions resulted in reduction of virus titers (Figure 7C), and the virus could regain the C-terminus after several passages in cell culture (Figure 8). These observations highlight the positive effect of the C-terminus of GP3 for virus replication.

Table 5 Leucine naturally exists in GP4 between strains

PRRSV strains	Amino acids of GP4	Accession no.
GD1404	MATPFL**F**LLVGFKCFVVSQ…	MF669720.1
Henan-A6	MATPFL**S**LLVGFKCFVVSQ…	KJ534541.1
PRRSV2/CN/F1228/2017	MATPFL**F**LLVGFKCFVVSQ…	MT416543.1
HB19-12	MATPFL**F**LLVGFKCFVVSQ…	MW651975.1
GXNN1396-p3	MATPFL**F**LLVGFKCFVVSQ…	MN660067.1
HeNan-A9	MATPFL**F**LLVGFKCFVVSQ…	KJ546412.1
SD54-1603	MATPFL**F**LLVGFKCFVVSQ…	MT093740.1
09HUN1	MATPFL**L**LLVGFKCFVVSQ…	JF268673.1
Henan-A12	MATPFL**F**LLVGFKCFVVSQ…	KJ819934.1

Table 5 Leucine naturally exists in GP4 between strains

The conserved amino acid Phenylalanine (Phe) is highlighted in blue at the seventh position in the listed strains. The mutated amino acids Serine (Ser) and Leucine (Leu) are highlighted in red.

Introducing a stop codon at the 209th position of GP3 caused one amino acid mutation in the signal peptide of GP4 (from Phe to Leu). The same residue is present in the 09HUN1 strain which was discovered in central China (Zhou et al., 2011) (Table 5) indicating that it does not prevent the generation of viable virus. I also confirmed that this mutation did not hinder virus rescue in cell culture. Furthermore, the rescued virus remained stable for at least 15 passages in cell culture (Figure 10B), and the virus titer was only moderately reduced with no statistic significant difference in comparison to wild type (Figure 10A). This suggests that the decrease in Δ209 titer is mainly due to the deletion of the C-terminal region of GP3, although a combined effect cannot be excluded. In Δ203, the deletion of the C-terminus results in one amino acid change in the mature GP4. It has been shown that the predicted cleavage site of the signal peptide remains the same as in the wild type, but it leads to a significant reduction in virus titer. In Δ227, the deletion of the C-terminal of GP3 alone, without any changes to GP4 amino acids, also leads to a significant decrease in virus titer. This highlights the critical role of the GP3 C-terminal region in viral replication.

Antiviral factor CLDNs are transmembrane proteins composed of intracellular N- and C-terminal tails, four transmembrane helices, two extracellular loops (large ECL1 and small ECL2), and one cytoplasmic loop. Previous report indicated that after the inoculation of PRRSV onto susceptible cells, most viral particles were kept out of the cells due to the interaction between GP3 and the ECL2 domain of CLDN4. Only a fraction of the viral particles binds to the cellular receptor CD163 and enters the cells(Ding et al., 2020). The transcription factor specificity protein 1 (SP1) has been reported to positively regulated the transcription of CLDN4 (Ikari et al., 2009; Senga, Mostov, Mitaka, Miyajima, & Tanimizu, 2012). Following viral entry into the cells, GP3 is produced early and causes ubiquitination of SP1 through an unknown mechanism. Subsequently, SP1 is degraded in a proteasome-mediated manner, leading to the downregulation of CLDN4 transcription and a decrease in CLDN4 levels. Consequently, a large number of viral particles can enter the cells (Ding et al., 2020). However, the authors did not further validate their hypothesis using full-length infectious virus. In this study, deletion of the C-terminus of GP3 resulted in a reduction in virus titer, possibly because the antiviral factor CLDN4 could not be regulated by GP3 due to its inability to bind to the C- terminus of GP3, thereby enabling CLDN4 to fully exert its antiviral activity and inhibit PRRSV replication. Our findings align well with the aforementioned hypothesis (Ding et al., 2020), potentially elucidating why the virus needs to regain the C-terminus.

4.2 GP3 requires an amphiphilic helix with a certain sequence to allow virus replication

To investigate the function of the amphiphilic helix of GP3 in virus replication several mutations were introduced. Since the N-terminus of GP4 overlaps with the C-terminus of GP3, substituting the amino acids of the amphipathic helical hydrophobic surface with Ala leads to the replacement of amino acids in the signal peptide region of GP4. Experimental results show that this does not affect the signal peptide cleavage of GP4-2A, but the protein expression level decreases (Figure 11D), which might be one of the reasons for the failure to rescue this virus.

Signal peptides direct proteins to the endoplasmic reticulum (ER) for secretion or membrane localization and are first recognized by the signal recognition particle (SRP) in the cytoplasm. Alterations in the sequence might reduce the binding affinity between the SRP and the signal peptide, thereby slowing down or partially preventing the protein's targeting to the ER (Rapoport, Jungnickel, & Kutay, 1996). Proteins that fail to be properly targeted to the ER may accumulate in the cytosol, where they are often tagged for degradation by the ubiquitin-proteasome system. Consequently, this would reduce the overall protein levels (Ciechanover, 1998). Furthermore, even though the signal peptide is cleaved, changes in its sequence can affect the nascent chain's folding in the ER. Misfolded proteins in the ER can induce stress and activate the unfolded protein response (UPR) and are often targeted for degradation via the ER-associated degradation (ERAD) pathway(Dobson, 2003). This can lead to a global reduction in protein synthesis to alleviate the stress, which might indirectly reduce the expression level of the protein(Ron & Walter, 2007). GP2, GP3, and GP4 are incorporated as a disulfide-linked heterotrimeric complex into the envelope of EAV (Wieringa et al., 2003), but details of the complex formation of the respective proteins of PRRSV have not been investigated. Therefore, if the expression of GP4-2A decreases, it might mean that fewer GP2/3/4 complexes are formed, leading to fewer infectious viral particles or the formation of non-infectious viral particles within the cells(M. Zhang et al., 2018). However, constructing 3H, 4H, and 7H did not affect the amino acids of GP4, yet also resulted in virus rescue failure or a decrease in viral titers (figure13 C and E), further illustrating the importance of the helix of GP3 in viral replication.

Exchanging the positions of two pairs of amino acids in the amphiphilic helix did also prevent virus rescue indicating that the sequence of the helix is essential for virus viability (Fig. 14). The corresponding changes in the signal peptide of Gp4 did not alter its cleavage suggesting that the failure to rescue virus is mainly due to the amino acid exchanges in the helix of Gp3. Furthermore, the two exchanges did not alter the membrane-binding properties of the helix indicating that the Gp3 with this mutation is still membrane-bound (figure 17). The requirement for a specific sequence suggests

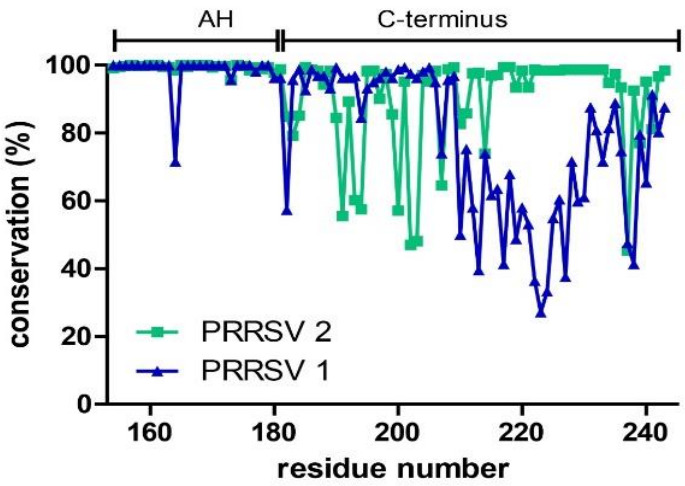

Figure 24 Amphiphilic helix of GP3 is conservation but not the C-terminus
To analyze conservation, a consensus sequence of the C-terminus of GP3 was compiled from all PRRSV-1 and PRRSV-2 sequences, and subjected to conservation analysis using bioinformatics tool. The resulting graph displays the percentage of amino acid conservation (y-axis) at each position (x-axis) of the consensus sequence derived from the GP3 sequences of both PRRSV1 and PRRSV2 in the database. AH, amphiphilic helix.

that the helix is rather (also) involved in binding to another protein, for example during formation of the Gp2/3/4 complex and or during virus entry by membrane fusion.

A sequence comparison of the entire C-terminus of GP3 from both PRRSV-1 and PRRSV-2 strains revealed that the amphiphilic helix of GP3, exhibits is highly conserved between virus strains (Figure 24). This further underscores that the exact sequence and not only the biophysical properties are crucial for virus rescue and replication. In contrast, the C-terminal part shows a large degree of variability between viruses which is in line with the less important role of this protein domain for virus replication.

4.3 Inhibitors for porcine reproductive and respiratory syndrome virus replication

In this study, five inhibitors were tested on both PRRSV-1 and PRRSV-2. It was demonstrated that Remdesivir, GS-441524, EIDD-2801, and Ribavirin effectively inhibit virus replication, thus showing potential for clinical treatment of PRRSV. Only GC376 showed no effect on virus replication. The published IC50 values of Remdesivir for coronavirus replication are roughly one order of magnitude lower than the

corresponding values determined here for PRRSV， the IC50 value of GS-441524 and Ribavirin are almost identical for both coronavirus and PRRSV. However, the IC50 value of Molnupiravir for PRRSV are roughly four factors of magnitude lower than the one for coronavirus (Table 6).

Table 6 Inhibitors for porcine reproductive and respiratory syndrome virus replication

Inhibitors	Type	Inhibition of Coronavirus IC50 (μM)	Inhibition of PRRSV-1 IC50 (μM)	Inhibition of PRRSV-2 IC50 (μM)
Remdesivir	RdRp Inhibitor	Yes (IC50=0.77)	Yes (IC50=6.78)	Yes (IC50=13.5)
GS-441524	RdRp Inhibitor	Yes (IC50=1.1)	Yes (IC50=1.386)	Yes (IC50=1.209)
Molnupiravir (EIDD-2801)	Ribonucleoside analogue	Yes (IC50=0.15)	Yes (IC50=100.7)	Yes (IC50=910.8)
Ribavirin	Guanosine (ribonucleic)analogue	Yes (IC50=109.5)	Yes (IC50=138.5)	Yes (IC50=57.35)
GC376	Protease inhibitor	Yes (IC50=0.9)	No	No

To determine the structural similarities between the target of remdesivir, the RNA-dependent polymerase (Rdp), I compared the structures of the proteins from coronavirus and PRRSV. I utilized alphafold 2 online software (https://colab.research.google.com/github/sokrypton/ColabFold/blob/main/AlphaFold2.ipynb#scrollTo=kOblAo-xetgx) to predict the structure of RdRp for PRRSV (Figure 25A), The program created five models in the form of PDB files and two data sets to evaluate the quality of the predicted models. One of these credibility scores was the “predicted local distance difference test” (pLDDT), which was more than 90 for the best model. Values between 70 and 90 indicate a high accuracy, where the prediction of the main chain of the protein is reliable.

The structure of RdRp for SARS-Cov-2 was obtained from the PDB database (PDB: 7BV1) (Figure 25B). Comparison of these two structures revealed a similar conformation with an RMSD (Root-Mean-Square Deviation) value of 3.128Å (Figure 25C). This similarity in conformation suggests a possible explanation why remdesivir inhibits both coronavirus and PRRSV replication. The structure of remdesivir bound to the active pocket of the RdP of SARS-CoV-2 revealed that remdesivir interacts with residues Lys551, Trp617, Asp618, Tyr619, Lys621, Cys622, Asp623, Leu758, Asp760, Asp761, Ala762, Trp800, Glu811, Phe812, Cys813, and Ser814 (red sticks in figure 25

D and E) (Khan, Kang, Ali, & Lai, 2021). By aligning the structures of RdRp of SARS-CoV-2 and PRRSV, I identified the amino acids present at the same positions. Seven amino acids including Lys336, Asp395, Cys399, Asp400, Asp509, Asp 510 and Phe551 (green sticks in figure 25 E) of RdRp of PRRSV are identical in SARS-CoV-2

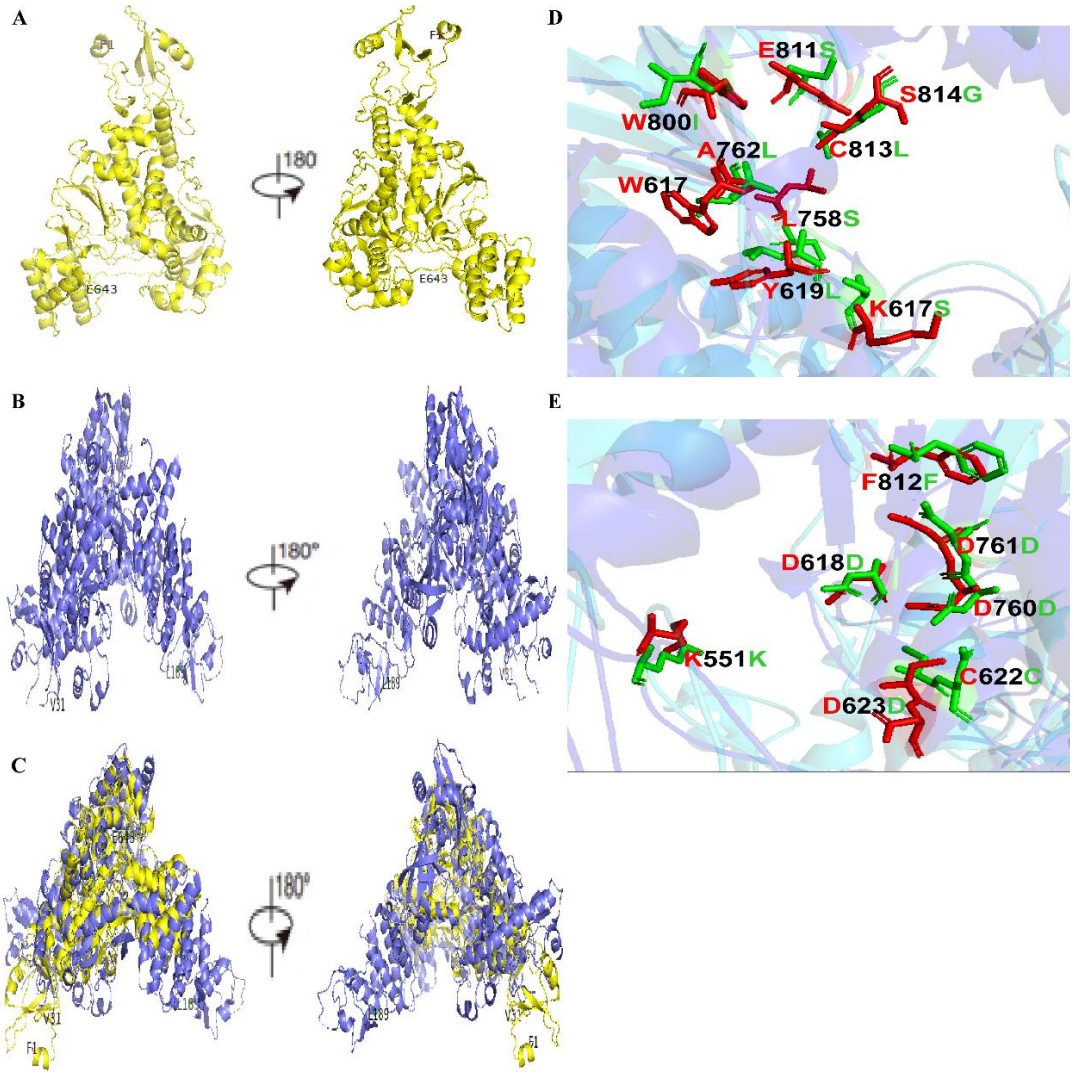

Figure 25 Prediction of structure of RdRp in PRRSV-2 and comparing to RdRp of SARS-Cov-2
(A) The predicted structure of RdRp of PRRSV and its reverse side. (B) The crystal conformation of RdRp of coronaviruses and its reverse side (PDB: 7bv1). (C) The aligned crystal conformation of RdRp of PRRSV and SARS-CoV-2 and their reverse side. (D and E) The aligned crystal conformation of RdRp of PRRSV and SARS-CoV-2. Those non-conserved and conserved residues of RdRp present at the same position in both coronaviruses and PRRSV are displayed in figure D and E, respectively, Amino acids of RdRp of SARS-CoV-2 that are important for remdesivir binding are highlighted as red sticks, while amino acids present at the same position in the RdRp of PRRSV are highlighted as green sticks. respectively

to Lys551, Asp618, Cys622, and Asp623, Asp760, Asp761 and Phe812 (red sticks figure 25 E) but nine amino acids are completely different including Ala394, Leu396,

Ser398, Ser508, Leu511, Ile545, Ser550, Leu552 and Gly553 (green sticks in figure 25D). This difference in the binding pocket might explain why remdesivir has lower affinity for the polymerase of PRRSV.

GS-441524 and remdesivir are closely related antiviral compounds developed by Gilead Sciences, both targeting RNA viruses through similar mechanisms. Clinically, remdesivir is approved for treating COVID-19 in humans, demonstrating reduced recovery times in hospitalized patients (Pruijssers et al., 2020; Sheahan et al., 2017). In contrast, GS-441524 has shown remarkable efficacy in treating feline infectious peritonitis (FIP), a fatal disease in cats caused by a feline coronavirus, but it is not approved for human use (Lo et al., 2017; Pedersen et al., 2019). These differences highlight remdesivir's clinical application in humans, while GS-441524 remains crucial for veterinary medicine. Considering the inhibition of remdesivir and GS-441524 tested in this study, both are potential candidates for the clinical treatment of PRRSV infection.

Molnupiravir broad-spectrum antiviral activity suggests potential applications for other RNA viruses, although more research is needed to confirm its efficacy against other pathogens. In this study, we confirmed the inhibition of molnupiravir of PRRSV-1 and PRRSV-2 replication. However, the potential mechanism of action of molnupiravir on the inhibition of PRRSV is still unclear. It is most likely similar to its mechanism against SARS-CoV-2(Kabinger et al., 2021). First, molnupiravir is metabolized into N4-hydroxycytidine (NHC), NHC is further phosphorylated inside the host cells to its active triphosphate form, NHC-TP (N4-hydroxycytidine triphosphate). Then the RdRp of PRRSV incorporates NHC-TP into its RNA during replication, mistaking it for the natural nucleosides cytidine (C) or uridine (U). Once incorporated, NHC can pair with either guanosine (G) or adenosine (A), leading to an increased mutation rate during subsequent rounds of RNA replication. This results in a high number of mutations in the viral genome. The accumulation of these mutations reaches a threshold known as error catastrophe, rendering the viral progeny nonviable and unable to propagate effectively. To confirm the action mechanism of molnupiravir on PRRSV, the next-generation sequencing (NGS) can be employed to analyze the mutation frequency and patterns. Furthermore, measuring the viability of viral progeny after multiple replication

cycles in the presence of molnupiravir, assessing the infectivity and genomic integrity of the progeny viruses are also needed.

It was found that ribavirin binds strongly to the active pocket of the RdRp of SARS-CoV-2 and interacts with residues Arg553, Asp618, Lys621, Lys798, Trp800, Glu811 and Ser814 (red sticks in figure 26) (Goswami, 2021). By aligning the experimentally determined structures of RdRp of SARS-CoV-2 and PRRSV, a RMSD value of 3.128Å was calculated. I observed that the amino acids of RdRp of PRRSV present at the

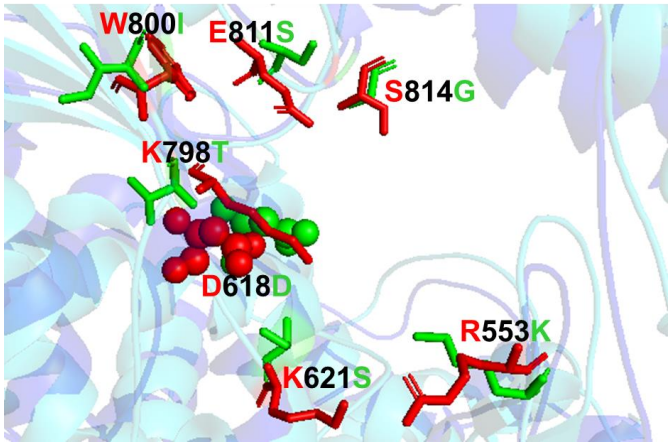

Figure 26 Prediction of crystal conformation of RdRp in PRRSV-2 and comparing to RdRp of SARS-Cov-2

The aligned crystal structures of RdRp of PRRSV-2 and coronavirus is depicted. Amino acids crucial for ribavirin binding in coronavirus RdRp are highlighted as red sticks, while amino acids occupying the corresponding positions in PRRSV RdRp are marked with green sticks. Residues shared between the RdRp of both coronaviruses and PRRSV are denoted by red and green spheres, respectively. The cyan structure is RdRp of SARS-Cov-2, the blue one is RdRp of PRRSV.

same positions as residues of RdRp of SARS-CoV-2 are Lys338, Asp395, Ser398, Thr543, Ile545, Ser550, and GLY553, (green sticks in figure 26) respectively, Only Asp395 (Sphere in green) of RdRp of PRRSV corresponds to Asp618 (Sphere in red) of RdRp of SARS-CoV-2 (Figure 26). The low number of identical amino acids present at the same positions may explain ribavirin's inhibition of PRRSV due to its binding to these residues at the active pocket of RdRp of PRRSV. However, only Asp395 of RdRp of PRRSV being the same as Asp618 of RdRp of SARS-CoV-2 may not be sufficient for ribavirin to bind to RdRp of PRRSV. Therefore, ribavirin's inhibition of PRRSV may not solely be due to its binding to RdRp, as it exhibits varying mechanisms on different

viruses.

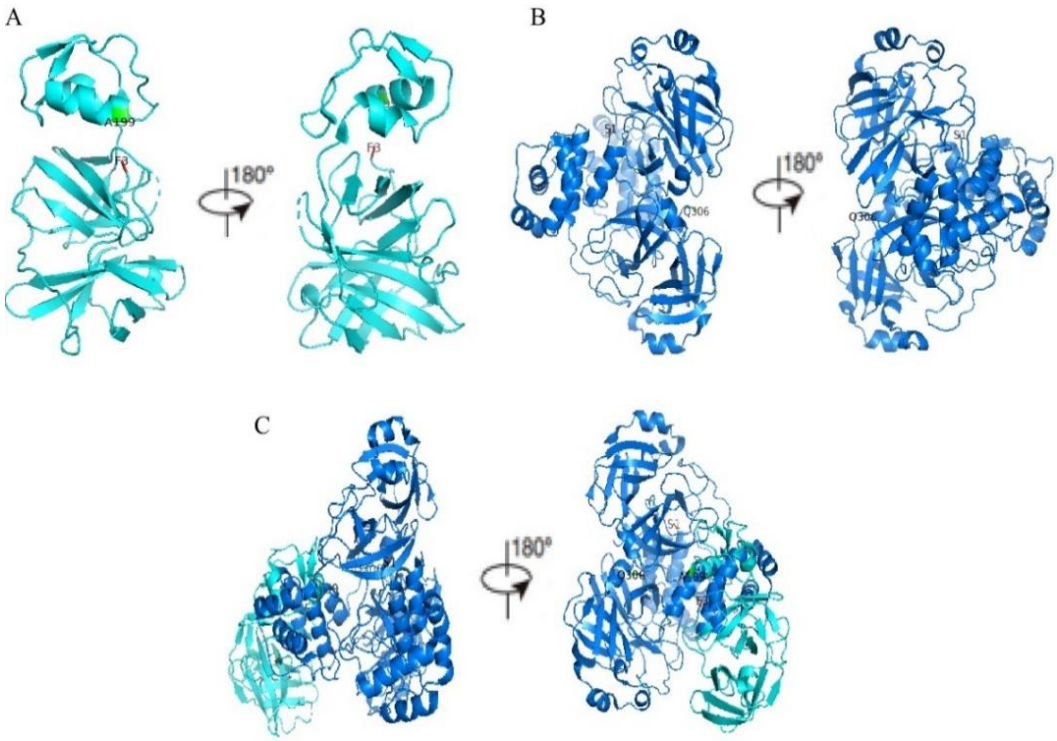

Figure 27 Comparison of crystal conformation of M^{pro} of PRRSV to M^{pro} of SARS-Cov-2
(A) The crystal conformation of the Mpro of PRRSV and its reversed side (PDB: 3fan). (B) The crystal conformation of the Mpro of SARS-CoV-2 and its reversed side (PDB: 6wtm). (C) The aligned crystal conformations of the Mpro of PRRSV and SARS-CoV-2, along with their respective reversed sides, are compared.

To elucidate why GC376, an inhibitor of the main protease (Mpro) inhibits replication of coronaviruses but not of PRRSV, I aligned the crystal structures of M^{pro} from coronavirus and PRRSV, both obtained from the PDB database (PRRSV: 3fan; Coronavirus: 6wtm) (Figure 27A and B). The results reveal an RMSD value of 7.952Å (Figure 27C), indicating significant structural differences between the two. This may explain why GC376 inhibits the replication of coronaviruses but not PRRSV.

5 Summary

The porcine reproductive and respiratory syndrome virus (PRRSV), an Arterivirus stands as one of the most impactful infectious pathogens, causing substantial economic losses in the swine industry. The minor glycoprotein Gp3 possesses an unusual hairpin-like membrane topology. The N- and C-terminus are exposed to the outside of the virus particle and anchoring to the membrane is achieved by an amphiphilic helix. The objectives of this study were to investigate the influence of the amphiphilic helix and the C-terminus of GP3 on viral replication in cell culture and to investigate whether the amphiphilic helix can be replaced by another amphiphilic helix with the same properties.

I demonstrate that deletion of the C-terminal region leads to a slowdown in virus growth compared to the wild-type virus. Notably, the virus regains the C-terminus of GP3 after serial passage in cell culture. Moreover, substituting amino acids in the hydrophilic face of the helix with alanine results in the failure to rescue the virus, while the exchange of hydrophilic amino acids with more hydrophobic ones either causes virus rescue failure or strong reduction in virus titer. Additionally, swapping the position of two pairs of amino acid within the amphiphilic helix, which maintains its hydrophobicity and amphiphilic character, prevents rescue of infectious virus particles. Intriguingly, despite these alterations, the amphiphilic helix with substituted amino acids retains its binding capacity to membranes. This underscores that the amphiphilic helix cannot be replaced by another amphiphilic helix with similar biophysical properties without affecting the virus's behavior.

Finally, five inhibitors were tested on PRRSV-1 and PRRSV-2 replication and it was shown that Remdesivir, GS-441524, EIDD-2801 and Ribavirin effectively inhibit virus replication whereas GC376 have no effect.

6 Zusammenfassung:

Struktur- und Funktionsforschung des Glykoproteins 3 des Porcinen Reproduktions- und Atemwegssyndrom-Viru

Das porzine reproduktive und respiratorische Syndromvirus (PRRSV), ein Arterivirus, gilt als einer der folgenschwersten infektiösen Pathogene, das beträchtliche wirtschaftliche Verluste in der Schweineindustrie verursacht. Das kleine Glykoprotein Gp3' besitzt eine ungewöhnliche haarförmige Membrantopologie. Der N- und C-Terminus sind außen am Viruspartikel freigelegt, und die Verankerung in der Membran wird durch eine amphiphile Helix erreicht. Die Ziele dieser Studie sind die Untersuchung des Einflusses der amphiphilen Helix und des C-Terminus von GP3 auf die virale Replikation in Zellkultur und die Untersuchung, ob die amphiphile Helix durch eine andere amphiphile Helix mit den gleichen Eigenschaften ersetzt werden kann. Wir zeigen, dass die Deletion des C-terminalen Bereichs zu einer Verlangsamung des Viruswachstums im Vergleich zum Wildtypvirus führt. Bemerkenswerterweise gewinnt das Virus nach wiederholter Passage in der Zellkultur den C-Terminus von GP3 zurück. Darüber hinaus führt die Substitution von Aminosäuren auf der hydrophilen Seite der Helix durch Alanin zum Versagen der Virusrettung, während der Austausch von hydrophilen Aminosäuren durch hydrophobere entweder zum Versagen der Virusrettung oder zu einer starken Reduktion der Virusmenge führt. Darüber hinaus verhindert der Austausch der Position von zwei Paaren von Aminosäuren innerhalb der amphiphilen Helix, die ihre Hydrophobie und amphiphilen Charakter beibehält, die Rettung infektiöser Viruspartikel. Interessanterweise behält die amphiphile Helix mit substituierten Aminosäuren trotz dieser Veränderungen ihre Bindungsfähigkeit an Membranen bei. Dies unterstreicht, dass die amphiphile Helix nicht durch eine andere amphiphile Helix mit ähnlichen biophysikalischen Eigenschaften ersetzt werden kann, ohne das Verhalten des Virus zu beeinträchtigen. Schließlich wurden fünf Inhibitoren auf PRRSV-1 und PRRSV-2 getestet, es wurde gezeigt, dass Remdesivir, GS-441524, EIDD-2801 und Ribavirin die Virusreplikation effektiv hemmen, was potenzielle

klinische Behandlungsmittel für PRRSV sein könnten, und dass GC376 keine Auswirkungen auf die Virusreplikation hat.

7 References

Agostini, M. L., Andres, E. L., Sims, A. C., Graham, R. L., Sheahan, T. P., Lu, X., . . . Denison, M. R. (2018). Coronavirus Susceptibility to the Antiviral Remdesivir (GS-5734) Is Mediated by the Viral Polymerase and the Proofreading Exoribonuclease. *mBio, 9*(2). doi:10.1128/mBio.00221-18

Agostini, M. L., Pruijssers, A. J., Chappell, J. D., Gribble, J., Lu, X., Andres, E. L., . . . Denison, M. R. (2019). Small-Molecule Antiviral β-d-N(4)-Hydroxycytidine Inhibits a Proofreading-Intact Coronavirus with a High Genetic Barrier to Resistance. *J Virol, 93*(24). doi:10.1128/jvi.01348-19

Almagro Armenteros, J. J., Tsirigos, K. D., Sønderby, C. K., Petersen, T. N., Winther, O., Brunak, S., . . . Nielsen, H. (2019). SignalP 5.0 improves signal peptide predictions using deep neural networks. *Nat Biotechnol, 37*(4), 420-423. doi:10.1038/s41587-019-0036-z

Amara, A., Penchala, S. D., Else, L., Hale, C., FitzGerald, R., Walker, L., . . . Khoo, S. (2021). The development and validation of a novel LC-MS/MS method for the simultaneous quantification of Molnupiravir and its metabolite ß-d-N4-hydroxycytidine in human plasma and saliva. *J Pharm Biomed Anal, 206*, 114356. doi:10.1016/j.jpba.2021.114356

Balasuriya, U. B., Go, Y. Y., & MacLachlan, N. J. (2013). Equine arteritis virus. *Vet Microbiol, 167*(1-2), 93-122. doi:10.1016/j.vetmic.2013.06.015

Balasuriya, U. B., & MacLachlan, N. J. (2004). The immune response to equine arteritis virus: potential lessons for other arteriviruses. *Vet Immunol Immunopathol, 102*(3), 107-129. doi:10.1016/j.vetimm.2004.09.003

Bautista, E. M., Meulenberg, J. J., Choi, C. S., & Molitor, T. W. (1996). Structural polypeptides of the American (VR-2332) strain of porcine reproductive and respiratory syndrome virus. *Arch Virol, 141*(7), 1357-1365. doi:10.1007/bf01718837

Beigel, J. H., Bao, Y., Beeler, J., Manosuthi, W., Slandzicki, A., Dar, S. M., . . . Davey, R. T. (2017). Oseltamivir, amantadine, and ribavirin combination antiviral therapy versus oseltamivir monotherapy for the treatment of influenza: a multicentre, double-blind, randomised phase 2 trial. *Lancet Infect Dis, 17*(12), 1255-1265. doi:10.1016/s1473-3099(17)30476-0

Benfield, D. A., Nelson, E., Collins, J. E., Harris, L., Goyal, S. M., Robison, D., . . . Chladek, D. (1992). Characterization of swine infertility and respiratory syndrome (SIRS) virus (isolate ATCC VR-2332). *J Vet Diagn Invest, 4*(2), 127-133.

Brockmeier, S. L., Palmer, M. V., & Bolin, S. R. (2000). Effects of intranasal inoculation of porcine reproductive and respiratory syndrome virus, Bordetella bronchiseptica, or a combination of both organisms in pigs. *Am J Vet Res, 61*(8), 892-899. doi:10.2460/ajvr.2000.61.892

Bryans, J. T., Crowe, M. E., Doll, E. R., & McCollum, W. H. (1957). Isolation of a filterable agent causing arteritis of horses and abortion by mares; its differentiation from the equine abortion (influenza) virus. *Cornell Vet, 47*(1), 3-41.

Calvert, J. G., Slade, D. E., Shields, S. L., Jolie, R., Mannan, R. M., Ankenbauer, R. G., & Welch, S. K. (2007). CD163 expression confers susceptibility to porcine reproductive and respiratory syndrome viruses. *J Virol, 81*(14), 7371-7379. doi:10.1128/jvi.00513-07

Chen, J. Z., Wang, Q., Bai, Y., Wang, B., Zhao, H. Y., Peng, J. M., . . . Tong, G. Z. (2014). Identification of two dominant linear epitopes on the GP3 protein of highly pathogenic porcine

reproductive and respiratory syndrome virus (HP-PRRSV). *Res Vet Sci, 97*(2), 238-243. doi:S0034-5288(14)00213-6 [pii]
10.1016/j.rvsc.2014.07.011

Chen, N., Cao, Z., Yu, X., Deng, X., Zhao, T., Wang, L., . . . Tian, K. (2011). Emergence of novel European genotype porcine reproductive and respiratory syndrome virus in mainland China. *J Gen Virol, 92*(Pt 4), 880-892. doi:10.1099/vir.0.027995-0

Cho, A., Saunders, O. L., Butler, T., Zhang, L., Xu, J., Vela, J. E., . . . Kim, C. U. (2012). Synthesis and antiviral activity of a series of 1'-substituted 4-aza-7,9-dideazaadenosine C-nucleosides. *Bioorg Med Chem Lett, 22*(8), 2705-2707. doi:10.1016/j.bmcl.2012.02.105

Christopher-Hennings, J., Nelson, E. A., Althouse, G. C., & Lunney, J. (2008). Comparative antiviral and proviral factors in semen and vaccines for preventing viral dissemination from the male reproductive tract and semen. *Anim Health Res Rev, 9*(1), 59-69. doi:10.1017/s1466252307001387

Ciechanover, A. (1998). The ubiquitin-proteasome pathway: on protein death and cell life. *Embo j, 17*(24), 7151-7160. doi:10.1093/emboj/17.24.7151

Crotty, S., Cameron, C. E., & Andino, R. (2001). RNA virus error catastrophe: direct molecular test by using ribavirin. *Proc Natl Acad Sci U S A, 98*(12), 6895-6900. doi:10.1073/pnas.111085598

Das, P. B., Dinh, P. X., Ansari, I. H., de Lima, M., Osorio, F. A., & Pattnaik, A. K. (2010). The minor envelope glycoproteins GP2a and GP4 of porcine reproductive and respiratory syndrome virus interact with the receptor CD163. *J Virol, 84*(4), 1731-1740. doi:10.1128/jvi.01774-09

Das, P. B., Vu, H. L., Dinh, P. X., Cooney, J. L., Kwon, B., Osorio, F. A., & Pattnaik, A. K. (2011). Glycosylation of minor envelope glycoproteins of porcine reproductive and respiratory syndrome virus in infectious virus recovery, receptor interaction, and immune response. *Virology, 410*(2), 385-394. doi:10.1016/j.virol.2010.12.002

de Lima, M., Ansari, I. H., Das, P. B., Ku, B. J., Martinez-Lobo, F. J., Pattnaik, A. K., & Osorio, F. A. (2009). GP3 is a structural component of the PRRSV type II (US) virion. *Virology, 390*(1), 31-36. doi:10.1016/j.virol.2009.04.017

de Vries, A. A., Chirnside, E. D., Horzinek, M. C., & Rottier, P. J. (1992). Structural proteins of equine arteritis virus. *J Virol, 66*(11), 6294-6303. doi:10.1128/jvi.66.11.6294-6303.1992

de Vries, A. A., Raamsman, M. J., van Dijk, H. A., Horzinek, M. C., & Rottier, P. J. (1995). The small envelope glycoprotein (GS) of equine arteritis virus folds into three distinct monomers and a disulfide-linked dimer. *J Virol, 69*(6), 3441-3448. doi:10.1128/jvi.69.6.3441-3448.1995

Dea, S., Gagnon, C. A., Mardassi, H., Pirzadeh, B., & Rogan, D. (2000). Current knowledge on the structural proteins of porcine reproductive and respiratory syndrome (PRRS) virus: comparison of the North American and European isolates. *Arch Virol, 145*(4), 659-688.

Ding, G., Liu, J., Shao, Q., Wang, B., Feng, J., Li, Y., . . . Xiao, Y. (2020). Porcine Reproductive and Respiratory Syndrome Virus Structural Protein GP3 Regulates Claudin 4 To Facilitate the Early Stages of Infection. *J Virol, 94*(20). doi:10.1128/jvi.00124-20

Doan, D. N., & Dokland, T. (2003). Structure of the nucleocapsid protein of porcine reproductive and respiratory syndrome virus. *Structure, 11*(11), 1445-1451. doi:10.1016/j.str.2003.09.018

Dobson, C. M. (2003). Protein folding and misfolding. *Nature, 426*(6968), 884-890. doi:10.1038/nature02261

Dokland, T. (2010). The structural biology of PRRSV. *Virus Res, 154*(1-2), 86-97. doi:10.1016/j.virusres.2010.07.029

Dunowska, M., Biggs, P. J., Zheng, T., & Perrott, M. R. (2012). Identification of a novel nidovirus associated with a neurological disease of the Australian brushtail possum (Trichosurus vulpecula). *Vet Microbiol, 156*(3-4), 418-424. doi:10.1016/j.vetmic.2011.11.013

Eastman, R. T., Roth, J. S., Brimacombe, K. R., Simeonov, A., Shen, M., Patnaik, S., & Hall, M. D. (2020). Remdesivir: A Review of Its Discovery and Development Leading to Emergency Use Authorization for Treatment of COVID-19. *ACS Cent Sci, 6*(5), 672-683. doi:10.1021/acscentsci.0c00489

Eisenberg, D., Weiss, R. M., & Terwilliger, T. C. (1982). The helical hydrophobic moment: a measure of the amphiphilicity of a helix. *Nature, 299*(5881), 371-374. doi:10.1038/299371a0

Elfiky, A. A. (2020). Ribavirin, Remdesivir, Sofosbuvir, Galidesivir, and Tenofovir against SARS-CoV-2 RNA dependent RNA polymerase (RdRp): A molecular docking study. *Life Sci, 253*, 117592. doi:10.1016/j.lfs.2020.117592

Faaberg, K., Balasuriya, U., Brinton, M., Gorbalenya, A., Leung, F., Nauwynck, H., . . . Yoo, D. J. V. t. N. r. o. t. i. c. o. t. o. v. E. A. P., Amsterdam. (2012). Family arteriviridae. 796-805.

Faaberg, K. S., Balasuriya, U. B., Brinton, M. A., Gorbalenya, A. E., & Yoo, D. (2012). Family Arteriviridae.

Faaberg, K. S., Even, C., Palmer, G. A., & Plagemann, P. G. (1995). Disulfide bonds between two envelope proteins of lactate dehydrogenase-elevating virus are essential for viral infectivity. *J Virol, 69*(1), 613-617. doi:10.1128/jvi.69.1.613-617.1995

Faaberg, K. S., & Plagemann, P. G. (1997). ORF 3 of lactate dehydrogenase-elevating virus encodes a soluble, nonstructural, highly glycosylated, and antigenic protein. *Virology, 227*(1), 245-251. doi:10.1006/viro.1996.8310

Feng, W., Laster, S. M., Tompkins, M., Brown, T., Xu, J. S., Altier, C., . . . McCaw, M. B. (2001). In utero infection by porcine reproductive and respiratory syndrome virus is sufficient to increase susceptibility of piglets to challenge by Streptococcus suis type II. *J Virol, 75*(10), 4889-4895. doi:10.1128/jvi.75.10.4889-4895.2001

Ferner, R. E., & Aronson, J. K. (2020). Remdesivir in covid-19. *Bmj, 369*, m1610. doi:10.1136/bmj.m1610

Firth, A. E., Zevenhoven-Dobbe, J. C., Wills, N. M., Go, Y. Y., Balasuriya, U. B. R., Atkins, J. F., . . . Posthuma, C. C. (2011). Discovery of a small arterivirus gene that overlaps the GP5 coding sequence and is important for virus production. *J Gen Virol, 92*(Pt 5), 1097-1106. doi:10.1099/vir.0.029264-0

Fu, L., Ye, F., Feng, Y., Yu, F., Wang, Q., Wu, Y., . . . Gao, G. F. (2020). Both Boceprevir and GC376 efficaciously inhibit SARS-CoV-2 by targeting its main protease. *Nat Commun, 11*(1), 4417. doi:10.1038/s41467-020-18233-x

Garcia, B., Sharma, N., Johnson, K., Salgado, J., & Wille, K. (2019). Clinical Outcomes of Paramyxovirus Infections in Lung Transplant Recipients Treated With Oral Ribavirin: A Two-Center Case Series. *Exp Clin Transplant, 17*(3), 393-397. doi:10.6002/ect.2017.0133

Gautier, R., Douguet, D., Antonny, B., & Drin, G. (2008). HELIQUEST: a web server to screen sequences with specific alpha-helical properties. *Bioinformatics, 24*(18), 2101-2102. doi:10.1093/bioinformatics/btn392

Gonin, P., Mardassi, H., Gagnon, C. A., Massie, B., & Dea, S. (1998). A nonstructural and antigenic glycoprotein is encoded by ORF3 of the IAF-Klop strain of porcine reproductive and respiratory syndrome virus. *Arch Virol, 143*(10), 1927-1940. doi:10.1007/s007050050430

Gordon, C. J., Tchesnokov, E. P., Feng, J. Y., Porter, D. P., & Götte, M. (2020). The antiviral compound remdesivir potently inhibits RNA-dependent RNA polymerase from Middle East respiratory syndrome coronavirus. *J Biol Chem, 295*(15), 4773-4779. doi:10.1074/jbc.AC120.013056

Gordon, C. J., Tchesnokov, E. P., Woolner, E., Perry, J. K., Feng, J. Y., Porter, D. P., & Götte, M. (2020). Remdesivir is a direct-acting antiviral that inhibits RNA-dependent RNA polymerase from severe acute respiratory syndrome coronavirus 2 with high potency. *J Biol Chem, 295*(20), 6785-6797. doi:10.1074/jbc.RA120.013679

Goswami, D. (2021). Comparative assessment of RNA-dependent RNA polymerase (RdRp) inhibitors under clinical trials to control SARS-CoV2 using rigorous computational workflow. *RSC Adv, 11*(46), 29015-29028. doi:10.1039/d1ra04460e

Graci, J. D., & Cameron, C. E. (2006). Mechanisms of action of ribavirin against distinct viruses. *Rev Med Virol, 16*(1), 37-48. doi:10.1002/rmv.483

Guo, C., Zhu, Z., Wang, X., Chen, Y., & Liu, X. (2017). Pyrithione inhibits porcine reproductive and respiratory syndrome virus replication through interfering with NF-κB and heparanase. *Vet Microbiol, 201*, 231-239. doi:10.1016/j.vetmic.2017.01.033

Halbur, P. G., Paul, P. S., Frey, M. L., Landgraf, J., Eernisse, K., Meng, X. J., . . . Rathje, J. A. (1996). Comparison of the antigen distribution of two US porcine reproductive and respiratory syndrome virus isolates with that of the Lelystad virus. *Vet Pathol, 33*(2), 159-170. doi:10.1177/030098589603300205

Halbur, P. G., Paul, P. S., Frey, M. L., Landgraf, J., Eernisse, K., Meng, X. J., . . . Rathje, J. A. (1995). Comparison of the pathogenicity of two US porcine reproductive and respiratory syndrome virus isolates with that of the Lelystad virus. *Vet Pathol, 32*(6), 648-660. doi:10.1177/030098589503200606

Hilgenfeld, R., & Peiris, M. (2013). From SARS to MERS: 10 years of research on highly pathogenic human coronaviruses. *Antiviral Res, 100*(1), 286-295. doi:10.1016/j.antiviral.2013.08.015

Holtkamp, D. J., Kliebenstein, J. B., Neumann, E. J., Zimmerman, J. J., Haley, C. A. J. J. o. S. H., & Production. (2013). Assessment of the economic impact of porcine reproductive and respiratory syndrome virus on United States pork producers. *21*(2), 72-84.

Ikari, A., Atomi, K., Takiguchi, A., Yamazaki, Y., Miwa, M., & Sugatani, J. (2009). Epidermal growth factor increases claudin-4 expression mediated by Sp1 elevation in MDCK cells. *Biochem Biophys Res Commun, 384*(3), 306-310. doi:10.1016/j.bbrc.2009.04.120

Johnson, C. R., Griggs, T. F., Gnanandarajah, J., & Murtaugh, M. P. (2011). Novel structural protein in porcine reproductive and respiratory syndrome virus encoded by an alternative ORF5 present in all arteriviruses. *J Gen Virol, 92*(Pt 5), 1107-1116. doi:10.1099/vir.0.030213-0

Johnson, W., Roof, M., Vaughn, E., Christopher-Hennings, J., Johnson, C. R., & Murtaugh, M. P. (2004). Pathogenic and humoral immune responses to porcine reproductive and

respiratory syndrome virus (PRRSV) are related to viral load in acute infection. *Vet Immunol Immunopathol, 102*(3), 233-247. doi:10.1016/j.vetimm.2004.09.010

Kabatek, A., & Veit, M. (2012). Folding and oligomerization of the gp2b/gp3/gp4 spike proteins of equine arteritis virus in vitro. *Viruses, 4*(3), 414-423. doi:10.3390/v4030414

Kabinger, F., Stiller, C., Schmitzová, J., Dienemann, C., Kokic, G., Hillen, H. S., . . . Cramer, P. (2021). Mechanism of molnupiravir-induced SARS-CoV-2 mutagenesis. *Nat Struct Mol Biol, 28*(9), 740-746. doi:10.1038/s41594-021-00651-0

Kappes, M. A., & Faaberg, K. S. (2015). PRRSV structure, replication and recombination: Origin of phenotype and genotype diversity. *Virology, 479-480*, 475-486. doi:10.1016/j.virol.2015.02.012

Kappes, M. A., Miller, C. L., & Faaberg, K. S. (2013). Highly divergent strains of porcine reproductive and respiratory syndrome virus incorporate multiple isoforms of nonstructural protein 2 into virions. *J Virol, 87*(24), 13456-13465. doi:10.1128/jvi.02435-13

Kapur, V., Elam, M. R., Pawlovich, T. M., & Murtaugh, M. P. (1996). Genetic variation in porcine reproductive and respiratory syndrome virus isolates in the midwestern United States. *J Gen Virol, 77 (Pt 6)*, 1271-1276. doi:10.1099/0022-1317-77-6-1271

Keffaber, K. K. J. a. a. s. p. n. (1989). Reproductive failure of unknown etiology.

Khan, F. I., Kang, T., Ali, H., & Lai, D. (2021). Remdesivir Strongly Binds to RNA-Dependent RNA Polymerase, Membrane Protein, and Main Protease of SARS-CoV-2: Indication From Molecular Modeling and Simulations. *Front Pharmacol, 12*, 710778. doi:10.3389/fphar.2021.710778

Lauck, M., Hyeroba, D., Tumukunde, A., Weny, G., Lank, S. M., Chapman, C. A., . . . Goldberg, T. L. (2011). Novel, divergent simian hemorrhagic fever viruses in a wild Ugandan red colobus monkey discovered using direct pyrosequencing. *PLoS One, 6*(4), e19056. doi:10.1371/journal.pone.0019056

Lee, C., & Yoo, D. (2005). Cysteine residues of the porcine reproductive and respiratory syndrome virus small envelope protein are non-essential for virus infectivity. *J Gen Virol, 86*(Pt 11), 3091-3096. doi:10.1099/vir.0.81160-0

Lee, C., & Yoo, D. (2006). The small envelope protein of porcine reproductive and respiratory syndrome virus possesses ion channel protein-like properties. *Virology, 355*(1), 30-43. doi:10.1016/j.virol.2006.07.013

Leyssen, P., De Clercq, E., & Neyts, J. (2006). The anti-yellow fever virus activity of ribavirin is independent of error-prone replication. *Mol Pharmacol, 69*(4), 1461-1467. doi:10.1124/mol.105.020057

Li, C., Zhuang, J., Wang, J., Han, L., Sun, Z., Xiao, Y., . . . Tian, K. (2016). Outbreak Investigation of NADC30-Like PRRSV in South-East China. *Transbound Emerg Dis, 63*(5), 474-479. doi:10.1111/tbed.12530

Li, G., Jiang, P., Li, Y., Wang, X., Huang, J., Bai, J., . . . Zeshan, B. (2009). Inhibition of porcine reproductive and respiratory syndrome virus replication by adenovirus-mediated RNA interference both in porcine alveolar macrophages and swine. *Antiviral Res, 82*(3), 157-165. doi:10.1016/j.antiviral.2009.02.202

Lin, Z., Li, Y., Gong, G., Xia, Y., Wang, C., Chen, Y., . . . Zhu, B. (2018). Restriction of H1N1 influenza virus infection by selenium nanoparticles loaded with ribavirin via resisting caspase-3 apoptotic pathway. *Int J Nanomedicine, 13*, 5787-5797. doi:10.2147/ijn.S177658

Lo, M. K., Jordan, R., Arvey, A., Sudhamsu, J., Shrivastava-Ranjan, P., Hotard, A. L., . . . Spiropoulou, C. F. (2017). GS-5734 and its parent nucleoside analog inhibit Filo-, Pneumo-, and Paramyxoviruses. *Sci Rep, 7*, 43395. doi:10.1038/srep43395

Loemba, H. D., Mounir, S., Mardassi, H., Archambault, D., & Dea, S. (1996). Kinetics of humoral immune response to the major structural proteins of the porcine reproductive and respiratory syndrome virus. *Arch Virol, 141*(3-4), 751-761. doi:10.1007/bf01718333

Long, F., Zhang, M., Yang, X., Liang, X., Su, L., An, T., . . . Chen, J. (2022). The Antimalaria Drug Artesunate Inhibits Porcine Reproductive and Respiratory Syndrome Virus Replication by Activating AMPK and Nrf2/HO-1 Signaling Pathways. *J Virol, 96*(3), e0148721. doi:10.1128/jvi.01487-21

Loula, T. J. A. P. (1991). Mystery pig disease.

Lunney, J. K., Fang, Y., Ladinig, A., Chen, N., Li, Y., Rowland, B., & Renukaradhya, G. J. (2016). Porcine Reproductive and Respiratory Syndrome Virus (PRRSV): Pathogenesis and Interaction with the Immune System. *Annu Rev Anim Biosci, 4*, 129-154. doi:10.1146/annurev-animal-022114-111025

Ma, C., Sacco, M. D., Hurst, B., Townsend, J. A., Hu, Y., Szeto, T., . . . Wang, J. (2020). Boceprevir, GC-376, and calpain inhibitors II, XII inhibit SARS-CoV-2 viral replication by targeting the viral main protease. *Cell Res, 30*(8), 678-692. doi:10.1038/s41422-020-0356-z

Malone, B., & Campbell, E. A. (2021). Molnupiravir: coding for catastrophe. *Nat Struct Mol Biol, 28*(9), 706-708. doi:10.1038/s41594-021-00657-8

Mardassi, H., Gonin, P., Gagnon, C. A., Massie, B., & Dea, S. (1998). A subset of porcine reproductive and respiratory syndrome virus GP3 glycoprotein is released into the culture medium of cells as a non-virion-associated and membrane-free (soluble) form. *J Virol, 72*(8), 6298-6306.

Mardassi, H., Massie, B., & Dea, S. (1996). Intracellular synthesis, processing, and transport of proteins encoded by ORFs 5 to 7 of porcine reproductive and respiratory syndrome virus. *Virology, 221*(1), 98-112. doi:10.1006/viro.1996.0356

Matczuk, A. K., Kunec, D., & Veit, M. (2013). Co-translational processing of glycoprotein 3 from equine arteritis virus: N-glycosylation adjacent to the signal peptide prevents cleavage. *J Biol Chem, 288*(49), 35396-35405. doi:M113.505420 [pii]

10.1074/jbc.M113.505420

Meng, X. J. (2000). Heterogeneity of porcine reproductive and respiratory syndrome virus: implications for current vaccine efficacy and future vaccine development. *Vet Microbiol, 74*(4), 309-329. doi:10.1016/s0378-1135(00)00196-6

Mengeling, W. L., Vorwald, A. C., Lager, K. M., & Brockmeier, S. L. (1996). Comparison among strains of porcine reproductive and respiratory syndrome virus for their ability to cause reproductive failure. *Am J Vet Res, 57*(6), 834-839.

Meulenberg, J. J. (2000). PRRSV, the virus. *Vet Res, 31*(1), 11-21. doi:10.1051/vetres:2000103

Meulenberg, J. J., Petersen-den Besten, A., De Kluyver, E. P., Moormann, R. J., Schaaper, W. M., & Wensvoort, G. (1995). Characterization of proteins encoded by ORFs 2 to 7 of Lelystad virus. *Virology, 206*(1), 155-163. doi:S0042-6822(95)80030-1 [pii]

Meulenberg, J. J., van Nieuwstadt, A. P., van Essen-Zandbergen, A., & Langeveld, J. P. (1997). Posttranslational processing and identification of a neutralization domain of the GP4

protein encoded by ORF4 of Lelystad virus. *J Virol, 71*(8), 6061-6067. doi:10.1128/jvi.71.8.6061-6067.1997

Molenkamp, R., van Tol, H., Rozier, B. C. D., van der Meer, Y., Spaan, W. J. M., & Snijder, E. J. (2000). The arterivirus replicase is the only viral protein required for genome replication and subgenomic mRNA transcription. *J Gen Virol, 81*(Pt 10), 2491-2496. doi:10.1099/0022-1317-81-10-2491

Murphy, B. G., Perron, M., Murakami, E., Bauer, K., Park, Y., Eckstrand, C., . . . Pedersen, N. C. (2018). The nucleoside analog GS-441524 strongly inhibits feline infectious peritonitis (FIP) virus in tissue culture and experimental cat infection studies. *Vet Microbiol, 219*, 226-233. doi:10.1016/j.vetmic.2018.04.026

Murtaugh, M. P., Elam, M. R., & Kakach, L. T. (1995). Comparison of the structural protein coding sequences of the VR-2332 and Lelystad virus strains of the PRRS virus. *Arch Virol, 140*(8), 1451-1460. doi:10.1007/bf01322671

Notkins, A. L., & Scheele, C. (1963). AN INFECTIOUS NUCLEIC ACID FROM THE LACTIC DEHYDROGENASE AGENT. *Virology, 20*, 640-642. doi:10.1016/0042-6822(63)90291-5

Owen, K. E., & Kuhn, R. J. (1997). Alphavirus budding is dependent on the interaction between the nucleocapsid and hydrophobic amino acids on the cytoplasmic domain of the E2 envelope glycoprotein. *Virology, 230*(2), 187-196. doi:10.1006/viro.1997.8480

Painter, W. P., Holman, W., Bush, J. A., Almazedi, F., Malik, H., Eraut, N., . . . Painter, G. R. (2021). Human Safety, Tolerability, and Pharmacokinetics of Molnupiravir, a Novel Broad-Spectrum Oral Antiviral Agent with Activity Against SARS-CoV-2. *Antimicrob Agents Chemother, 65*(5). doi:10.1128/aac.02428-20

Pedersen, N. C., Kim, Y., Liu, H., Galasiti Kankanamalage, A. C., Eckstrand, C., Groutas, W. C., . . . Chang, K. O. (2018). Efficacy of a 3C-like protease inhibitor in treating various forms of acquired feline infectious peritonitis. *J Feline Med Surg, 20*(4), 378-392. doi:10.1177/1098612x17729626

Pedersen, N. C., Perron, M., Bannasch, M., Montgomery, E., Murakami, E., Liepnieks, M., & Liu, H. (2019). Efficacy and safety of the nucleoside analog GS-441524 for treatment of cats with naturally occurring feline infectious peritonitis. *J Feline Med Surg, 21*(4), 271-281. doi:10.1177/1098612x19825701

Perera, K. D., Galasiti Kankanamalage, A. C., Rathnayake, A. D., Honeyfield, A., Groutas, W., Chang, K. O., & Kim, Y. (2018). Protease inhibitors broadly effective against feline, ferret and mink coronaviruses. *Antiviral Res, 160*, 79-86. doi:10.1016/j.antiviral.2018.10.015

Pruijssers, A. J., George, A. S., Schäfer, A., Leist, S. R., Gralinksi, L. E., Dinnon, K. H., 3rd, . . . Sheahan, T. P. (2020). Remdesivir Inhibits SARS-CoV-2 in Human Lung Cells and Chimeric SARS-CoV Expressing the SARS-CoV-2 RNA Polymerase in Mice. *Cell Rep, 32*(3), 107940. doi:10.1016/j.celrep.2020.107940

Ramírez-Olivencia, G., Estébanez, M., Membrillo, F. J., & Ybarra, M. D. C. (2019). Use of ribavirin in viruses other than hepatitis C. A review of the evidence. *Enferm Infecc Microbiol Clin (Engl Ed), 37*(9), 602-608. doi:10.1016/j.eimc.2018.05.008

Rapoport, T. A., Jungnickel, B., & Kutay, U. (1996). Protein transport across the eukaryotic endoplasmic reticulum and bacterial inner membranes. *Annu Rev Biochem, 65*, 271-303. doi:10.1146/annurev.bi.65.070196.001415

Rathnayake, A. D., Zheng, J., Kim, Y., Perera, K. D., Mackin, S., Meyerholz, D. K., . . . Chang, K. O. (2020). 3C-like protease inhibitors block coronavirus replication in vitro and improve survival in MERS-CoV-infected mice. *Sci Transl Med, 12*(557). doi:10.1126/scitranslmed.abc5332

Robinson, S. R., Abrahante, J. E., Johnson, C. R., & Murtaugh, M. P. (2013). Purifying selection in porcine reproductive and respiratory syndrome virus ORF5a protein influences variation in envelope glycoprotein 5 glycosylation. *Infect Genet Evol, 20*, 362-368. doi:10.1016/j.meegid.2013.09.022

Ron, D., & Walter, P. (2007). Signal integration in the endoplasmic reticulum unfolded protein response. *Nat Rev Mol Cell Biol, 8*(7), 519-529. doi:10.1038/nrm2199

Rosenke, K., Hansen, F., Schwarz, B., Feldmann, F., Haddock, E., Rosenke, R., . . . Jarvis, M. A. (2021). Orally delivered MK-4482 inhibits SARS-CoV-2 replication in the Syrian hamster model. *Nat Commun, 12*(1), 2295. doi:10.1038/s41467-021-22580-8

Rowland, R. R., Lawson, S., Rossow, K., & Benfield, D. A. (2003). Lymphoid tissue tropism of porcine reproductive and respiratory syndrome virus replication during persistent infection of pigs originally exposed to virus in utero. *Vet Microbiol, 96*(3), 219-235. doi:10.1016/j.vetmic.2003.07.006

Scavone, C., Brusco, S., Bertini, M., Sportiello, L., Rafaniello, C., Zoccoli, A., . . . Capuano, A. (2020). Current pharmacological treatments for COVID-19: What's next? *Br J Pharmacol, 177*(21), 4813-4824. doi:10.1111/bph.15072

Schleuning, M., Buxbaum-Conradi, H., Jäger, G., & Kolb, H. J. (2004). Intravenous ribavirin for eradication of respiratory syncytial virus (RSV) and adenovirus isolates from the respiratory and/or gastrointestinal tract in recipients of allogeneic hematopoietic stem cell transplants. *Hematol J, 5*(2), 135-144. doi:10.1038/sj.thj.6200358

Senga, K., Mostov, K. E., Mitaka, T., Miyajima, A., & Tanimizu, N. (2012). Grainyhead-like 2 regulates epithelial morphogenesis by establishing functional tight junctions through the organization of a molecular network among claudin3, claudin4, and Rab25. *Mol Biol Cell, 23*(15), 2845-2855. doi:10.1091/mbc.E12-02-0097

Shah, J. N., & Chemaly, R. F. (2011). Management of RSV infections in adult recipients of hematopoietic stem cell transplantation. *Blood, 117*(10), 2755-2763. doi:10.1182/blood-2010-08-263400

Sheahan, T. P., Sims, A. C., Graham, R. L., Menachery, V. D., Gralinski, L. E., Case, J. B., . . . Baric, R. S. (2017). Broad-spectrum antiviral GS-5734 inhibits both epidemic and zoonotic coronaviruses. *Sci Transl Med, 9*(396). doi:10.1126/scitranslmed.aal3653

Shi, X., Chang, Y., Zhang, X., Wang, L., Li, C., Jiang, K., . . . Zhang, G. (2015). Small interfering RNA targeting nonstructural protein1 α (nsp1α) of porcine reproductive and respiratory syndrome virus (PRRSV) can reduce the replication of PRRSV in MARC-145 cells. *Res Vet Sci, 99*, 215-217. doi:10.1016/j.rvsc.2015.01.015

Snijder, E. J., Dobbe, J. C., & Spaan, W. J. (2003). Heterodimerization of the two major envelope proteins is essential for arterivirus infectivity. *J Virol, 77*(1), 97-104. doi:10.1128/jvi.77.1.97-104.2003

Snijder, E. J., Kikkert, M., & Fang, Y. (2013). Arterivirus molecular biology and pathogenesis. *J Gen Virol, 94*(Pt 10), 2141-2163. doi:10.1099/vir.0.056341-0

Snijder, E. J., van Tol, H., Pedersen, K. W., Raamsman, M. J., & de Vries, A. A. (1999). Identification of a novel structural protein of arteriviruses. *J Virol, 73*(8), 6335-6345. doi:10.1128/jvi.73.8.6335-6345.1999

Snijder, E. J. J. S. I. o. V. (2002). Arterivirus.

Song, J., Shen, D., Cui, J., & Zhao, B. (2010). Accelerated evolution of PRRSV during recent outbreaks in China. *Virus Genes, 41*(2), 241-245. doi:10.1007/s11262-010-0507-2

Spilman, M. S., Welbon, C., Nelson, E., & Dokland, T. (2009). Cryo-electron tomography of porcine reproductive and respiratory syndrome virus: organization of the nucleocapsid. *J Gen Virol, 90*(Pt 3), 527-535. doi:10.1099/vir.0.007674-0

Sun, L., Li, Y., Liu, R., Wang, X., Gao, F., Lin, T., . . . Yuan, S. (2013). Porcine reproductive and respiratory syndrome virus ORF5a protein is essential for virus viability. *Virus Res, 171*(1), 178-185. doi:10.1016/j.virusres.2012.11.005

Tchesnokov, E. P., Feng, J. Y., Porter, D. P., & Götte, M. (2019). Mechanism of Inhibition of Ebola Virus RNA-Dependent RNA Polymerase by Remdesivir. *Viruses, 11*(4). doi:10.3390/v11040326

Thaa, B., Sinhadri, B. C., Tielesch, C., Krause, E., & Veit, M. (2013). Signal peptide cleavage from GP5 of PRRSV: a minor fraction of molecules retains the decoy epitope, a presumed molecular cause for viral persistence. *PLoS One, 8*(6), e65548. doi:10.1371/journal.pone.0065548

PONE-D-13-06268 [pii]

Thacker, E. L., Halbur, P. G., Ross, R. F., Thanawongnuwech, R., & Thacker, B. J. (1999). Mycoplasma hyopneumoniae potentiation of porcine reproductive and respiratory syndrome virus-induced pneumonia. *J Clin Microbiol, 37*(3), 620-627. doi:10.1128/jcm.37.3.620-627.1999

Thanawongnuwech, R., Thacker, E. L., & Halbur, P. G. (1998). Influence of pig age on virus titer and bactericidal activity of porcine reproductive and respiratory syndrome virus (PRRSV)-infected pulmonary intravascular macrophages (PIMs). *Vet Microbiol, 63*(2-4), 177-187. doi:10.1016/s0378-1135(98)00245-4

Tian, K., Yu, X., Zhao, T., Feng, Y., Cao, Z., Wang, C., . . . Gao, G. F. (2007). Emergence of fatal PRRSV variants: unparalleled outbreaks of atypical PRRS in China and molecular dissection of the unique hallmark. *PLoS One, 2*(6), e526. doi:10.1371/journal.pone.0000526

Van Breedam, W., Van Gorp, H., Zhang, J. Q., Crocker, P. R., Delputte, P. L., & Nauwynck, H. J. (2010). The M/GP(5) glycoprotein complex of porcine reproductive and respiratory syndrome virus binds the sialoadhesin receptor in a sialic acid-dependent manner. *PLoS Pathog, 6*(1), e1000730. doi:10.1371/journal.ppat.1000730

van der Linden, I. F., Voermans, J. J., van der Linde-Bril, E. M., Bianchi, A. T., & Steverink, P. J. (2003). Virological kinetics and immunological responses to a porcine reproductive and respiratory syndrome virus infection of pigs at different ages. *Vaccine, 21*(17-18), 1952-1957.

van Nieuwstadt, A. P., Meulenberg, J. J., van Essen-Zanbergen, A., Petersen-den Besten, A., Bende, R. J., Moormann, R. J., & Wensvoort, G. (1996). Proteins encoded by open reading frames 3 and 4 of the genome of Lelystad virus (Arteriviridae) are structural proteins of the virion. *J Virol, 70*(7), 4767-4772. doi:10.1128/jvi.70.7.4767-4772.1996

Veit, M., Matczuk, A. K., Sinhadri, B. C., Krause, E., & Thaa, B. (2014). Membrane proteins of arterivirus particles: structure, topology, processing and function. *Virus Res, 194*, 16-36. doi:S0168-1702(14)00397-9 [pii]
10.1016/j.virusres.2014.09.010

Verheije, M. H., Welting, T. J., Jansen, H. T., Rottier, P. J., & Meulenberg, J. J. (2002). Chimeric arteriviruses generated by swapping of the M protein ectodomain rule out a role of this domain in viral targeting. *Virology, 303*(2), 364-373. doi:10.1006/viro.2002.1711

Vu, H. L., Kwon, B., Yoon, K. J., Laegreid, W. W., Pattnaik, A. K., & Osorio, F. A. (2011). Immune evasion of porcine reproductive and respiratory syndrome virus through glycan shielding involves both glycoprotein 5 as well as glycoprotein 3. *J Virol, 85*(11), 5555-5564. doi:10.1128/jvi.00189-11

Vuong, W., Khan, M. B., Fischer, C., Arutyunova, E., Lamer, T., Shields, J., . . . Lemieux, M. J. (2020). Feline coronavirus drug inhibits the main protease of SARS-CoV-2 and blocks virus replication. *Nat Commun, 11*(1), 4282. doi:10.1038/s41467-020-18096-2

Wahl, A., Gralinski, L. E., Johnson, C. E., Yao, W., Kovarova, M., Dinnon, K. H., 3rd, . . . Garcia, J. V. (2021). SARS-CoV-2 infection is effectively treated and prevented by EIDD-2801. *Nature, 591*(7850), 451-457. doi:10.1038/s41586-021-03312-w

Wang, M., Cao, R., Zhang, L., Yang, X., Liu, J., Xu, M., . . . Xiao, G. (2020). Remdesivir and chloroquine effectively inhibit the recently emerged novel coronavirus (2019-nCoV) in vitro. *Cell Res, 30*(3), 269-271. doi:10.1038/s41422-020-0282-0

Wei, D., Hu, T., Zhang, Y., Zheng, W., Xue, H., Shen, J., . . . Aisa, H. A. (2021). Potency and pharmacokinetics of GS-441524 derivatives against SARS-CoV-2. *Bioorg Med Chem, 46*, 116364. doi:10.1016/j.bmc.2021.116364

Wei, Z., Tian, D., Sun, L., Lin, T., Gao, F., Liu, R., . . . Yuan, S. (2012). Influence of N-linked glycosylation of minor proteins of porcine reproductive and respiratory syndrome virus on infectious virus recovery and receptor interaction. *Virology, 429*(1), 1-11. doi:S0042-6822(12)00167-5

Welch, S. K., & Calvert, J. G. (2010). A brief review of CD163 and its role in PRRSV infection. *Virus Res, 154*(1-2), 98-103. doi:10.1016/j.virusres.2010.07.018

Welch, S. K., Jolie, R., Pearce, D. S., Koertje, W. D., Fuog, E., Shields, S. L., . . . Calvert, J. G. (2004). Construction and evaluation of genetically engineered replication-defective porcine reproductive and respiratory syndrome virus vaccine candidates. *Vet Immunol Immunopathol, 102*(3), 277-290. doi:10.1016/j.vetimm.2004.09.022

Wensvoort, G., Terpstra, C., Pol, J. M., ter Laak, E. A., Bloemraad, M., de Kluyver, E. P., . . . et al. (1991). Mystery swine disease in The Netherlands: the isolation of Lelystad virus. *Vet Q, 13*(3), 121-130. doi:10.1080/01652176.1991.9694296

Wieringa, R., De Vries, A. A., Post, S. M., & Rottier, P. J. (2003). Intra- and intermolecular disulfide bonds of the GP2b glycoprotein of equine arteritis virus: relevance for virus assembly and infectivity. *J Virol, 77*(24), 12996-13004. doi:10.1128/jvi.77.24.12996-13004.2003

Wieringa, R., de Vries, A. A., Raamsman, M. J., & Rottier, P. J. (2002). Characterization of two new structural glycoproteins, GP(3) and GP(4), of equine arteritis virus. *J Virol, 76*(21), 10829-10840.

Wieringa, R., de Vries, A. A., & Rottier, P. J. (2003). Formation of disulfide-linked complexes between the three minor envelope glycoproteins (GP2b, GP3, and GP4) of equine arteritis virus. *J Virol, 77*(11), 6216-6226. doi:10.1128/jvi.77.11.6216-6226.2003

Wieringa, R., de Vries, A. A., van der Meulen, J., Godeke, G. J., Onderwater, J. J., van Tol, H., . . . Rottier, P. J. (2004). Structural protein requirements in equine arteritis virus assembly. *J Virol, 78*(23), 13019-13027. doi:78/23/13019 [pii]

10.1128/JVI.78.23.13019-13027.2004

Wills, R. W., Doster, A. R., Galeota, J. A., Sur, J. H., & Osorio, F. A. (2003). Duration of infection and proportion of pigs persistently infected with porcine reproductive and respiratory syndrome virus. *J Clin Microbiol, 41*(1), 58-62. doi:10.1128/jcm.41.1.58-62.2003

Wills, R. W., Gray, J. T., Fedorka-Cray, P. J., Yoon, K. J., Ladely, S., & Zimmerman, J. J. (2000). Synergism between porcine reproductive and respiratory syndrome virus (PRRSV) and Salmonella choleraesuis in swine. *Vet Microbiol, 71*(3-4), 177-192. doi:10.1016/s0378-1135(99)00175-3

Wills, R. W., Zimmerman, J. J., Yoon, K. J., Swenson, S. L., McGinley, M. J., Hill, H. T., . . . Nelson, E. A. (1997). Porcine reproductive and respiratory syndrome virus: a persistent infection. *Vet Microbiol, 55*(1-4), 231-240. doi:10.1016/s0378-1135(96)01337-5

Wissink, E. H., Kroese, M. V., van Wijk, H. A., Rijsewijk, F. A., Meulenberg, J. J., & Rottier, P. J. (2005). Envelope protein requirements for the assembly of infectious virions of porcine reproductive and respiratory syndrome virus. *J Virol, 79*(19), 12495-12506. doi:79/19/12495 [pii]

10.1128/JVI.79.19.12495-12506.2005

Wissink, E. H. J., Kroese, M. V., Maneschijn-Bonsing, J. G., Meulenberg, J. J. M., van Rijn, P. A., Rijsewijk, F. A. M., & Rottier, P. J. M. (2004). Significance of the oligosaccharides of the porcine reproductive and respiratory syndrome virus glycoproteins GP2a and GP5 for infectious virus production. *J Gen Virol, 85*(Pt 12), 3715-3723. doi:10.1099/vir.0.80402-0

Wootton, S. K., & Yoo, D. (2003). Homo-oligomerization of the porcine reproductive and respiratory syndrome virus nucleocapsid protein and the role of disulfide linkages. *J Virol, 77*(8), 4546-4557. doi:10.1128/jvi.77.8.4546-4557.2003

Wu, W. H., Fang, Y., Farwell, R., Steffen-Bien, M., Rowland, R. R., Christopher-Hennings, J., & Nelson, E. A. (2001). A 10-kDa structural protein of porcine reproductive and respiratory syndrome virus encoded by ORF2b. *Virology, 287*(1), 183-191. doi:10.1006/viro.2001.1034

Wu, W. H., Fang, Y., Rowland, R. R., Lawson, S. R., Christopher-Hennings, J., Yoon, K. J., & Nelson, E. A. (2005). The 2b protein as a minor structural component of PRRSV. *Virus Res, 114*(1-2), 177-181. doi:10.1016/j.virusres.2005.06.014

Xie, J., Zhou, H., Cui, J., Chen, Y., Zhang, M., Deng, S., . . . Zhang, G. (2014). Inhibition of porcine reproductive and respiratory syndrome virus by specific siRNA targeting Nsp9 gene. *Infect Genet Evol, 28*, 64-70. doi:10.1016/j.meegid.2014.08.008

Yang, M., Xiang, Q., Zhang, X., Li, X., Sylla, S., & Ding, Z. (2014). RNA interference targeting nucleocapsid protein inhibits porcine reproductive and respiratory syndrome virus replication in Marc-145 cells. *J Microbiol, 52*(4), 333-339. doi:10.1007/s12275-014-3419-3

Yang, Y., Liu, Y., Lou, R., Lei, Y., Li, G., Xu, Z., & You, X. (2023). Glycyrrhiza polysaccharides inhibits PRRSV replication. *Virol J, 20*(1), 140. doi:10.1186/s12985-023-02052-9

Ye, G., Wang, X., Tong, X., Shi, Y., Fu, Z. F., & Peng, G. (2020). Structural Basis for Inhibiting Porcine Epidemic Diarrhea Virus Replication with the 3C-Like Protease Inhibitor GC376. *Viruses, 12*(2). doi:10.3390/v12020240

Yu, M., Liu, X., Sun, L., Chen, C., Ma, G., Kitamura, Y., . . . Liu, W. (2010). Subcellular localization and topology of porcine reproductive and respiratory syndrome virus E protein. *Virus Res, 152*(1-2), 104-114. doi:10.1016/j.virusres.2010.06.012

Yun, S. I., & Lee, Y. M. (2013). Overview: Replication of porcine reproductive and respiratory syndrome virus. *J Microbiol, 51*(6), 711-723. doi:10.1007/s12275-013-3431-z

Zhang, A., Zhao, L., Li, N., Duan, H., Liu, H., Pu, F., . . . Xiao, S. (2017). Carbon Monoxide Inhibits Porcine Reproductive and Respiratory Syndrome Virus Replication by the Cyclic GMP/Protein Kinase G and NF-κB Signaling Pathway. *J Virol, 91*(1). doi:10.1128/jvi.01866-16

Zhang, H., Luo, Q., He, Y., Zheng, Y., Sha, H., Li, G., . . . Zhao, M. (2023). Research Progress on the Development of Porcine Reproductive and Respiratory Syndrome Vaccines. *Vet Sci, 10*(8). doi:10.3390/vetsci10080491

Zhang, M., Han, X., Osterrieder, K., & Veit, M. (2021). Palmitoylation of the envelope membrane proteins GP5 and M of porcine reproductive and respiratory syndrome virus is essential for virus growth. *PLoS Pathog, 17*(4), e1009554. doi:10.1371/journal.ppat.1009554

Zhang, M., Krabben, L., Wang, F., & Veit, M. (2018). Glycoprotein 3 of Porcine Reproductive and Respiratory Syndrome Virus Exhibits an Unusual Hairpin-Like Membrane Topology. *J Virol, 92*(15). doi:10.1128/JVI.00660-18

Zhang, M., & Veit, M. (2018). Differences in signal peptide processing between GP3 glycoproteins of Arteriviridae. *Virology, 517*, 69-76. doi:10.1016/j.virol.2017.11.026

Zhou, Z., Ni, J., Cao, Z., Han, X., Xia, Y., Zi, Z., . . . Tian, K. (2011). The epidemic status and genetic diversity of 14 highly pathogenic porcine reproductive and respiratory syndrome virus (HP-PRRSV) isolates from China in 2009. *Vet Microbiol, 150*(3-4), 257-269. doi:10.1016/j.vetmic.2011.02.013

8 Acknowledgements

In what feels like the blink of an eye, three remarkable years have passed. I am profoundly grateful for the privilege of undertaking my PhD studies at the esteemed Institute of Virology at the Free University of Berlin. Throughout this transformative journey, I have not only acquired academic achievements and honed my scientific experimental skills, but I have also gleaned invaluable life lessons. While the path of a PhD is undoubtedly challenging, the setbacks and failures encountered during my research have served as profound teachers. To the compassionate and supportive individuals who have generously assisted me on this odyssey, I offer my heartfelt gratitude.

First and foremost, I am deeply thankful to my supervisor, PD. Dr. Michael Veit, for his unwavering guidance, encouragement, and mentorship. His expertise, patience, and constructive feedback have been invaluable assets throughout the research process. I am truly fortunate to have had such a dedicated mentor. I would like to thank Prof. Dr. Benedikt Kaufer for valuable suggestions, insightful questions, and support during the institute seminars, which help a lot in my project.

I am also grateful to the members of my doctoral committee for their valuable insights, suggestions, and support. Their expertise in their respective fields has enriched the quality of this thesis and broadened my understanding of the subject matter.

I would like to express my sincere appreciation to all the members of Veit's lab for their valuable assistance throughout my PhD journey. Dr. Minze Zhang provided a lot of instruction to my project, and Dr. Xiaorong Meng given many helpful suggestions, as well as PhD students Dina Abdulrahman, Amirreza Ohadi, Richard Kempa and Jun Ma. I am grateful for the collaborative and stimulating environment of the lab, which allowed me to learn from my colleagues and to grow both professionally and personally.

I would also like to extend my deep appreciation to all the members at the Institute of Virology for their support and help. Dr. Jakob Trimpert, Dr. Dusan Kunec, Dr. Xiaoyuan Lin, Dr. Ahmed Kheimar, Dr. Ludwig Krabben, Dr. Azza Abdelgawad, Dr. Yu You, Dr. Na Xing. PhD students Thomas Höfler, Jana Reich, Giulia Aimola, Mariana

Nascimento, Ricardo Vidal, Yingnan Cheng, Lisa Kossak, Sabsabi Mohammad, Dilan Serdar, Daria Vladimirova, Christine Langner, Yulin Cong, Louis Cairn, Jiyoon Kim, Jinzhao Ban. I will always cherish the memories and experiences I shared with them.

My sincere thanks to our technicians in the institute, Ann Reum, Annett Neubert, Michaela Zeitlow, Sebastian Bischofberger, Axel Teigeler and Constantin Rudolph for their great assist during the work and for making lab life easier. Thanks to our secretary Katharina Malik for her help during the work.

Furthermore, I would like to express my gratitude to all of my teachers, friends, and members of family especially grandparents, parents, uncles, brothers and sisters for their unwavering support, understanding, and encouragement. Their belief in me and their encouragement during both the highs and lows of this journey have been a constant source of motivation.

In addition, thanks to China Scholarship Council (CSC) for the funding support.

To summary, the completion of a doctoral degree does not signify an end, but rather a new beginning. I believe that the journey of obtaining a PhD has bestowed upon me invaluable spiritual wealth, which will serve as an inexhaustible source of motivation for my future endeavors, continuously inspiring me to overcome one challenge after another.

9 Publications in recent years

Papers:

1、**QIAN Bang**, LI Yanmin, ZHU xueliang, ZHANG Xueyan, Niyokwishimira Alfred, DOU Yongxi，ZHANG Zhidong. Establishment of an iELISA method for detection of antibody againist PPRV based on H protein epitope peptide. Acta veterinaria et Zootechnica Sinica. 2021.01.000，Doi:10.11843(In Chinese).

2、**QIAN Bang**, LIU Zhen-dong, ZHAO Yin, LI Jing, PRAJAPATI Meera, LI Yan-min, SUN Yue-feng, DOU Yong-xi. Establishment of Chemiluminescence Immunoassay for the Detection of Peste des Petits Ruminants Virus H Protein Antibodies[J]. Biotechnology Bulletin, 2023, 39(5): 120-129(In Chinese).

3、Zhang, M., **Qian, B**., & Veit, M. (2024). Engineering and characterizing porcine reproductive and respiratory syndrome virus with separated and tagged genes encoding the minor glycoproteins. Veterinary microbiology, 294, 110125. https://doi.org/10.1016/j.vetmic.2024.110125

4、Alfred, N., **Qian, B**., Qin, X., Yin, X., Prajapati, M., Dou, Y., Li, Y., & Zhang, Z. (2021). Inhibition of eIF2α Phosphorylation by Peste des Petits Ruminant Virus Phosphoprotein Facilitates Viral Replication. Frontiers in veterinary science, 8, 645571. https://doi.org/10.3389/fvets.2021.645571

5、Niyokwishimira, A., Dou, Y., **Qian, B**., Meera, P., & Zhang, Z. (2018). Reverse Genetics for Peste des Petits Ruminants Virus: Current Status and Lessons to Learn from Other Non-segmented Negative-Sense RNA Viruses. Virologica Sinica, 33(6), 472–483. https://doi.org/10.1007/s12250-018-0066-6

Patents:

1、iELISA detecting method and application for Peste des petits ruminant virus H protein antibody. DOU Yongxi, **QIAN Bang**, LI Yanmin, ZHU xueliang,ZHANG Xueyan, ZHANG Zhidong. No.202010563205.6 (In Chinese)

2、Establishment and Application of Chemiluminescence Immunoassay Detecting Method Against PPRV H Protein Antibody Based on Epitope Multipeptide. **QIAN Bang**, DOU Yongxi, ZHU xueliang, Meng Xuelian, Zhang Xueyan, ZHAO Shuaiyang, SUN Yuefeng, ZHANG Zhidong, LI Yanmin, No.202011130996.X (In Chinese)

Poster:

An amphiphilic helix of GP3 is essential for porcine reproductive and respiratory syndrome virus replication. **Bang Qian,** Minze Zhang, Michael Veit. Poster, 03/2024, 33rd Annual Meeting of the Society for Virology, Vienna, Austria.

10 Fundings of this thesis

Funding provided by China Scholarship Council (CSC) for me during the whole period of phD. Also, this work was supported by the German research foundation [grant no: Ve 141/18-1] to Michael Veit.

11. Conflict of interests

There are no conflicts of interests.

12. Selbständigkeitserklärung

Selbständigkeitserklärung Hiermit bestätige ich, dass ich die vorliegende Arbeit selbständig angefertigt habe. Ich versichere, dass ich ausschließlich die angegebenen Quellen und Hilfen Anspruch genommen habe.

Berlin, Germany, am 09.2024 Bang Qian